

**UNIVERSIDADE FEDERAL DO RIO GRANDE DO SUL  
INSTITUTO DE GEOCIÊNCIAS  
PROGRAMA DE PÓS-GRADUAÇÃO EM GEOCIÊNCIAS**

**CONTRIBUIÇÃO A EVOLUÇÃO TECTONO-  
ESTRATIGRÁFICA E TERMOCRONOLÓGICA DA  
REGIÃO NOROESTE DE MOÇAMBIQUE - ÁFRICA**

**MARCOS MÜLLER BICCA**

ORIENTADORA – Prof<sup>a</sup>. Dra. Andrea Ritter Jelinek  
COORIENTADOR – Prof. Dr. Ruy Paulo Philipp

Volume Único

Porto Alegre – 2017

**UNIVERSIDADE FEDERAL DO RIO GRANDE DO SUL  
INSTITUTO DE GEOCIÊNCIAS  
PROGRAMA DE PÓS-GRADUAÇÃO EM GEOCIÊNCIAS**

**CONTRIBUIÇÃO A EVOLUÇÃO TECTONO-  
ESTRATIGRÁFICA E TERMOCRONOLÓGICA DA  
REGIÃO NOROESTE DE MOÇAMBIQUE - ÁFRICA**

**MARCOS MÜLLER BICCA**

**ORIENTADORA – Prof<sup>a</sup>. Dra. Andrea Ritter Jelinek  
COORIENTADOR – Prof. Dr. Ruy Paulo Philipp**

**BANCA EXAMINADORA**

Prof. Dr. Léo Afraneo Hartmann – Instituto de Geociências, Universidade Federal do Rio Grande do Sul

Prof. Dr. Felipe Guadagnin – Instituto de Geologia, Universidade Federal do Pampa

Prof. Dr. Maurício Parra Amézquita – Instituto de Energia e Ambiente, Universidade de São Paulo

Tese de Doutorado apresentada como requisito parcial para a obtenção do Título de Doutor em Ciências.

Porto Alegre – 2017

# **UNIVERSIDADE FEDERAL DO RIO GRANDE DO SUL**

**Reitor:** Rui Vicente Oppermann

**Vice-Reitor:** Jane Fraga Tutikian

## **INSTITUTO DE GEOCIÊNCIAS**

**Diretor:** André Sampaio Mexias

**Vice-Diretor:** Nelson Luiz Sambaqui Gruber

Bicca, Marcos Müller

Contribuição a evolução tectono-estratigráfica e termocronológica da região noroeste de Moçambique – África. / Marcos Müller Bicca.

- Porto Alegre: IGEO/UFRGS, 2017.

[165 f.] il.

Tese (Doutorado).- Universidade Federal do Rio Grande do Sul.  
Programa de Pós-Graduação em Geociências. Instituto de Geociências.  
Porto Alegre, RS - BR, 2017.

Orientador(es): Andrea Ritter Jelinek

Coorientador(es): Ruy Paulo Philipp

1. Noroeste de Moçambique. 2. Termocronologia. 3. Evolução estratigráfica. 4. Tectônica. I. Título.

CDU 550.4

---

Catalogação na Publicação

Biblioteca Instituto de Geociências - UFRGS

Renata Cristina Grun

CRB 10/1113

## AGRADECIMENTOS

Em primeiro lugar gostaria de agradecer a minha família por ter acreditado em mim, me apoiado e incentivado durante todo o meu tempo de graduação e mestrado e doutorado.

E segundo lugar gostaria de agradecer aos meus orientadores Andrea e Ruy por todo o empenho, dedicação, ensinamentos e incentivos ao longo dos quatro anos do doutorado e também ao Prof. Claiton, João Marcelo e ao Adriano pela colaboração no primeiro artigo.

Por fim, quero agradecer também ao Cnpq por fornecer a minha bolsa de estudos durante o doutorado, e também a Vale Moçambique pela disponibilização dos dados do perfil estratigráfico do furo de sondagem que compõem o primeiro artigo desta tese.

A TODOS, MUITO OBRIGADO!!!

## RESUMO

O estudo da região noroeste de Moçambique demonstrou a importância de processos tectônicos distais (compressivos) e proximais (distensivos) na reativação de estruturas antigas do embasamento cristalino, influenciando em aspectos estruturais, sedimentares e erosivos. A caracterização tectono-estratigráfica na bacia rifte Moatize-Minjova demonstrou a forte influência de remobilização de estruturas noroeste regionais na sua configuração, sedimentação e magmatismo. A geração de espaço de acomodação na bacia foi impulsionada por esforços tectônicos na margem sul-sudoeste do Gondwana enquanto as estruturas registradas em escala de afloramento caracterizaram a influência de esforços distensivos/transtrativos pós-depositionais atribuídos à separação Jurássico-Cretácica entre as placas da África e Antártica. A análise sedimentológica permitiu determinar na Formação Moatize (Permiano Inferior ao Superior) litofácies depositadas em sequências cíclicas marcadas por sucessões de alta e baixa energia, as quais permitiram definir associações de litofácies atribuídas a planície de inundação, depósitos de crevasse e canal fluvial caracterizando um sistema fluvial meandrante estando as camadas de carvão associados a lagos e pântanos em meandros abandonados. Esta sequência foi progradada por litofácies arenosas grossas a conglomeráticas com estratificações cruzadas planares e acanaladas pertencentes à Formação Matinde, composta por macroformas de leito de migração frontal e lateral associadas a um sistema fluvial entrelaçado. As medidas de paleocorrente nestas duas formações sugerem um paleofluxo para norte-noroeste. A análise de proveniência na Formação Matinde forneceu idades entre o Mesoproterozóico e Cambriano, que abrange importantes momentos de formação e deformação crustal nos domínios geotectônicos do norte de Moçambique. As populações de idades entre 950-550 Ma permitiram a definição de uma área fonte da região sul-sudoeste, juntamente com os dados de paleocorrente para norte-noroeste, correspondente aos domínios do Complexo Nampula e da Suite Guro.

As análises térmicas das amostras do embasamento forneceram idades entre o Mesozoico e o Cenozoico e uma espessura denudada de ~ 2-3,5 km

desde o Triássico Superior. Os estágios iniciais foram marcados por taxas de denudação muito baixas (1-10 m/Ma) atingindo ~ 500 m até o Cretáceo Inferior sofrendo um leve aumento até o Paleoceno (3-17 m/Ma). Altas taxas de denudação de 31-47 m/Ma trouxeram as amostras para as condições superficiais. A denudação inicial está associada a processos distensivos/transtratativos produzidos pela dissolução do Gondwana. O Jurássico Superior e o Cretáceo Superior foi um período de grande desenvolvimento do Oceano Índico e o início da deriva N-S da Antártica em relação à placa Africana. O período entre o Cretáceo Inferior e o Paleoceno, marca o desenvolvimento da margem africana e a reconfiguração dos padrões de drenagem na placa Africana. O último evento forneceu taxas de resfriamento da ordem de 1,17 a 0,88 °C/Ma, implicando na denudação de ~ 1,5 a 2 km desde o início do Neogeno até os tempos recentes. Este último evento foi relacionado ao desenvolvimento de topografia dinâmica induzida pela movimentação da pluma do manto do Rifte do Leste Africano.

## ABSTRACT

The study of the northwestern region of Mozambique demonstrated the importance of distal (compressive) and proximal (extensional) tectonic processes in the reactivation of old structures of the crystalline basement, influencing structural, sedimentary and erosive aspects. The tectono-stratigraphic characterization in the Moatize-Minjova rifte basin demonstrated the strong influence of remobilization of northwest regional structures in its configuration, sedimentation and magmatism. Accommodation space generation in Permian times were driven by tectonic efforts on the south-southwestern margin of Gondwana, while the outcrop scale structures characterized the influence of post-depositional extensional/transtractive efforts attributed to the Jurassic-Cretaceous separation between the African and Antarctic plates. The sedimentary analysis allowed to determine in the Moatize Formation (Lower-Upper Permian) lithofacies deposited in cyclic sequences marked by deposits of high and low energy, which allowed to define associations of lithofacies attributed to floodplain, crevasse and fluvial channel deposits characterizing a meandering fluvial system, being the coal layers associated with lakes and swamps in abandoned meanders. This sequence was grade by coarse sandy to conglomerate lithofacies with planar and through-cross bedding belonging to the Matinde Formation, composed of frontal and lateral migration bed macroforms associated to a braided fluvial system. The paleocurrent measurements in these two formations suggest a north-northwest paleoflux. The provenance analysis in the Matinde Formation provided ages between the Mesoproterozoic and Cambrian, which covers important crustal formation and deformation moments in the geotectonic domains of northern Mozambique. Populations between 950-550 Ma allowed the definition of a source area of the south-southwest region, together with the north-northwest paleocurrent data, corresponding to the Nampula Complex and Guro Suite domains.

The thermal analyzes of the basement samples provided ages between the Mesozoic and the Cenozoic and a denuded thickness of ~ 2-3.5 km since Upper Triassic times. The initial stages denoted to very low denudation rates (1-10 m/Ma)

reaching ~ 500 m until the Lower Cretaceous when the region undergoes a brief increase until the Paleocene (3-17 m/Ma). High denudation rates of 31-47 m/Ma brought the samples to the present surface conditions. Initial denudation is associated with extensional/transpressive processes produced by the dissolution of Gondwana. The Upper Jurassic to Upper Cretaceous was a period of great development of the Indian Ocean and the beginning of the N-S drift of Antarctica in relation to the African plate. The period between the Lower Cretaceous and the Paleocene marks the development of the African margin and the reconfiguration of drainage patterns on the African plate. The last event provided cooling rates in the order of 1.17 to 0.88 °C/Ma implying denudation of ~ 1.5 to 2 km from the beginning of Neogene to recent times which was attributed to the development of dynamic topography induced by the movement of the mantle plume of the East African Rift.

## SUMÁRIO

|                                                                              |     |
|------------------------------------------------------------------------------|-----|
| RESUMO.....                                                                  | 1   |
| ABSTRACT .....                                                               | 3   |
| SUMÁRIO.....                                                                 | 5   |
| TEXTO EXPLICATIVO DA ESTRUTURA DA TESE .....                                 | 6   |
| 1. INTRODUÇÃO.....                                                           | 7   |
| 1.2. Localização da Área e Contexto Geológico Simplificado .....             | 8   |
| 1.3. Problema Científico e Justificativa Metodológica .....                  | 13  |
| 1.4. Síntese Integradora.....                                                | 17  |
| REFERÊNCIAS .....                                                            | 22  |
| 2. ARTIGO NO PRELO NA REVISTA <i>JOURNAL OF AFRICAN EARTH SCIENCES</i> ..... | 32  |
| 3. ARTIGO SUBMETIDO À REVISTA <i>JOURNAL OF AFRICAN EARTH SCIENCES</i> ..... | 91  |
| 4. ARTIGO SUBMETIDO À REVISTA <i>TECTONOPHYSICS</i> .....                    | 131 |

## TEXTO EXPLICATIVO DA ESTRUTURA DA TESE

Esta tese está estruturada em formato de artigos científicos, publicados e/ou submetidos em periódicos. Consequentemente, sua organização compreende as seguintes partes principais:

1- Introdução, na qual é feita uma abordagem sobre o estado da arte, procurando-se caracterizar os principais trabalhos desenvolvidos na região e arredores. Além disso, é apresentada a localização da área e o contexto geológico simplificado; problemática e justificativa para aplicação dos métodos empregados para o desenvolvimento da tese; e a síntese integradora a qual é composta por uma análise resumida e integradora dos dados obtidos nesta tese, salientando as suas contribuições para o aprimoramento do conhecimento geológico científico da região de estudo.

Os itens seguintes consistem no corpo principal desta tese, onde são apresentados os artigos submetidos à revistas nacionais e internacionais com corpo editorial indexado, com autoria principal do doutorando e colaboradores (incluindo orientadores). Nestes artigos encontram-se os resultados obtidos no decorrer do desenvolvimento da tese bem como a avaliação e interpretação dos dados com discussão e conclusão.

## 1. INTRODUÇÃO

Em termos gerais, o estudo abordou aspectos estratigráficos, tectônicos, geocronológicos e termocronológicos do Cinturão Moçambicano e bacias adjacentes, contribuindo para o aprimoramento do modelo evolutivo regional durante o Mesozóico (Permiano-Cretácico). O principal estímulo para o desenvolvimento desta tese foi a carência de trabalhos de detalhe que abrangessem análises isotópicas pertinentes a avaliação dos processos tectônicos que afetaram a região após a sua formação. Os primeiros estudos geológicos em Moçambique foram desenvolvidos ainda no século XIX com foco principal nas ocorrências de carvão que se distribuíam amplamente nas camadas do Supergrupo Karoo. Foi apenas na década de 80 que os primeiros trabalhos de mapeamento geológico de reconhecimento, e trabalhos mais detalhados, para exploração mineral foram desenvolvidos na região, em parceria com o governo de Moçambique (Hunting, 1984; Pinna *et al.*, 1993).

Mais recentemente, os trabalhos realizados pelo GTK Consortium, de 2002 a 2007, que consistiu em uma parceria entre os Serviços Geológicos de Moçambique e da Finlândia (GTK), apresentaram uma caracterização mais detalhada do território de Moçambique, definidos em folhas geológicas em escala 1:250.000. Neste projeto foram integrados todos os dados geológicos disponíveis, combinados com dados geofísicos, de imagens de satélites, análises litogeoquímicas e dados isotópicos (U-Pb com TIMS e SHRIMP e análises Sm-Nd). Os dados geocronológicos obtidos durante este projeto são pouco representativos, dispersos e não atendem as dimensões e a complexidade da geologia na região de estudo, não permitindo o seu pleno entendimento. Diversas unidades tiveram seu posicionamento estratigráfico definido a partir unicamente de observações de campo e dados geofísicos.

Desde então, alguns trabalhos pertencentes a este grupo tem sido publicados em revistas internacionais de prestígio, agregando novos dados geocronológicos aplicados à evolução das entidades geotectônicas regionais e bacias Neoproterozóicas relacionadas a elas, porém abrangendo predominantemente a região nordeste de Moçambique (Viola *et al.*, 2008; Bingen *et al.*, 2009; Thomas

*et al.*, 2010; Ueda *et al.*, 2012a e 2012b; Grantham *et al.*, 2013; Macey *et al.*, 2010; 2013). Entretanto, pouco foi desenvolvido concernente ao desenvolvimento da superfície durante o período Fanerozóico envolvendo a evolução deposicional das bacias Karoo empregando conceitos clássicos de análise estratigráfica e tectônica de bacias sedimentares (Miall, 1992; 1996).

Discussão semelhante pode ser aplicada aos estudos termocronológicos, que possuem relações intrínsecas com a história de denudação de cinturões orogênicos contribuindo diretamente para o entendimento de processos erosivos e deposicionais. A aplicação destes métodos restringe-se aos domínios nordeste de Moçambique, destinados a compreender a evolução tardi-tectônica do cinturão orogênico através de análises por termocronômetros de alta e média temperatura (Daszinnies, 2006; Daszinnies *et al.*, 2009), assim como, definir os seus estágios evolutivos tardios (Fanerozóicos) no que tange processos de denudação/exumação da superfície a partir de termocronômetros de mais baixa temperatura (< 300°C; Emmel *et al.*, 2011; Bauer *et al.*, 2016).

Neste contexto, a proposta desta tese foi contribuir com novos dados estruturais, sedimentológicos e de proveniência para as sequências do Supergrupo Karoo e termocronológicos para região, concentrando a coleta de amostras, e consequentemente, a realização de análises em unidades estratégicas para o entendimento da evolução estrutural e termotectônica do Cinturão Moçambicano. E assim, aprimorar o conhecimento ao identificar e datar eventos tectônicos tardios, que condicionaram a evolução deste cinturão durante o Fanerozóico através de análises de traços de fissão em apatitas.

## 1.2. Localização da Área e Contexto Geológico Simplificado

Este estudo foi desenvolvido na região noroeste de Moçambique, nos arredores da província de Tete, região centro-leste da África. Em termos gerais, a região de estudo comprehende rochas atribuídas aos ciclos orogênicos Proterozóicos apresentando uma ampla assembleia de rochas metamórficas de baixo a alto grau (orto e para derivadas) e rochas ígneas intrusivas (Fig. 1A e 1B). O continente Africano é composto por um mosaico de cráticos e faixas móveis

Arqueanas, amalgamados por cinturões dobrados Proterozóico-Cambrianos e cobertos por uma associação de sedimentos indeformados e rochas extrusivas de idades Neoproterozóica, Carbonífera Superior-Jurássica Inferior e Cretácica-Quaternária.

O embasamento cristalino é composto por uma assembleia heterogênea de orto e paragnasses, granulitos, migmatitos e rochas ígneas de diferentes níveis crustais (GTK Consortium, 2006). Estas associações correspondem, em sua maior parte, a rochas de idade Mesoproterozóicas (~1300-930 Ma) que foram retrabalhadas pela orogenia Pan-Africana (Neoproterozóica-Cambriana - Pinna, 1993; Hanson, 2003; Grantham *et al.*, 2003). Esta orogenia ocorreu em dois estágios principais. O primeiro estágio de amalgamação é caracterizado pela colisão das associações do terreno Gondwana Leste e Oeste, formando o Orógeno do Leste Africano com *trend* Norte - Sul (~ 550 Ma). O segundo estágio é marcado pela colisão do recém-formado Gondwana Norte com o Gondwana Sul (Orogenia Kuunga, ~ 500 Ma) com um *trend* principal Leste – Oeste (Fig. 1A) (Ueda *et al.*, 2012; Macey *et al.*, 2013).

O norte de Moçambique pode ser dividido em dois grandes domínios Mesoproterozóicos separados pelo proeminente Cinturão Lúrio Neoproterozóico-Paleozoico (Fig. 1B) (Viola *et al.*, 2008), o qual compreende uma série de zonas de cisalhamento anastomosadas com orientação NE-SW e é representado principalmente pelo Complexo Granulítico Ocua, que ocorre dominante no nordeste de Moçambique, enquanto que o segmento sudoeste do Cinturão Lurio está parcialmente coberto (Fig. 1B). O significado do Cinturão Lurio ainda é controverso. Alguns autores acreditam que ele representa uma importante zona de sutura que se liga com os cinturões Damara-Lufilian-Zambezi (Sacchi *et al.*, 2000, Grantham *et al.*, 2003). Outros sugerem que ele representa uma zona de acomodação, especialmente devido às semelhanças entre os complexos metamórficos ao norte e ao sul do Cinturão Lurio, e devido a uma aparente diminuição da tensão ao longo do cinturão de nordeste para sudoeste (Viola *et al.*, 2008; Bingen *et al.* 2009).

Os dois domínios, ao norte e ao sul do Cinturão Lurio, compartilham uma história similar de crescimento crustal durante o Mesoproterozóico. O Complexo Nampula, ao sul do cinturão, desenvolveu-se entre 1125 e 1035 Ma, enquanto o Cinturão Irumide Sul é uma região estrutural e metamorficamente complexa de rochas ígneas mesoproterozóicas relacionadas a rochas magmáticas volumosas de 1300-930 Ma (GTK Consortium) atribuídas a um ambiente de arco continental, acompanhadas de metamorfismo de alta temperatura/baixa pressão (Fritz *et al.*, 2013).

O Complexo Nampula forma um grande bloco crustal contíguo que consiste em ortognaisses e rochas metassedimentares com metamorfismo de alto grau (Bingen *et al.*, 2009; Macey *et al.*, 2010). Os ortogneisses do segmento sudoeste do Complexo Nampula (Fig. 1B) são interpretados como remanescentes do arco magmático continental Mesoproterozóico (cerca de 1100 Ma, Chaúque, 2012). A porção sudoeste do Complexo Nampula (Fig. 1B), compreendida na área de estudo desta tese, é atribuído às nappes frontais dos grupos Chimoio-Macossa e Mungari (Chaúque, 2012), constituídos por paragneisses de baixo a alto grau, as quais estão em contato tectônico direto com as rochas do craton do Kalahari. A nappe de Mungari inclui as associações da Suite Guro que compõem uma associação intrusiva bimodal Neoproterozóica (Fig. 1B) (Chaúque *et al.*, 2017).

Análises U-Pb em zircão de rochas graníticas indicam uma idade de cristalização magmática de  $867 \pm 15$  Ma. A datação do núcleo de zircões metamórficos mostra idades de recristalização em ~ 850-839 Ma, relacionada com falhas distensivas, enquanto as bordas metamórficas forneceram uma idade de  $512 \pm 4$  Ma relacionada com a Orogenia Pan-Africana (GTK Consortium 2006). Na margem nordeste da área cratônica ocorrem rochas metavulcânicas metassedimentares e félsicas de baixo a médio grau (cerca de 800 Ma) do Grupo Rushinga que podem representar uma margem passiva de idade Neoproterozóica (Barton *et al.*, 1991; Hargrove *et al.*, 2003, GTK Consortium 2006, Chaúque, 2012).

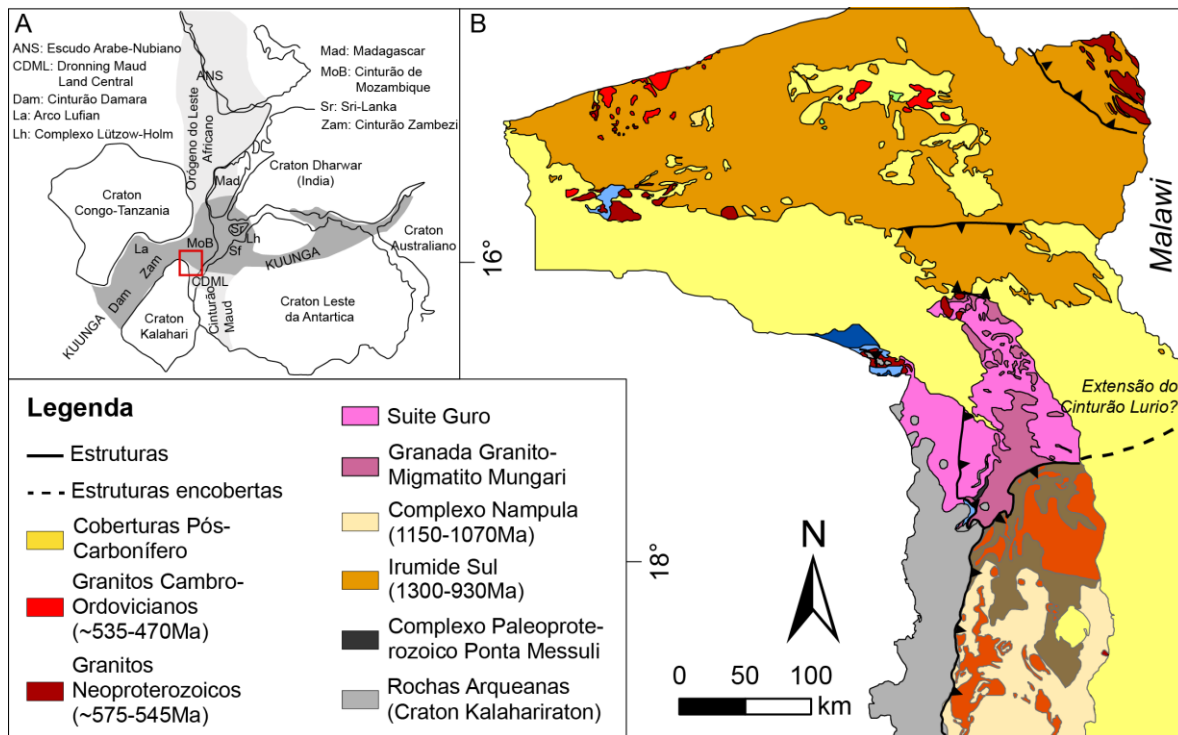


Figura 1: A) Reconstrução da margem leste da África ao final da amalgamação do Gondwana (Meert, 2003); B) Mapa geológico simplificado da região noroeste de Moçambique (Macey *et al.*, 2013).

A orogênese colisional Pan-Africana foi seguida pela intrusão de granitos tardi-pós-tectônicos no Neoproterozóico (cerca de 575-545 Ma) e K-granito no Cambriano-Ordoviciano (cerca de 530-495 Ma) (Jacobs *et al.*, 2008, Ueda *et al.*, 2012, Macey *et al.*, 2013, Grantham *et al.*, 2013). Este último predomina na porção oriental do Complexo Nampula (Fig. 1B), devido ao processo de delaminação crustal que levou a uma história de resfriamento prolongada durante os períodos Cambriano e Ordoviciano (Jacob *et al.*, 2008; Emmel *et al.*, 2014). Estas rochas Pré-Cambrianas a Cambrianas foram parcialmente cobertas pelos depósitos vulcanossedimentares Fanerozóicos do Supergrupo Karoo e sequências mais jovens (GTK Consortium, 2006).

As sequências sedimentares e ígneas da região se depositaram em riftes intracontinentais associados às estruturas do embasamento, as quais possuem direções preferenciais noroeste-sudeste e leste-oeste. Estes depósitos são representados por dois supergrupos distintos: o supergrupo Karoo (Carbonífero

Superior – Jurássico Inferior) e depósitos contemporâneos ao rifte da margem leste Africana (Jurássico Superior ao Recente) (GTK Consortium, 2006).

O Supergrupo Karoo (SK) comprehende uma sucessão de rochas sedimentares continentais, seguidas por derrames de lavas básicas e extrusões riolíticas, que atestam um processo de separação do Gondwana. A história deposicional do Supergrupo Karoo é composta por sequências glaciogênicas, fluvio-lacustres, fluviais e magmáticas. Em geral, a sedimentação do Supergrupo Karoo comprehende uma mudança progressiva das condições glaciais para as condições úmidas e frias para condições quentes, semiáridas e finalmente quentes e áridas (Johnson *et al.*, 1996). Sequências correlacionáveis a esses grupos, que mais ou menos podem ser observadas em todas as bacias de Karoo na África, seguem uma sequencia de ambientes glaciais, deltaicos, fluviais, lacustres e eólicos, principalmente devido à mudanças climáticas (aridificação) durante a deriva norte de Gondwana (Catuneanu *et al.*, 2005).

A Formação Vúzi corresponde a base da sequência, depositada em um ambiente flúvio-glacial (Consórcio GTK, 2006, Fernandes *et al.*, 2015). As litologias mais expressivas comprehendem conglomerados fluviais, diamictitos, arenitos e ritmitos intercalados, folhelhos carbonosos e finas camadas de carvão no topo da sequência, repousando discordantemente sobre o embasamento cristalino Pré-Cambriano (GTK Consortium, 2006; Vasconcelos *et al.*, 2014; Fernandes *et al.*, 2015; Lakshminarayana, 2015). Os depósitos de Vúzi mostram uma importante assembleia palinológica que indica uma idade Sakmariana (Wopfner e Kreuser, 1986, Weiss e Wopfner, 1997). Não obstante, estudos desenvolvidos por Pereira *et al.* (2014) e Lopes *et al.* (2014) que, datando os diamictitos do topo desta formação, atribuíram uma idade Kunguriana-Roadiana (Permiano Médio-Superior), sendo mais jovem que a última idade regional proposta. Poucas idades radiométricas U-Pb estão disponíveis para as sequências cronocorrelatas à Formação Vúzi, sendo descritas no grupo Dwyka da Namíbia e da África do Sul, obtidas a partir de camadas de tufos indicando idades de  $302 \pm 3,0$  Ma e  $299 \pm 3,2$  Ma para as rochas da Namíbia e  $288 \pm 3,0$  Ma e  $289 \pm 3,8$  Ma para a África do Sul (Bangert *et al.*, 1999). A formação Vúzi transiciona

gradualmente para a Formação Moatize que consiste em sua maior parte, de arenitos carbonosos, arenitos arcoseanos e arenitos conglomeráticos ocasionais. Ainda ocorrem arenitos de finos com argila ou micáceo e folhelhos carbonosos com camadas cíclicas de carvão (Cairncross, 2001). A idade absoluta destas formações de carvão não está bem definida e a maior parte provém do registro palinológico, permitindo posicionar o seu ciclo deposicional durante todo o Permiano (Daber, 1984; Pereira *et al.*, 2014).

A Formação de Moatize é sobreposta pelos depósitos da Formação Matinde de idade Permo-Triássica (GTK Consortium, 2006; Pereira *et al.*, 2016), compreendendo uma espessa sucessão intercalada de arenitos muito grosseiros e conglomerados polimíticos, com ocorrências subordinadas de siltitos (GTK Consortium, 2006). A sequência sedimentar atribuída ao topo do Supergrupo Karoo é dominada por depósitos aluviais grosseiros com estratificação cruzada da Formação Cádzi (GTK Consortium, 2006) a qual é classicamente posicionada entre o Permiano Superior e o Triássico Inferior (GTK Consortium, 2006). Entretanto, devido à idade atribuída à formação inferior a esta, fica evidente a necessidade de um aprimoramento dos estudos geocronológicos referentes a estas formações, ou até mesmo, quanto à sua correlação em termos estratigráficos. O ciclo basinal do Supergrupo Karoo é encerrado pelo magmatismo bimodal (195-180 Ma, Sm-Nd; 181 Ma, U-Pb TIMS) atribuído a um estágio inicial da dissolução de supercontinente Gondwana (GTK Consortium, 2006).

As sequências do SK foram parcialmente erodidas e sobrepostas por depósitos sedimentares associados aos estágios sin- e pós- abertura do Oceano Índico acompanhados por rochas vulcânicas e associações carbonáticas e alcalinas (dados  $^{40}\text{K}$ - $^{40}\text{Ar}$  forneceram idades entre ~ 106-166 Ma) marcando um novo pulso de rifteamento na margem leste Africana (GTK Consortium, 2006).

### 1.3. Problema Científico e Justificativa Metodológica

Cinturões orogênicos consistem em zonas alongadas, comumente arqueadas, de rochas altamente deformadas que se desenvolveram durante

processos da orogênese em ambiente de margens convergentes, envolvendo encurtamento intraplaca, espessamento crustal e soerguimento topográfico. Orógenos antigos, os quais já tiveram a sua topografia reduzida por processos erosivos, marcam a localização de antigos e inativos limites de placas, fornecendo informações importantes referentes aos movimentos das placas tectônicas no passado (Kearey *et al.*, 2009). Os orógenos Pré-Cambrianos compreendem províncias crustais exumadas, sendo que a maioria destas províncias contém rochas com um amplo intervalo de idades e registram mais de um período de deformação, metamorfismo e plutonismo. Algumas seções das províncias crustais correspondem a rochas “novas”, derivadas do manto, denominada de juvenis, enquanto que outras partes são formadas por rochas originadas a partir do retrabalhamento da crosta antiga (Conde, 2005).

A maioria das províncias crustais e orógenos são compostos por terrenos, os quais são considerados os blocos básicos para a construção dos continentes e a colisão entre os terrenos é o processo principal para o crescimento continental. Estes terrenos apresentam um registro semelhante de idades isotópicas e exibem uma história pós-amalgamação semelhante. A maioria dos terrenos colide com a crosta continental ao longo de falhas transcorrentes ou zonas de subducção, sendo suturadas aos continentes. A crosta continental pode ser fragmentada e separada por processos de rifteamento ou por falhas transcorrentes (Conde, 2005). Os terrenos, que compõem as províncias crustais, são limitados por zonas de sutura, que são lineamentos entre as províncias crustais. Estas zonas correspondem a indícios da presença de zonas de subducção ou limites de placa. Megassuturas são aglomerados de cinturões orogênicos unidos por um limite de placas comum (Kearey *et al.*, 2009).

O norte de Moçambique comprehende rochas geradas em ciclos orogênicos desde o Arqueano até o Cambriano. Estes processos deixaram diversas estruturas crustais que demonstraram vital importância na reconfiguração crustal concernentes aos processos tectônicos tardios, taxas de sedimentação e estilos deposicionais em bacias sedimentares e taxas de denudação. As bacias sedimentares possuem em seu registro importantes pistas dos eventos que

ocorreram nas rochas do embasamento adjacente, que atuaram como área fonte para o seu preenchimento (Fedó *et al.*, 2003; Hawkesworth *et al.*, 2010).

O Supergrupo Karoo compreende sequências vulcanossedimentares depositadas em um intervalo de tempo entre o Carbonífero Superior e o Jurássico Médio. Estas sequências estão amplamente depositadas em bacias de antepaís, sag e em riftes intracontinentais em toda a região centro-sul da África (Catuneanu *et al.*, 2005). Estas bacias são cronocorrelatas a outras bacias sedimentares na América do Sul, Antártica e Austrália, sendo que algumas compartilham eventos deposicionais relacionados a eventos tectônicos compressivos ocorridos na margem sul-sudoeste do Supercontinente Gondwana (Milani e Ramos, 1998; Zerfass *et al.*, 2003; 2004; 2005; Milani e De Wit, 2008). Em todas as bacias Africanas é possível observar uma correlação em seus registros sedimentares referente a uma mudança progressiva das condições glaciais para as condições úmidas e frias para condições quentes, semiáridas e finalmente quentes e áridas, a qual ocorre aproximadamente no limite entre o Permiano e o Triássico (Johnson *et al.*, 1996; Catuneanu *et al.*, 2005).

Em Moçambique, pouco tem sido feito em termos de aprimoramento tectono-estratigráfico para aperfeiçoamento dos modelos deposicionais e prospectivos. Os modelos vigentes apenas restringem-se a uma determinação superficial, caracterizando-os como ambientes glaciogênicos (Formação Vúzi), fluvial e lacustre (Formação Moatize) e fluvial (Formações Matinde e Cádzi) (Cairncross, 2001; GTK Consortium, 2006). O último estágio deposicional desta bacia é marcado por um evento magmático atribuído às primeiras fases da separação entre as placas da África e Antártica (Castaing, 1991; Salman e Abdul, 1995). Com este viés, o objetivo deste trabalho residiu em aplicar conceitos clássicos de estratigrafia, interpretação de fácies sedimentares e ambientes deposicionais (Miall, 1996; 2016), a partir do qual é possível correlacionar padrões de sedimentação e estruturas sedimentares a processos deposicionais e, por conseguinte a ambientes deposicionais. Aliado ao estudo estratigráfico foi realizada uma análise estrutural da bacia para identificar possíveis correlações

com episódios tectônicos distais da margem do Gondwana, posicionando-os nos ciclos evolutivos da bacia.

Para caracterizar o comportamento do embasamento adjacente a bacia, propusemos a aplicação de um estudo de proveniência através do método U-Pb em zircões detriticos, tendo em vistas a ausência de trabalhos de proveniência nas bacias sedimentares da região. Este método é uma técnica amplamente utilizada para a determinação de idades de formação e/ou metamorfismo em minerais ricos em urânio (principalmente o zircão) permitindo a correlação destas idades com a base de dados regionais de datações disponíveis para as rochas adjacentes à bacia (Cawood, 2012; Guadagnin *et al.*, 2012; Bicca *et al.*, 2013; Oliveira *et al.*, 2014).

Uma das questões importantes referente aos estudos tectônicos associados à evolução tardia de orógenos é a determinação das taxa dos processos térmicos e erosivos que definem a sua evolução. Estes taxas podem ser determinadas através da modelagem de dados termocronológicos, para caracterizar a história térmica destas rochas (Hodges, 2003). No tocante a região de estudo, o único trabalho trazendo informações termocronológicas foi desenvolvido nas sequências sedimentares do Supergrupo Karoo (Fernandes *et al.*, 2015), onde foi possível identificar que as idades térmicas por traços de fissão de apatita encontram-se entre 146 e 84 Ma, e, são portanto mais jovens do que a idade estratigráfica das amostras, além do que, o modelo térmico indica um episódio de resfriamento rápido entre 240 e 230 Ma implicando em 2500-3000 m de denudação. A partir deste modelo foi possível identificar ainda um segundo período, também de resfriamento rápido, a partir de 6 Ma implicando em 1000 - 1500m de denudação. Os autores correlacionaram o primeiro episódio ao principal evento de deformação compressiva no *Cape Fold Belt* na África do Sul, que transferiu o estresse para o norte em sistemas de falhas transtensionais pré-existentes nas bacias do Karoo, causando inversão tectônica e elevação, enquanto que o segundo período de resfriamento rápido e denudação foi relacionado com a propagação do Sistema Rift do Leste Africano em Moçambique.

No intuito de estudar estes processos tectônicos tardios, que afetaram as rochas da área de estudo adjacentes às bacias Karoo, utilizamos o método de traços de fissão em apatitas (60 – 120°C) para reconstruir a história de exumação e soerguimento destas rochas desde o último evento registrado e correspondente aos 5 km superiores da crosta continental (Stockli, 2005; Reiners e Brandon, 2006; Lisker *et al.*, 2009).

#### 1.4. Síntese Integradora

O desenvolvimento do trabalho envolvendo a análise estratigráfica e tectônica do Supergrupo Karoo na região noroeste de Moçambique integrado com dados da literatura (Castaing, 1991; Cairncross, 2001; Catuneanu *et al.*, 2005) revelou importantes aspectos concernentes aos processos tectônicos tardios do cinturões orogênicos a noroeste de Moçambique. A atividade tectônica reconhecida demonstrou um importante controle na sedimentação e transporte das Formações Moatize e Matinde do Supergrupo Karoo depositadas na bacia rifte Moatize-Minjova. Esta bacia situa-se sobre um importante sitio estrutural da região e demonstrou a forte influência de remobilização de estruturas noroeste regionais na sua configuração, sedimentação e magmatismo. Os estágios de subsidência/acomodação da bacia foram impulsionados por esforços tectônicos na margem sul-sudoeste do Gondwana gerados pela Orogenia Gondwanides. Anteriormente, a subsidência das bacias rifte do leste da África (Carbonífero Superior-Jurássico Superior) era atribuída aos processos de rifteamento do Supercontinente Gondwana envolvendo esforços distensivos. Enquanto que neste trabalho, foi possível determinar que as influências dos esforços compressivos de sul-sudoeste também se fizeram presentes no noroeste de Moçambique movimentando estruturas regionais noroeste em regime transtrativo, deformando as camadas de carvão (Permiano) durante a sua evolução.

As estruturas registradas em escala de afloramento caracterizaram apenas a influência de esforços distensivos/transtrativos pós-deposicionais atribuídos aos processos de separação Jurássico-Cretácica entre as placas da África e Antártica. Em termos de sedimentação foi possível reconstruir os paleoambientes

deposicionais para duas formações depositadas entre o Permiano e o Triássico Inferior. A Formação Moatize (Permiano Inferior ao Superior) abrange jazidas significativas de carvão na região e foi analisada detalhadamente a partir de afloramentos e de um perfil de sondagem (~500 m) permitindo a identificação de litofácies carbonosas, finas (folhelhos), arenosas com laminações tipo *ripples*, *hammoky* e *wavy*, como também estratificações cruzadas planares e acanaladas. A deposição desta sequência demonstra características deposicionais cíclicas marcadas por sucessões de alta e baixa energia. Estas características levaram a definição de cinco associações de litofácies atribuídas à planície de inundação, depósitos de crevasse *splay* e canal de crevasse, e canal fluvial caracterizando um sistema fluvial mandrante, estando as camadas de carvão associados a lagos e pântanos em meandros abandonados.

A análise estratigráfica de afloramentos e de uma seção de ~300m de profundidade permitiu definir que as sequências da Formação Moatize foram progradadas por litofácies arenosas grossas a conglomeráticas com estratificações cruzadas planares e acanaladas pertencentes à Formação Matinde. As relações internas e estruturais desta litofácies permitiram a definição de macroformas de leito de migração frontal e lateral associadas a um sistema fluvial entrelaçado. As medidas de paleocorrente sugerem um paleofluxo para norte-noroeste.

Neste modelo as camadas de carvão estão associadas com os depósitos de lagos e pântanos de planície de inundação e meandros abandonados da Formação Moatize. Nestes termos, as camadas de carvão devem apresentar distribuições laterais e verticais variadas e descontínuas, sendo necessário um mapeamento mais detalhado de toda a região da determinar a sua ocorrência.

A identificação de paleocorrente para o norte-noroeste a partir das análises estratigráficas realizadas neste trabalho e por Key *et al.* (2015) foram interpretadas como representativas de uma provável inversão do Rio Zambezi (que drena atualmente a região) durante a deposição das sequências Permo-Triássico do norte de Moçambique. Este comportamento foi também estudado através de dados de proveniência com U-Pb em zircões detriticos da Formação Matinde. Em

litolíticas de arenitos grossos a conglomeráticos, provavelmente relacionados a um rejuvenescimento topográfico na área fonte durante o Permiano por processos tectônicos.

Os espectros de idades U-Pb observados mostraram apenas idades mais antigas em relação à idade de deposição da sequência, que reflete a história do cinturão orogênico subjacente como esperado em ambientes intracratônicos (Cawood *et al.*, 2012). A morfologia do zircão, as texturas internas e as idades fornecem informações sobre a história geotectônica do cinturão subjacente em termos de idades ígneas e metamórficas, permitindo a definição de quatro grupos de idades principais: i) 1.130-1.005 Ma; ii) 992-859 Ma; iii) 637-563 Ma; E iv) 549-493 Ma. As primeiras e as últimas são as mais proeminentes proveniências dos sedimentos de Karoo, destacando-se dois importantes eventos de geração, consumo e deformação crustais dos Supercontinentes Rodinia e Gondwana. As medições de paleocorrentes e a imaturidade do arenito amostrado sugerem áreas fontes localizadas em algum lugar no sul da Bacia de Moatize-Minjova, devido à preservação das bordas metamórficas.

A população de idades mais antigas reflete a maior componente crustal no norte de Moçambique, refletindo principalmente idades de cristalização magmática, como evidenciado pelo crescimento oscilatório nos grãos de zircão, característica comum nesta população. O final do Mesoproterozóico foi um momento importante de geração crustal para todos os domínios geotectônicos do norte de Moçambique. Esta população encontra-se na faixa de idades do segmento sudoeste do Complexo Nampula (Chaúque, 2012), ao sul da área de amostragem. Após os eventos de espessamento crustal e cavalgamentos resultantes da Orogenia Pan-Africana (~550-480 Ma), a região sul da Bacia Moatize-Minjova provavelmente formou um alto topográfico juntamente com toda a porção nordeste de Moçambique. Nestes locais se originaram as cabeceiras dos rios e afluentes que banharam a bacia do Proto-Zambeze, como sugerido por Key *et al.* (2015) e por esta tese.

As idades contidas entre ~550 Ma e 480 Ma são atribuídas a eventos magmáticos e metamórficos comuns na região devido ao metamorfismo de alto

grau produzido pela Orogenia Pan-Africana e, portanto, não são bons marcadores para determinar a proveniência sedimentar. Por outro lado, as idades entre ~ 950Ma e 550Ma não ocorrem com ampla distribuição e correspondem a importantes períodos de evolução geotectônica da crosta na região. Estas idades foram relacionadas aos dados de U-Pb de Manjate (2015) para a Suite Guro e rochas associadas posicionadas a leste-sudeste da área amostrada, como também as idades em torno de ~ 850 Ma. As idades em torno de ~ 630 Ma e 560Ma referem-se a eventos distintos de deformação e magmatismo ao longo do norte do cinturão de Moçambique, que são registrados no nordeste de Moçambique em rochas metamórficas e magmáticas (~635 Ma, Macey *et al.*, 2013; 635 Ma e 570-590 Ma, Grantham *et al.*, 2013). Esta população não está fortemente impressa na porção sudoeste do Complexo de Nampula e na Suite Guro /Granada granito-migmatito Mungari/Granito Chacocoma, embora estejam presentes nas idades de zircão individuais apresentadas por Chaúque (2012) e Manjate (2015). Dados de concentrações e taxas de Th/U também são compatíveis com as áreas fonte sugeridas, predominando razões  $\text{Th}/\text{U} > 0,1$ . Outras fontes a nordeste da área apresentaram razões  $\text{Th}/\text{U} < 0,1$ , atribuídas a uma origem metamórfica (Hartmann e Santos, 2004), além de concentrações muito altas de U ( $> 1000 \text{ ppm}$ ), as quais não foram observadas nos zircões da Formação Matinde.

As histórias térmicas determinadas para as rochas do embasamento cristalino do noroeste de Moçambique a partir das análises de termonocronologia por traços de fissão em apatitas (TFA) indicam que processos intensos de exumação afetaram amplamente a região durante a Era Mesozóica. As idades centrais TFA e as máximas paleotemperaturas modeladas puderam ser atribuídas à períodos de importantes atividade tectônica regional e local e à dinâmica mantélica associados com a abertura do Oceano Índico e do Sistema Rifte do Leste Africano. As idades mais antigas são compatíveis com os últimos estádios da atividade tectônica da *Cape Fold Belt*, podendo representar episódios de resfriamento causados por erosão e denudação associados à reativações estruturais distais. Esta proposta é pertinente e bem qualificada já através da

análise estratigráfica da Bacia Karoo , onde foram observadas evidências de uma sedimentação possante nas bacias Karoo do Vale do Zambezi ainda no Permiano. Estas idades estão de acordo com o trabalho de Fernandes *et al.* (2015) em amostras sedimentares do Supergrupo Karoo na Bacia Moatize-Minjova e com os dados de Van Der Beek *et al.* (1998) para o norte do Malawi, demonstrando que se trata de eventos de denudação regionais. As demais idades são todas mais jovens que o magmatismo do Supergrupo Karoo, responsável por alterar o comportamento térmico crustal durante a sua atividade. No Jurássico Médio (170-166 Ma) ocorre o início da abertura da bacia da Somália através da Zona de Falha Davie (Mahanjane, 2014), compreendendo estágios iniciais de separação do Gondwana. Durante estes processos as maiores espessuras denudadas são da ordem de 300 m, em um período entre o Triássico superior ao Jurássico médio, implicando em taxas de resfriamento inferiores a 0.3 °C/Ma.

Um padrão semelhante é observado entre o Jurássico Médio e Cretáceo Inferior, com espessuras denudadas da ordem de 300 m, que podem estar associados à reativações dos padrões estruturais NW-SE e N-S que predominam na região. As paleotemperaturas máximas em torno de 150 Ma são frequentes nos modelos térmicos, também documentadas na Malawi e associados a uma nova fase de rifte na margem leste da África (Van der Beek *et al.*, 1998). Este momento está documentado na região sul do Malawi com o desenvolvimento de magmatismo alcalino (~130-100 Ma) associado com tectônica distensiva (Eby *et al.*, 1995). Dados K-Ar de rochas vulcânicas, associações carbonatíticas e alcalinas no norte de Moçambique (GTK Consortium, 2006) forneceram idades entre ~106-166 Ma, configurando um importante estágio de fluxo térmico na placa continental Africana. Este período compreende os primeiros estágios de *drift* da Antártida para o sul em relação à África (Mahanjane, 2012; Castelino *et al.*, 2015) e a deriva de Madagáscar para o sul da margem da Tanzânia pela zona de cisalhamento Davie (140 Ma a 90 Ma, Emmel *et al.*, 2011; Mahanjane, 2014). Esses argumentos estão de acordo com a intensificação da denudação observada em toda a área de estudo, desde o Cretáceo Superior até o Paleoceno Médio, com espessuras erodidas variando entre 254 e 1659 m, devido ao

desenvolvimento da margem de Moçambique. Processos semelhantes durante o Cretáceo Inferior e Superior são também descritos por Belton e Raab (2010) para a área cratônica do Kalahari e por Emmel *et al.* (2011) para a porção nordeste de Moçambique, corroborando o modelo elevação regional da margem leste da placa africana.

Taxas de denudação de 31-47 m/Ma e espessuras de 1,5-2 km de superfície denudada trouxeram as amostras até as condições térmicas atuais a partir de ~40 Ma, atingindo desde o Triássico espessuras da ordem de 2,5-3,5 km. Condições semelhantes foram detectadas nas sequências de Karoo na bacia Moatize-Minjova implicando em 1-1,5 km de denudação a partir de 6 Ma (Fernandes *et al.*, 2015). Estas taxas elevadas foram atribuídas a mudanças na topografia do norte de Moçambique devido à movimentação para norte da placa Africana, resultando na movimentação mantélica produzida pela pluma do Sistema Rifte do Leste Africano atuante na região nordeste da África (Moucha e Forte, 2011). As elevadas taxas de sedimentação na bacia *offshore* de Moçambique (Castelino *et al.*, 2015) corroboram as taxas de denudação continentais, entretanto, demandam uma carga maior provavelmente suprida por área ainda mais interiores da placa Africana, implicando em alterações topográficas e nos padrões fluviais da bacia do Rio Zambezi.

## REFERÊNCIAS

- Barton, C.M., Carney, J.N., Crow, M.J., Dunkley, P.N., Simango, S., 1991. The Geology of the Country around Rushinga and Nyamapanda. Zimbabwe Geological Survey Bulletin, 92.
- Bangert, B., Stollhofen, H., Lorenz, V., Armstrong, R., 1999. The geochronology and significance of ash-fall tuffs in the glaciogenic Carboniferous-Permian Dwyka Group of Namibia and South Africa. Journal of African Earth Sciences 29, 33–49.

- Bauer, F.U., Jacobs, J., Emmel, B.U., van Soest, M.C., 2016. New (U-Th)/He titanite data from a complex orogen-passive margin system: A case study from northern Mozambique. *Journal of African Earth Sciences* 120, 56-69.
- Belton, D.X., Raab, M.J., 2010. Cretaceous reactivation and intensified erosion in the Archean–Proterozoic Limpopo Belt, demonstrated by apatite fission track thermochronology. *Tectonophysics* 480, 99–108.
- Bicca, M.M., Chemale Jr., F., Jelinek, A.R., Christie Helouise Engelmann de Oliveira, C.H.E.O., Guadagnin, F., Armstrong, R., 2013. Tectonic evolution and provenance of the Santa Bárbara Group, Camaquã Mines region, Rio Grande do Sul, Brazil 48, 173–192.
- Bicca, M.M., Philipp, R.P., Jelinek, A.R., Ketzer, J.M.M., Scherer, C.M.S., Jamal, D.L., Reis, A.D., 2017. Permian-Early Triassic Tectonic and Stratigraphy of the Karoo Supergroup in Northwestern Mozambique. *Journal of African Earth Sciences*. Article in press.
- Bingen, B., Jacobs, J., Viola, G., Henderson, I.H.C., Skar, O., Boyd, R., Thomas, R.J., Solli, A., Key, R.M., Daudi, E.X.F., 2009. Geochronology of the Precambrian crust in the Mozambique belt in NE Mozambique, and implications for Gondwana assembly. *Precambrian Research* 70, 231–255.
- Cairncross, B., 2001. An overview of Permian (Karoo) coal deposits of Southern Africa. *Journal of African Earth Sciences* 33, 529–562.
- Casting, C., 1991. Post-Pan-African tectonic evolution of South Malawi in relation to the Karroo and Recent East African Rift Systems. *Tectonophysics* 191, 55-73.
- Castelino, J.A., Reichert, C., Klingelhofer, F., Aslanian, D., Jokat, W., 2015. Mesozoic and Early Cenozoic sediment influx and morphology of the Mozambique Basin. *Marine and Petroleum Geology* 66, 890-905.<http://dx.doi.org/10.1016/j.marpetgeo.2015.07.028>.

- Catuneanu, O., Wopfner, H., Eriksson, P.G., Cairncross, B., Rubidge, B.S., Smith, R.M.H., Hancox, P.J., 2005. The Karoo basins of south-central Africa. *Journal of African Earth Sciences* 43, 211–253.
- Cawood, P., Hawkesworth, C., Dhuime, B., 2012. The continental record and generation of the continental crust. *Geological Society of America Bulletin* 125, 14–32.
- Chaúque, F. R., 2012. Contribution to the knowledge of the tectonic evolution of the Mozambique Belt, Mozambique. Thesis (Ph.D) - Institute of Geosciences, University of São Paulo, São Paulo, 187pp.
- Chaúque, F. R., Cordani, U.G., Jamal, D.L., Onoe, A.T., 2017. The Zimbabwe Craton in Mozambique: A brief review of its geochronological pattern and its relation to the Mozambique Belt. *Journal of African Earth Sciences*. doi: 10.1016/j.jafrearsci.2017.01.021.
- Condie, K. C. 2005. Earth as an Evolving Planetary System. Elsevier, Amsterdam, 447p.
- Daber, R., 1984. Plantas fósseis de Moçambique, 9. Ciência e Tecnologia, Maputo, pp. 77-81.
- Daszinnies, M.C., 2006. The Phanerozoic Thermo-tectonic Evolution of Northern Mozambique Constrained by  $^{40}\text{Ar}/^{39}\text{Ar}$ , Fission Track and (U–Th)/He Analyses. PhD Thesis University of Bremen 227.
- Daszinnies, M.C., Jacobs, J., Wartho, J.-A., Grantham, G.H., 2009. Post Pan-African thermo-tectonic evolution of the north Mozambican basement and its implication for Gondwana rifting. Inferences from  $^{40}\text{Ar}/^{39}\text{Ar}$  hornblende, biotite and titanite fission-track dating. In: Lisker, F., Ventura, B., Glasmacher, U. (Eds.), *Thermochronological Methods: From Palaeotemperature Constraints to Landscape Evolution Models*: Geological Society of London, Special Publications 324, 25–50.
- Eby, R M., Roden-Tice, G.N., Krueger, H.L., Ewing, W., Faxon, E.H., Woolley, A.R., 1995. Geochronology and cooling history of the northern part of the

- Chilwa Alkaline Province, Malawi. *Journal of African Earth Sciences* 20(3-4), 215-288.
- Emmel, B., Kumar, R., Ueda, K., Jacobs, J., Daszinnies, M.C., Thomas, R.J., Matola, R., 2011. Thermochronological history of an orogen-passive margin system — an example from N Mozambique. *Tectonics* 30. <http://dx.doi.org/10.1029/2010TC002714>.
- Emmel, B., Kumar, R., Jacobs, J., Ueda, K., Van Zuijen, M., R.J., Matola, R., 2014. The low-temperature thermochronological record of sedimentary rocks from the central Rovuma Basin (N Mozambique) — Constraints on provenance and thermal history. *Gondwana Research* 25, 1216–1229.
- Fedo, C.M., Sircombe, K.N., Rainbird, R.H., 2003. Detrital zircon analysis of the sedimentary record. In: Hanchar, J.M., Hoskin, P.W.O. (Eds.), *Zircon. Reviews in Mineralogy and Geochemistry* 53, 277–303.
- Fernandes, P., Cogné, N., Chew, D.M., Bruno Rodrigues, B., Jorge, R.C.G.S., Marques, J., Jamal, D., Vasconcelos, L., 2015. The thermal history of the Karoo Moatize-Minjova Basin, Tete Province, Mozambique: An integrated vitrinite reflectance and apatite fission track thermochronology study. *Journal of African Earth Sciences* 112, 55-72.
- Fritz, H., Abdelsalam, M., Ali, K.A., Bingen, B., Collins, A.S., Fowler, A.R., Ghebreab, W., Hauzenberger, C.A., Johnson P.R., Kusky, T.M., Macey, P., Muhongo, S., Stern, R. J., Viola, G., 2013. Orogen styles in the East African Orogen: A review of the Neoproterozoic to Cambrian tectonic evolution. *Journal of African Earth Sciences* 86, 65–106.
- Grantham, G.H., Maboko, M., Eglington, B.M., 2003. A review of the evolution of the Mozambique Belt and implications for the amalgamation for Rodinia and Gondwana. In: Yoshida, M., Windley, B.F., Dasgupta, S. (Eds.), *Proterozoic East Gondwana: Supercontinent Assembly and Breakup*. Geological Society of London, Special Publications 206, 401–426.

- Grantham, G.H., Macey, P.H., Horie, K., Kawakami, T., Ishikawa, M., Satish-Kumar, M., Tsuchiya, N., Graser, P., Azevedo, S., 2013. Comparison of the metamorphic history of the Monapo Complex, northern Mozambique and Balchenfjella and Austhameren areas, Sør Rondane, Antarctica: Implications for the Kuunga Orogeny and the amalgamation of N and S Gondwana. *Precambrian Research* 234, 85– 135.
- GTK Consortium, 2006. Explanation of geological maps of sheets: Songo (1532), Cazula/Zóbuè (1533-1534), Mecumbura/Chioco (1631-1632), Tete (1633) and Tambara (1634). Ministério dos Recursos Minerais, Direcção Nacional de Geologia, Maputo.
- Guadagnin, F., Chemale Jr., F., Dussin, I.A., Jelinek, A.R., Santos, M.N., Borba, M.L., Justino, D., Bertotti,A.L.,Alessandretti, L., 2010. Depositional age and provenance of the Itajaí Basin, Santa Catarina State, Brazil: implications for SW Gondwana correlation. *Precambrian Res.* 180, 156–182.
- Hanson, R.E., 2003. Proterozoic geochronology and tectonic evolution of southern Africa. *Geological Society, Special Publications* 206, 427-463.
- Hargrove, U.S., Hanson, R.E., Martin, M.W., Blenkinsop, T.G., Bowring, S.A., Walker, N., Munyanyiwa, H., 2003.Tectonic evolution of the Zambezi orogenic belt: geochronological, structural, and petrological constraints from northern Zimbabwe. *Precambrian Research* 123, 159–186.
- Hartmann, L. A., Santos, J.O.S., 2004. Predominance of high Th/U, magmatic zircon in Brazilian shield sandstones. *Geology* 32, 73–76.
- Hawkesworth, C., Dhuime, B., Pietranik, A., Cawood, P., Kemp, T., and Storey, C., 2010. The Generation and Evolution of the Continental Crust: *Journal of the Geological Society* 167, 229–248.
- Hodges, K.V. 2003. Geochronology and thermochronology in orogenic systems. In: Turekian, K.K.; Holland, H.D. (eds.) *Treatise on Geochemistry*, Oxford, UK: Elsevier, 263–292.

- Jacobs, J., Bingen, B., Thomas, R.J., Bauer, W., Wingate, M.T.D., Feitio, P., 2008. Early Palaeozoic orogenic collapse and voluminous late-tectonic magmatism in Dronning Maud Land and Mozambique: insights into the partially delaminated orogenic root of the East African–Antarctic Orogen? In: Satish-Kumar, M., et al. (Ed.), *Geodynamic Evolution of East Antarctica: A Key to the East–West Gondwana Connection*: Geological Society of London, Special Publications 308, 69–90.
- Johnson, M.R., Van Vuuren, C.J., Hegenberger, W.F., Key, R., Shoko, U., 1996. Stratigraphy of the Karoo Supergroup in southern Africa—an overview. *Journal of African Earth Sciences* 23, 3-15.
- Kearey, P.; Klepeis, K.A.; Vine, F.J. 2009. *Global tectonics*. Wiley-Blackwell, John Wiley & Sons 3, 495p
- Key, R.M., Cotterill, F.P.D., Moore, A.E., 2015. The Zambezi River: An Archive of Tectonic Events Linked to the Amalgamation and Disruption of Gondwana and Subsequent Evolution of the African Plate. *South African Journal of Geology* 118(4), 425-438.
- Klausen, M.B., 2009. The Lebombo monocline and associated feeder dyke swarm: diagnostic of a successful and highly volcanic rifted margin? *Tectonophysics* 468, 42-62.
- Lakshminarayana, G., 2015. Geology of Barcode type coking coal seams, Mecondezi sub-basin, Moatize Coalfield, Mozambique. *International Journal of Coal Geology* 146, 1–13.
- Lisker, F., Ventura, B. & Glasmacher, U.A. 2009. Apatite Thermochronology in modern geology. In: Lisker, F., Ventura, B. & Glasmacher, U.A. (Eds.), *Thermochronological Methods: From Paleotemperature Constraints to Landscape Evolution Models*. London, Geological Society, Special Publications, 324: 1-23.
- Macey, P.H., Miller, J.A., Rowe, C.D., Grantham, G.H., Siegfried, P., Armstrong, R.A., Kemp, J., Bacalau, J., 2013. Geology of the Monapo Klippe, NE

- Mozambique and its significance for assembly of central Gondwana. *Precambrian Research* 233, 259– 281.
- Macey, P.H., Thomas, R.J., Grantham, G.H., Ingram, B.A., Jacobs, J., Armstrong, R.A., Roberts, M.P., Hollick, L., Bingen, B., de Kock, G., Bauer, W., Gonzales, E., Bjerkgård, T., Henderson, I.H.C., Cronwright, M., Harley, S., Solli, A., Nordgulen, Ø., Viola, G., Motuza, G., Daudi, E.X.F., Manhica, V., 2010. Mesoproterozoic geology of the Nampula Block, northern Mozambique: tracing fragments of Mesoproterozoic crust in the heart of Gondwana. *Precambrian Research* 182, 124–148.
- Mahanjane, E.S., 2012. A geotectonic history of the northern Mozambique Basin including the Beira High – a contribution for the understanding of its development. *Marine and Petroleum Geology* 36, 1–12. <http://dx.doi.org/10.1016/j.marpetgeo.2012.05.007>.
- Mahanjane, E.S., 2014. The Davie Fracture Zone and adjacent basins in the offshore Mozambique Margin - A new insights for the hydrocarbon potential. *Marine and Petroleum Geology* 57, 561–571. <http://dx.doi.org/10.1016/j.marpetgeo.2014.06.015> 2012.05.007.
- Manjate, V. A., 2011. Geocronologia da região de Gondola-Nhamatanda, centro de 33 Moçambique. Dissertação de Mestrado - São Paulo : IGc/USP. 82 pp. (unpubl.).
- Manjate, V. A., 2015. Caracterização Geocronológica dos granitoides do Complexo de Bárue e da Suíte de Guro, Centro-Oeste de Moçambique, e suas relações com a metalogênese. Thesis (Ph.D) - Institute of Geosciences, University of São Paulo, São Paulo, 149pp. (unpubl.)
- Miall, A.D., 1992. Alluvial deposits. In: Walker. R.G. James, N.P. (eds), *Facies Models: Response to sea-level change*. InGeoL Association, Canada, Saint john's Newfoundland, 119-142 pp.
- Miall, A.D., 1996. *The Geology of Fluvial Deposits. Sedimentary Facies, Basin Analysis, and Petroleum Geology*. Springer, Berlin, 582 pp.

- Milani, E.J., de Wit, M.J., 2008. Correlations between the classic Paraná and Cape-Karoo sequences of South America and southern Africa and their basin infills flanking the Gondwanides: du Toit revisited. Geological Society, London, Special Publications, 294, 319–342.
- Milani, E.J., Ramos, V.A., 1998. Orogenias paleozóicas no domínio sul-occidental do Gondwana e os ciclos de subsidência da Bacia do Paraná. Revista Brasileira de Geociências 28, 473–484.
- Norconsult Consortium, 2007. Mineral resources management capacity building project. Republic of Mozambique, Component 2: Geological Infrastructure Development Project, Geological Mapping Lot 1, Report.
- Reiners, P. W., Brandon, M. T., 2006. Using thermochronology to understand orogenic erosion. Annual Review of Earth and Planetary Sciences, 34:419–466.
- Oliveira, C.H.E.O., Chemale Jr, F., Jelinek, A.R., Bicca, M.M., Philipp, R.P., U–Pb and Lu–Hf isotopes applied to the evolution of the late to post-orogenic transtensional basins of the dom feliciano belt, Brazil. Precambrian Research 246, 240–255.
- Pereira, Z., Fernandes, P., Lopes, G., Marques, J., Vasconcelos, L., 2016. The Permian–Triassic transition in the Moatize–Minjova Basin, Karoo Supergroup, Mozambique: A palynological perspective. Review of Palaeobotany and Palynology 226, 1–19.
- Pereira, Z., Lopes, G., Fernandes, P., Marques, J., 2014. Palinoestratigrafia da Sondagem ETA 72 da Bacia Carbonífera de Moatize-Minjova, Província de Tete, Moçambique. In: Vasconcelos, L. (Ed.), Livro de Resumos, 2 Congresso Nacional de Geologia e 12 Congresso de Geoquímica dos Países de Língua Portuguesa, Maputo, Moçambique, pp. 67-71.
- Pinna, P., Jourde, G., Calvez, J.Y., Mroz, J.P., Marques, J.M., 1993. The Mozambique Belt in northern Mozambique; Neoproterozoic (1100–850 Ma)

- crustal growth and tectogenesis, and superimposed Pan-African (800–550 Ma) tectonism. *Precambrian Research* 62, 1–59.
- Sacchi, R., Cadoppi, P., Costa, M., 2000. Pan-African reactivation of the Lurio segment of the Kibaran Belt system: a reappraisal from recent age determinations in northern Mozambique. *Journal of African Earth Sciences* 30, 629–639.
- Salman, G., Abdula, I., 1995. Development of the Mozambique and Ruvuma sedimentary basins, offshore Mozambique. *Sedimentary Geology* 0738, 7–41.
- Stockli, D. F. 2005. Application of low-temperature thermochronometry to extensional tectonic settings. In: Reiners, P.W.; Ehlers, T.A. (eds.). *Low-Temperature Thermochronology: Techniques, Interpretations and Applications*. Washington, Mineralogical Society of America, Reviews in Mineralogy and Geochemistry, 58:411–448.
- Ueda, K., Jacobs, J., Thomas, R.J., Kosler, J., Jourdan, F., Matola, R., 2012a. Delamination-induced late-tectonic deformation and high-grade metamorphism of the Proterozoic Nampula Complex, northern Mozambique. *Precambrian Research* 196–197, 275–294.
- Ueda, K., Jacobs, J., Thomas, R.J., Kosler, J., Horstwood, M.S.A., Wartho, J.-A., Jourdan, F., Emmel, B., Matola, R., 2012b. Postcollisional high-grade metamorphism, orogenic collapse, and differential cooling of the East African Orogen of northeast Mozambique. *Journal of Geology* 120, 507–530.
- Van der Beek, P., Mbede, E., Andriessen, P., Delvaux, D., 1998. Denudation history of the Malawi and Rukwa Rift flanks (East African Rift System) from apatite fission track thermochronology. *Journal of African Earth Sciences* 26, 363–385.

- Vasconcelos, L., Chafy, A., Xerinda, L., 2014. Determination of the limit of oxidation in zones of sub-outcropping Chipanga Coal Seam, Moatize Coal Basin, Mozambique. *Journal of African Earth Sciences* 99, 554–567.
- Viola, G., Henderson, I.H.C., Bingen, B., Thomas, R.J., Smethurst, M.A., de Azavedo, S., 2008. Growth and collapse of a deeply eroded orogen: insights from structural and geochronological constraints on the Pan-African evolution of NE Mozambique. *Tectonics* 27, TC5009. <http://dx.doi.org/10.1029/2008TC002284>.
- Zerfass, H., Lavina, E.L., Schultz, C.L., Garcia, A.J.V., Faccini, U.F., Chemale Jr., F., 2003. Sequence-stratigraphy of continental strata of Southernmost Brazil: a contribution to Southwestern Gondwana palaeogeography and palaeoclimate. *Sedimentary Geology* 161, 85– 105.
- Zerfass, H., Chemale Jr., F., Schultz, C.L., Lavina, E.L., 2004. Tectonics and sedimentation in Southern South America during Triassic. *Sedimentary Geology* 166, 265–292.
- Zerfass, H., Chemale Jr., F., Lavina, E.L., 2005. Tectonic control of the Triassic Santa Maria units of the Paraná Basin, Southernmost Brazil, and its correlation to the Waterberg Basin, Namibia. *Gondwana Research* 8 (2), 163–176.

## 2. ARTIGO NO PRELO NA REVISTA JOURNAL OF AFRICAN EARTH SCIENCES

### Accepted Manuscript

Permian-Early Triassic tectonics and stratigraphy of the Karoo Supergroup in northwestern Mozambique

Marcos Müller Bicca, Ruy Paulo Philipp, Andrea Ritter Jelinek, João Marcelo Medina Ketzer, Claiton Marlon dos Santos Scherer, Daúd Liace Jamal, Adriano Domingos dos Reis



PII: S1464-343X(17)30107-3

DOI: [10.1016/j.jafrearsci.2017.03.003](https://doi.org/10.1016/j.jafrearsci.2017.03.003)

Reference: AES 2839

To appear in: *Journal of African Earth Sciences*

Received Date: 2 May 2016

Revised Date: 21 February 2017

Accepted Date: 6 March 2017

Please cite this article as: Bicca, M.M., Philipp, R.P., Jelinek, A.R., Ketzer, J.M.M., dos Santos Scherer, C.M., Jamal, D.L., dos Reis, A.D., Permian-Early Triassic tectonics and stratigraphy of the Karoo Supergroup in northwestern Mozambique, *Journal of African Earth Sciences* (2017), doi: 10.1016/j.jafrearsci.2017.03.003.

This is a PDF file of an unedited manuscript that has been accepted for publication. As a service to our customers we are providing this early version of the manuscript. The manuscript will undergo copyediting, typesetting, and review of the resulting proof before it is published in its final form. Please note that during the production process errors may be discovered which could affect the content, and all legal disclaimers that apply to the journal pertain.

1 PERMIAN-EARLY TRIASSIC TECTONICS AND STRATIGRAPHY OF THE  
2 KAROO SUPERGROUP IN NORTHWESTERN MOZAMBIQUE

3

4 Marcos Müller Bicca<sup>a\*</sup>

5 Ruy Paulo Philipp<sup>a</sup>

6 Andrea Ritter Jelinek<sup>a</sup>

7 João Marcelo Medina Ketzer<sup>b</sup>

8 Claiton Marlon dos Santos Scherer<sup>a</sup>

9 Daúd Liace Jamal<sup>c</sup>

10 Adriano Domingos dos Reis<sup>a</sup>

11

12 \* Corresponding author

13 E-mail addresses: [marcos.mb83@gmail.com](mailto:marcos.mb83@gmail.com) (M.M. Bicca); [ruy.philipp@ufrgs.br](mailto:ruy.philipp@ufrgs.br) (R.P.  
14 Philipp); [andrea.jelinek@ufrgs.br](mailto:andrea.jelinek@ufrgs.br) (A.R. Jelinek); [jketzer@pucrs.br](mailto:jketzer@pucrs.br) (J.M.M. Ketzer);  
15 [claiton.scherer@ufrgs.br](mailto:claiton.scherer@ufrgs.br) (C.M.S. Scherer); [daudjamal1@gmail.com](mailto:daudjamal1@gmail.com) (D. Jamal);  
16 [a\\_d\\_reis@hotmail.com](mailto:a_d_reis@hotmail.com) (A.D. Reis).

17

18 <sup>a</sup>Instituto de Geociências – Universidade Federal do Rio Grande do Sul, Campus do Vale.  
19 Av. Bento Gonçalves, 9500, Porto Alegre, Rio Grande do Sul, CEP 91509-900, Brazil.

20

21 <sup>b</sup>Petroleum and Natural Resources Institute, Pontifícia Universidade Católica do Rio  
22 Grande do Sul (PUCRS), Av. Ipiranga 6681, CEP 90619-900, Porto Alegre, Brazil.

23

24   <sup>c</sup>Departamento de Geologia, Universidade Eduardo Mondlane, Av. Moçambique km 1,5,  
25   Caixa Postal 257 Maputo, Mozambique

26

27   **Highlights**

28

- 29   • Permian Gondwanic tectonics led to intra-plate subsidence and sedimentation;
- 30   • Early Permian post-glaciation isostatic rebound led to high subsidence rates;
- 31   • NW-SE faults controlled Moatize-Minjova graben subsidence in Permian times;
- 32   • Fluvial plane environment dominated during Permian in the Moatize-Minjova  
33       graben;
- 34   • Paleozambezi river provided sediment for central and western southern Africa  
35       basins

36

37   **Abstract**

38       The Gondwana continent was the base of great basin inception, sedimentation and  
39       magmatism throughout the Cambrian to Middle Jurassic periods. The Northwestern  
40       Mozambique igneous and metamorphic basement assemblages host the NW-trending  
41       Moatize Minjova Basin, which has great economic potential for coal and gas mining. This  
42       rift basin was activated by an S-SW stress field during the Early Permian period, as  
43       constrained by regional and field scale structural data. Tectonically induced subsidence in  
44       the basin, from the reactivation of NW-SE and NNE-SSW regional structures is well  
45       recorded by faults, folds and synsedimentary fractures within the Early Late Permian  
46       Moatize Formation. NW-SE, N-S and NE-SW field structures consist of post-Karoo

47 reactivation patterns related to a NNE-SSW extension produced by the Pangea breakup and  
48 early inception stages of the Great East African Rift System. The Early Late Permian  
49 sequences of the Moatize-Minjova Basin are composed of fluvial meandering, coal-bearing  
50 beds of the Moatize Formation, which comprises mostly floodplain, crevasse splay and  
51 fluvial channel lithofacies associations, deposited in a cyclic pattern. This sequence was  
52 overlapped by a multiple-story, braided fluvial plain sequence of the Matinde Formation  
53 (Late Permian – Early Triassic). Lithofacies associations in the Matinde Formation and its  
54 internal relationships suggest deposition of poorly channelized braided alluvial plain in  
55 which downstream and probably lateral accretion macroforms alternate with gravity flow  
56 deposits. NW paleoflow measurements suggest that Permian fluvial headwaters were  
57 located somewhere southeast of the study area, possibly between the African and Antarctic  
58 Precambrian highlands.

59

60 **Keywords:** Mozambique, Karoo Supergroup, Moatize-Minjova Basin, Tectonic and  
61 Sedimentation, Early Late Permian

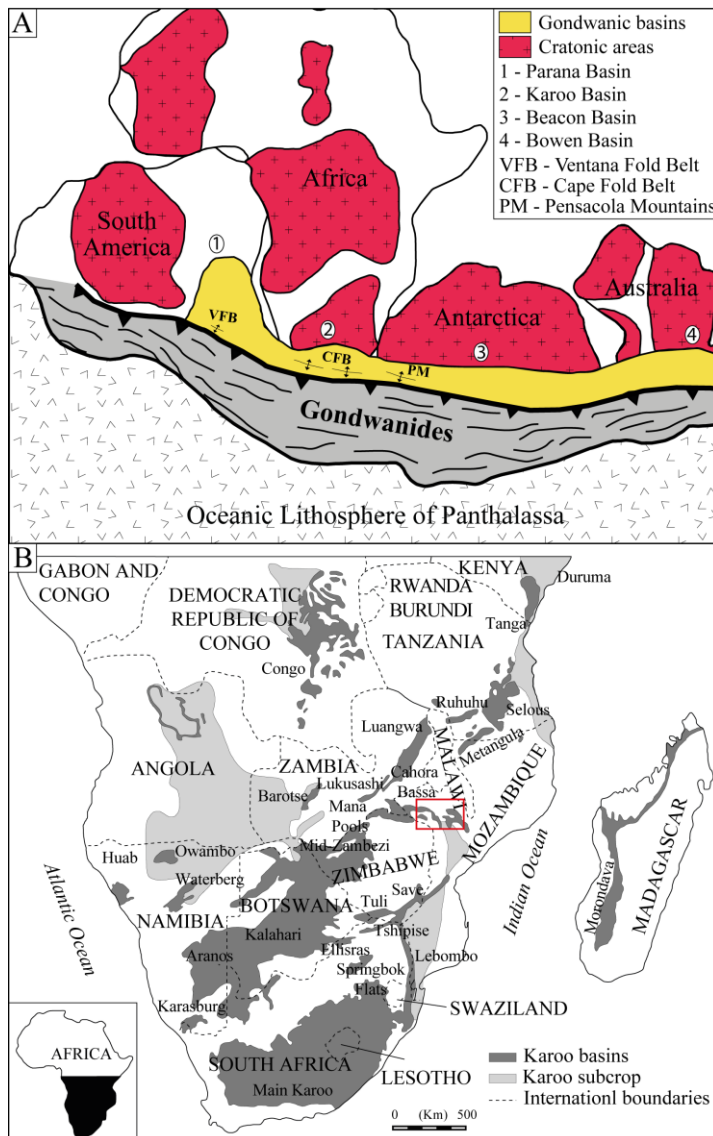
62

### 63 **1. Introduction**

64 The Gondwana volcano-sedimentary successions of the Karoo Supergroup are  
65 widely distributed throughout South and Central Africa, hosted in retroarc-foreland  
66 (continental margin), sag and rift (intracontinental) type basins and its record preserves one  
67 of the largest testimonies of Gondwana evolution (Fig. 1A and Fig. 1B). This Supergroup  
68 was named after the Main Karoo Basin, located in South Africa, which is one of the most  
69 economically important basins, showing the most complete stratigraphic record (Smith et  
70 al., 1993), ranging in age from Late Carboniferous to Middle Jurassic.

71       The Karoo basins' evolution is related to the tectonic events of the southern  
72   Gondwana margin (Gondwanides Orogeny), analogous to the Paraná and other smaller  
73   basins in the South America, Beacon (Antarctica) and Bowen (Australia) basins (Fig. 1A)  
74   (Smith et al., 1993; Trouw & de Wit, 1999; Catuneanu et al., 2005; Holz et al., 2006;  
75   Milani & de Wit, 2008; Alessandretti et al., 2013; Linol et al., 2015; Alessandretti et al.,  
76   2015). The Karoo and Paraná basin studies were the most detailed, showing great economic  
77   potential for natural gas, oil and coal. Coal bearing layers are the most common economic  
78   resource exploited in African and Brazilian basins, all Permian in age. These two basins  
79   share similarities within its stratigraphy framework and hierarchy among depositional  
80   cycles (Smith, 1993; Milani & de Wit, 2008; Linol et al., 2015).

81       The study of the stratigraphic record in these basins is particularly important to  
82   understand the Phanerozoic evolution of Gondwana. In this context, our study brings  
83   previous and new stratigraphic data from the successions of Karoo Supergroup from the  
84   Tete region in northwestern Mozambique, combined with a regional overview with  
85   stratigraphically and chronologically correlated basins in Africa, providing an insight into  
86   the Gondwanic/Pangea tectonics and deposition during Early Permian - Early Triassic  
87   boundaries.



88

89 Figure 1: A) Regional tectonic setting of the southern margin of Gondwana during the  
90 Phanerozoic, illustrating the convergence and collisional tectonics developed  
91 (Gondwanides Orogeny) due to the interaction between the paleocontinent plate and the  
92 oceanic lithosphere of Panthalassa (after Milani & de Wit, 2008; and Holz et al. 2006). B)  
93 Distribution of Karoo basins in south-central Africa (modified from Catuneanu et al.,  
94 2005). The red polygon indicates the study area.

95

96 We aimed to point out the Gondwanides Orogeny influence during the Karoo basin  
97 sedimentary infilling in northwestern Mozambique, despite its great distance from the

98 orogeny center and corroborating with the model of crustal tectonic transference leading to  
99 intraplate subsidence and basin formation (Milani, 1997; Zerfass et al., 2003; Zerfass et al.,  
100 2004; Zerfass et al., 2005; Linol et al., 2015).

101 For this purpose, we provide a structural characterization of the basement and  
102 adjacent Karoo sedimentary rocks, which we have integrated with those previously  
103 described in the literature, to improve the understanding of the graben architectural control  
104 during basin evolution. We also describe the Moatize and Matinde fluvial formations based  
105 on a borelog, and from outcrops identifying distinct lithofacies and lithofacies associations.

106

## 107 **2. Geologic and Tectonic Settings**

108 Northwestern Mozambique comprises a complex assemblage of igneous and  
109 metamorphic rocks, predominantly Mesoproterozoic (north-northeastward) and  
110 Neoproterozoic (southwestward) in age (Fig. 2B and 2C), and partially covered and  
111 intruded by Phanerozoic plutonic-volcanic-sedimentary sequences comprising the Karoo  
112 Supergroup and Post-Karoo units (GTK Consortium, 2006). These Precambrian  
113 assemblages partially preserve the records of two distinct orogenic events: 1) Late  
114 Mesoproterozoic (1.35 – 1.0 Ga); and 2) Neoproterozoic-Early Paleozoic Pan-African  
115 Orogeny (Hanson, 2003). The first one corresponds to the Rodinia Supercontinent  
116 geotectonic heritage, defined by intrusive granitic suites, associated with the Tete Gabro-  
117 Anorthosite stratiform Suite, whose emplacement was controlled by deep NW-SE trending  
118 ductile shear zones. The second one occurred in two stages. The first one comprises the N–  
119 S oriented East Africa Orogeny (EAO; Stern, 1994), referring to events of about 650 – 620  
120 Ma in age (Fritz et al., 2013), and the younger one represents an E–W oriented orogeny that  
121 produces the Damara-Zambezi-Lurio Belts (Kuunga Orogeny; Meert, 2003), comprising

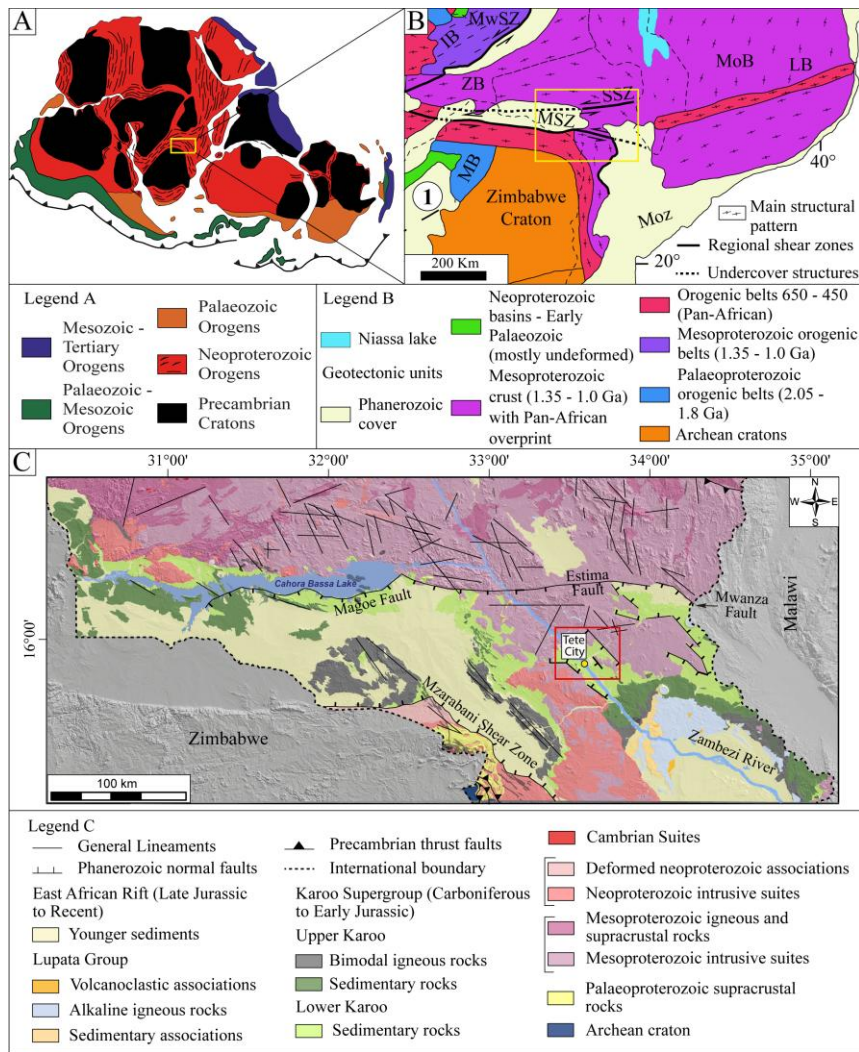
122 600–500 Ma events (Fritz et al., 2013; Fig. 2A and 2B). The Pan-African orogenesis  
123 partially imprints its tectonic patterns on the fabric of the older basement rocks.

124 North-northeast basement rocks comprise a large Mesoproterozoic landmass of  
125 supracrustal and intrusive assemblages, showing inherited magmatic rheology, or partially  
126 deformed by Pan-African Orogeny events. Otherwise, southwest units are grouped, such as  
127 the Zambezi Belt (ZB) which represents the easternmost section of a transcontinental Pan-  
128 African mobile belt system between the Congo and Kalahari cratons in southern Africa  
129 (Shackleton, 1996). This system also comprises the Lufilian Arc and Damara Belt (Fig. 2).  
130 In northeast Zimbabwe the ZB has an E-W trend, converging to a NW-SE trend in  
131 northwest Mozambique. These assemblages were deformed by Pan-African south-vergent  
132 thrusting, associated in places with transcurrent or transpressional shearing, followed by  
133 north-vergent back-thrusting (e.g. Barton et al., 1991 and 1993; Hanson et al. 1994;  
134 Hargrove et al., 2003; Hanson, 2003).

135 The Pan-African Orogeny left important structural zones (NW-SE and E-W  
136 trending) in northwest Mozambique, which were fundamental for Phanerozoic sedimentary  
137 basins development. One of the greatest structures is the Sanangoe Shear Zone (SSZ),  
138 which is an E-W trending transpressional ductile structure, crossing the central part of study  
139 area, over a distance of about 350 km in Mozambique (Fig. 2B). Westwards, this shear  
140 zone is largely concealed below Karoo and the younger rocks of the mid-Zambezi rift.

141 According to GTK Consortium (2006), the SSZ represents a Pan-African  
142 connection between the West and South Gondwana (Macey et al., 2013), generally similar  
143 in structural aspects and timing to the Mwembeshi Shear Zone (MSZ) (GTK Consortium,  
144 2006; Fig. 2B). Deformed granitoids surrounding this large structure confirm its ductile  
145 behavior during the Pan-African tectonics. Its likely relationship with the Cahora Bassa

146 Basin (E-W graben in the Cahora Bassa Lake area; Fig. 2) depocenter also highlights its  
 147 importance during Phanerozoic tectonic evolution.



148

149 Figure 2: A) Reconstruction map of Gondwana during Phanerozoic times (after Gray et al.,  
 150 2007; Cordani et al., 2013; and Rapela et al., 2015). B) Simplified Precambrian tectonic  
 151 framework of the study area (after Hanson, 2003). 1 - Archean western limit (Zimbabwe);  
 152 IB - Irumide Belt; LB - Lurio Belt; MB - Magondi Belt; MoB - Mozambique Belt; Moz -  
 153 Mozambique Country; MSZ - Mzarabani Shear Zone; MwSZ - Mwembeshi Shear Zone;  
 154 SSZ - Sanangoe Shear Zone; ZB - Zambezi Belt. C) Simplified geological map of  
 155 northwestern Mozambique (after GTK Consortium map sheets: Songo (1532),  
 156 Cazula/Zóbuè (1533-1534), Mecumbura/Chioco (1631-1632), Tete (1633) and Tambara  
 157 (1634)).

158     **2.1. Basin settings and stratigraphy**

159         As a general approach, the Karoo Supergroup (KS) comprises all contemporaneous  
160         Late Carboniferous to Middle Jurassic volcano-sedimentary deposits in Central-Southern  
161         Africa (Fig. 1B). Two main tectonic fronts may have influenced subsidence processes of  
162         the Karoo basins: the southern convergent orogenic margin of Gondwana and the northern  
163         Tethyan divergent margin. In the former, extensional/transtensional tectonic movements  
164         predominated and propagated southwards into the Gondwana continent (Bumby &  
165         Guiraud, 2005). In the southern margin of Gondwana, subduction, accretion and mountain  
166         building, regionally called Gondwanides Orogeny (Du Toit, 1927), or locally the Cape  
167         Orogeny (margin of Southern Africa plate), also produced important structural  
168         rearrangements across Precambrian African and South American plates (Milani & Ramos,  
169         1998; Zerfass et al., 2003; Zerfass et al., 2004; Zerfass et al., 2005; Linol et al., 2015).

170         In this study, we focused on the KS sequences from the northwestern Mozambique  
171         area, which were preferentially deposited in intracratonic half grabens, grouped as the  
172         Zambezi Valley basins. The Zambezi River is one of the great modern African rivers with  
173         an ancient history, and may have contributed for Early Permian-Early Triassic Karoo basin  
174         sedimentation, with a northwestern to western paleoflow (Key et al., 2015). The Zambezi  
175         Valley is an E-W trending graben (Cahora Bassa Basin, Fig. 1B and 2C), which inflects SE,  
176         following the Zimbabwe Cratonic northeastern margin, assuming a NW-SE trend (Moatize-  
177         Minjova Basin) in the Tete city region (Fig. 2B and 2C). The valley is bounded by  
178         Precambrian structures and the basin evolution follows distinct reactivation periods that  
179         occurred in Phanerozoic times (Castaing, 1991; GTK Consortium, 2006; Fernandes et al.,  
180         2015), under a transtensional stress regime associated with the NW-SE sinistral Zambezi  
181         pre-transform fault system (Castaing, 1991). In northwestern Mozambique, the Magoe-

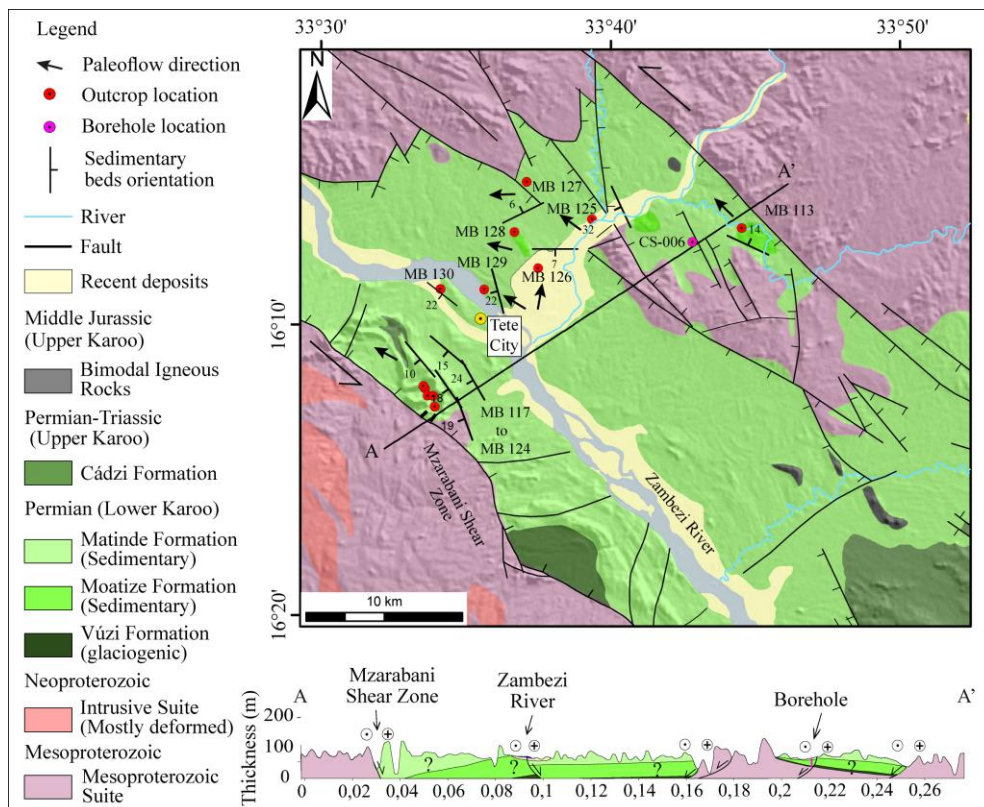
182 Estima–Mwanza fault zone (Fig. 2C) defines a major Pre-Karoo crustal weakness zone that  
183 controlled basin inception since the Permian (Lakshminarayana, 2015). This large scale  
184 crustal discontinuity resembles the Sanangoe ductile shear zone trend.

185 Our study was conducted in the Moatize-Minjova Basin, which is a NW-oriented  
186 graben (Fig. 3). Northeastern and southwestern basin boundaries are against deformed  
187 Mesoproterozoic and Neoproterozoic crystalline basement rocks. The former shows  
188 marginal high strain shear zones, NW-oriented, while the latter consists of highly folded  
189 metamorphic rocks, were the axial plane trends range between NW to N-S and E-W  
190 (Hargrove et al., 2003).

191 In general, the Karoo Supergroup sedimentation comprises a progressive shift from  
192 glacial to cool, moist conditions to warm, semi-arid and finally hot and arid conditions  
193 (Johnson et al., 1996). Classically, the KS is divided into five major groups, according to  
194 the stratigraphic record registered in the Main Karoo Basin of South Africa, from the base  
195 to the top as: Dwyka, Ecca, Beaufort, Stormberg (sedimentary and magmatic), and  
196 Drakensberg (magmatic). Correlatable sequences of these groups, which more or less can  
197 be observed in all Karoo Basins in Africa, follow a sequence of glacial, deltaic, fluvial,  
198 lacustrine and aeolian environments, mostly due to climatic changes (aridification) during  
199 the Gondwana northward drift (Catuneanu et al., 2005).

200 The base of KS sequence in the Moatize-Minjova Basin is attributed to the Vúzi  
201 Formation glaciogenic deposits (GTK Consortium, 2006; Fernandes et al., 2015), which  
202 classically correlate with the Dwyka Group, which has accumulated through Late  
203 Carboniferous–Early Permian (Wopfner, 2002; Catuneanu, 2004; Catuneanu et al., 2005).  
204 These correspond mostly to interbedded tillites, diamictites, rhythmites and sandstones,  
205 resting unconformably over the Precambrian crystalline basement (GTK Consortium, 2006;

206 Vasconcelos et al., 2014; Fernandes et al., 2015; Lakshminarayana, 2015). Vúzi deposits  
 207 show an important palynological assemblage, indicating early to middle Sakmarian age  
 208 (Wopfner & Kreuser, 1986; Weiss & Wopfner, 1997). Notwithstanding, recent  
 209 palynological studies developed by Pereira et al. (2014) and Lopes et al. (2014) dating  
 210 diamictite beds from the top of the Vúzi Formation, assigned it a Kungurian-Roadian age  
 211 (Lower-Middle Permian), younger than the previous regional proposed age. A few  
 212 available U-Pb radiometric ages published for the Dwyka Group of Namibia and South  
 213 Africa, obtained from tuff beds, indicate ages of  $302 \pm 3.0$  Ma and  $299 \pm 3.2$  Ma for the  
 214 Namibian rocks, and  $288 \pm 3.0$  Ma and  $289 \pm 3.8$  Ma for the latter (Bangert et al., 1999).



215  
 216 Figure 3: Detailed geological and structural map of the Moatize-Minjova Basin (compiled  
 217 and modified from GTK Consortium, 2006), showing the location of the borehole and all  
 218 the outcrops described in this work.  
 219

220        The top sequence of the Vúzi Formation comprises interbedded diamictites and thin  
221    coal beds, marking a gradational transition to the conformably overlain Moatize Formation.  
222    The latter is made of interbedded carbonaceous mudstones, rhythmites, sandstones and  
223    cyclic coal deposits (Cairncross, 2001; Lakshminarayana, 2015). The Moatize Formation in  
224    the Moatize-Minjova Basin has six main coal seams, known locally from bottom to top as  
225    Sousa Pinto, Chipanga, Bananeiras, Intermédia, Grande Falésia and André (Vasconcelos et  
226    al., 2014). Lithofacies assemblages of the Moatize Formation were interpreted by  
227    Lakshminarayana (2015) as a delta plain-mire depositional environment, representing a  
228    periglacial condition. The absolute age of these coal-bearing formations is not well  
229    constrained and most are derived from palynological records, which allow to place the  
230    Moatize Formation between the end of Early to Middle Ecca Group (Early-Late Permian;  
231    Catuneanu et al., 2005). Plant macrofossils and palynomorphs suggest a Lower to Middle  
232    Permian age for the top part of the Moatize Formation (Daber, 1984), which may be  
233    correlated with the Middle-Upper Ecca Group. However, Pereira et al. (2014) found a  
234    Kungurian/Roadian age (Lower – Middle Permian) for the basal sequences of the Moatize  
235    Formation, positioning its depositional cycle throughout the Early-Late Permian.

236        Overlaying the Moatize Formation there are mostly cross-bedded coarse grained  
237    alluvial deposits from the Matinde and Cádzi Formations (GTK Consortium, 2006). The  
238    Matinde Formation was assumed to be of an Early to Middle Permian age, comparable to  
239    the Middle/Upper Ecca Group (GTK Consortium, 2006). However, a recent palynological  
240    revision of the Matinde Formation has indicated that was deposited in the latest Permian,  
241    close to the Permian-Triassic boundary (Pereira et al., 2016). The latter, on the other hand,  
242    is classically correlated to the Beaufort Group, positioned between the Late Permian to  
243    Early Triassic age. Bimodal magmatism erupted between 195-180 Ma ended the basinal

244 cycle and is attributed to an early aborted stage of the Gondwana breakup (GTK  
245 Consortium, 2006), and correlated to the Stormberg Group from the Main Karoo Basin.

246

### 247 **3. Structural and stratigraphic analysis methods**

248 In this study, we adopt a methodology in which we integrate stratigraphic and  
249 tectonic data acquired in the field and from remote sensing images, with those available in  
250 the literature. During fieldwork we obtained stratigraphic and structural data from outcrops  
251 and one coal exploration borehole (CS\_006A), in which we gathered the main sedimentary  
252 attributes (e.g., texture, lithology), and structures related to basin inception and infilling  
253 control. The sedimentary facies framework and facies architecture of the studied interval  
254 are based on this data.

255 The regional distributions of the sedimentary lithofacies and architecture of the  
256 Moatize and Matinde Formations were examined in one deep borehole of about 500 m in  
257 depth and in natural exposures and road cuts (only Matinde and the top of Moatize  
258 Formations) throughout the area of Moatize-Minjova Basin (Fig. 3).

259 The facies analysis was based in the scheme of Miall (1992), to interpret facies  
260 associations and deduct its depositional systems. The lithofacies definition and  
261 classification used is based in Miall's (1978; 1996) facies code, in which the first letter  
262 represents the grain size and the second letter represents the sedimentary structure (Tab. 1).  
263 In order to clarify the three-dimensional relationships of the sedimentary units, these  
264 elements were mapped and logged, and documented as field sketches, photos and maps.  
265 Paleocurrent measurements were collected from stratified beds (planar and through cross-  
266 beds), and also from imbricated clasts, observed in conglomeratic facies in order to  
267 determine sediment dispersal patterns within the Moatize and Matinde formations.

268 Structural and tectonic data were acquired from a compilation of geological maps of  
 269 the Mozambican Geological Survey (1:250,000 scale). We also used a SRTM (Shuttle  
 270 Radar Topography Mission) image to generated a shaded relief model for tracing regional  
 271 lineaments ( $N = 1,568$ ; Fig. 4), from which we generated rose diagrams that allow us to  
 272 identify major structural lineament patterns within the basin and in the Precambrian  
 273 basement in the study area. We use length and frequency rose diagrams to identify major  
 274 lineaments populations. Our aim was to discriminate evidences of a possible chronology of  
 275 structural reactivations within the complex geological framework in the area, using  
 276 evidence of episodes of deformation, sedimentation and related magmatic activity.  
 277 Subsequently, we undertook geological mapping in selected areas throughout the basin area  
 278 and overlaying basement rocks, in order to complete our tectonic data acquisition by  
 279 measuring fault plans orientation and kinematic indicators, which we integrated to produce  
 280 a preliminary strain model for the study area. Fractures, in this work, are those structures  
 281 without any evidence of movement (slickenlines, fault mirror, etc.), and for fault  
 282 classification, we took into account the relationships between fault plane dipping and  
 283 slickenlines dipping within this plane (Angelier, 1994).

284

285 Table 1: Lithofacies description for Moatize and Matinde Formations (based on Miall, 1992  
 286 and 1996).

| Facies Code              | Facies Description and Structures                                                                                                                                 | Depositional process            |
|--------------------------|-------------------------------------------------------------------------------------------------------------------------------------------------------------------|---------------------------------|
| <b>Moatize Formation</b> |                                                                                                                                                                   |                                 |
| Gm                       | Conglomerate and conglomeratic coarse-sandstone, matrix (silt and mud) supported. Presents muddy intraclasts and extrabacinal clasts 0.3 a 4 cm (0.5 cm average). | Cohesive (plastic) debris flow. |

|           |                                                                                                                                                                                                                                                    |                                                                                                                 |
|-----------|----------------------------------------------------------------------------------------------------------------------------------------------------------------------------------------------------------------------------------------------------|-----------------------------------------------------------------------------------------------------------------|
| <b>St</b> | Micaceous (muscovite) medium to coarse-sandstone, sometimes conglomeratic, poorly to moderately selected, with sets of 5 to 50 cm thick of trough cross-stratification. Foresets are commonly marked by intraclasts.                               | Migration of 3D dunes, under lower flow regime.                                                                 |
| <b>Sl</b> | Micaceous (muscovite) medium to coarse-sandstone, sometimes conglomeratic, poorly to moderately selected, with low angle cross-stratification.                                                                                                     | Bedforms migration under transitional conditions between lower and upper regime.                                |
| <b>Sr</b> | Micaceous (muscovite) very fine to fine-sandstone, moderately to well selected, with critical to subcritical ripple cross-lamination of 0.5 to 2 cm thick.                                                                                         | Migration of ripple cross-lamination under lower regime conditions, with variation on traction/suspension rate. |
| <b>Sm</b> | Sand, medium grained. Homogeneous. Mostly massive. Sometimes shows a very tenuous horizontal lamination. Lenticular (sigmoid) shape and irregular contact with adjacent facies are common (convex up and concave up).                              | Sediment-gravity flow deposits                                                                                  |
| <b>Sh</b> | Sand, very fine to fine. Commonly interbedded with Sr. Horizontal lamination and parting lineation.                                                                                                                                                | Planar bed flow (upper flow regime).                                                                            |
| <b>Fl</b> | Pelite with very fine to fine-sandstone wavy/linsen bedding of 0.3 to 5 cm thick, with ripple cross-lamination. Sometimes foresets are marked by mud layers. At the top of the sequence it presents 1 to 2 m thick and fine horizontal lamination. | Interchange of ripple cross-lamination and mud decantation. Represent overbank or abandoned channels deposits.  |
| <b>Fm</b> | Massive carbonaceous pelite, with <0.5 cm thick of very fine to fine-sandstone linsen bedding and ripple cross-lamination.                                                                                                                         | Decantation of suspended mud sediments.                                                                         |
| <b>C</b>  | Coal                                                                                                                                                                                                                                               | Aggradational accumulation of organic matter on peat.                                                           |

#### Matinde Formation

|           |                                                                                                                                                                                                                                                                              |                                                                                                              |
|-----------|------------------------------------------------------------------------------------------------------------------------------------------------------------------------------------------------------------------------------------------------------------------------------|--------------------------------------------------------------------------------------------------------------|
| <b>Gm</b> | Massive or crudely bedded gravel. The matrix is composed by fine to coarse sand. Clasts are irregular and angular of most red colored granitic composition with casts of probably intrabasinal pelitic clasts. Transition to St/Sp is probably gradual. Weak or non-grading. | Plastic debris flow (highstrength, viscous).                                                                 |
| <b>St</b> | Arcosic sand, medium to very coarse and sometimes pebbly. Trough cross-beds are found interbedded with Sp. Its overlap on Fl show load casts marks.                                                                                                                          | Sinuous-crested and linguoid dunes. Migration of subaqueous ripples and dunes under low to high flow energy. |
| <b>Sp</b> | Arcosic sand, medium to coarse and sometimes pebble. Planar cross-beds of mostly 10 cm to <1 m.                                                                                                                                                                              | Linguoid and transverse bars, sand waves (lower flow regime).                                                |
| <b>Sl</b> | Arcosic sand, fine to medium grained with low angle planar cross-stratification.                                                                                                                                                                                             | Humpback or washed-out dunes.                                                                                |

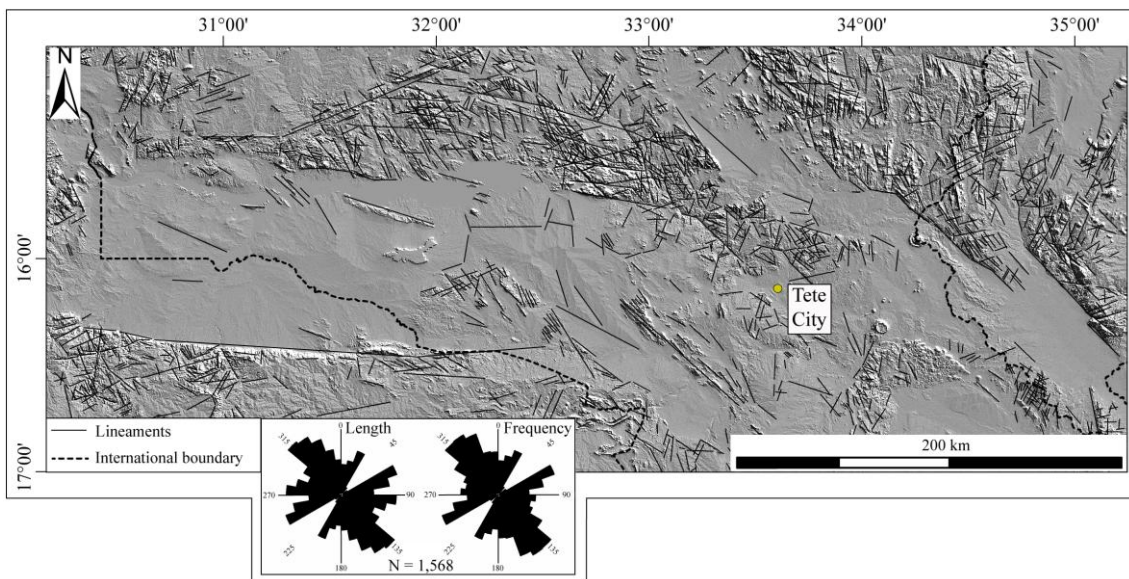
287

## 288 4. Results

### 289 4.1. Regional tectonic and structural analysis (Lineaments)

290 Structural analysis created from the 1,568 lineaments identified in the shaded relief  
 291 map (Fig. 4) allow visualizing a complex web of cross-cutting structures, mostly attributed  
 292 to Precambrian basement rocks, with some extending to Karoo rocks and a few to Post-  
 293 Karoo volcano-sedimentary rocks. Dissected valleys, crests and fluvial incision patterns are  
 294 the major relief features observed.

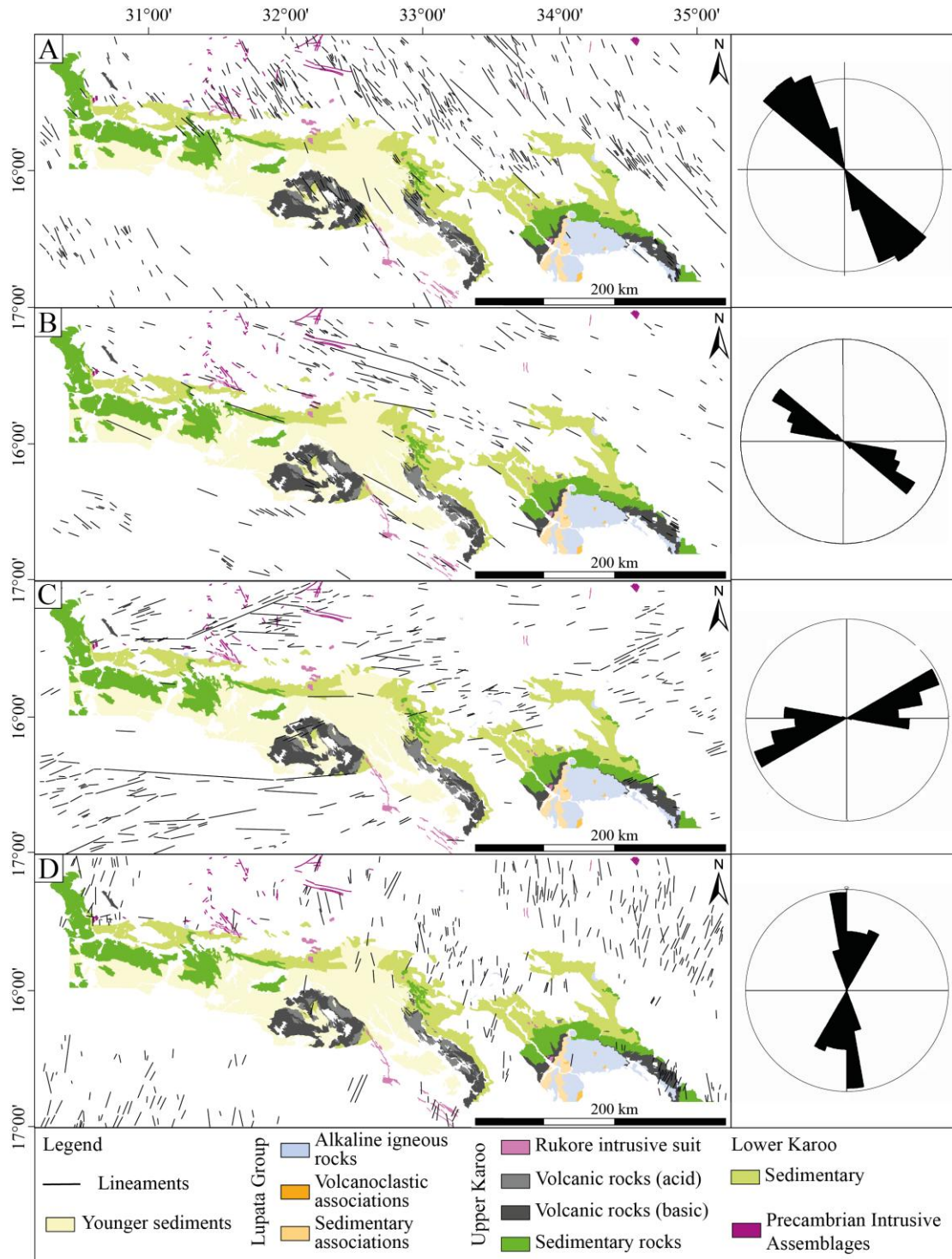
295 The structural rose diagrams produced from the traced lineaments allowed the  
 296 definition of six structural populations that may have a close relation with pre-, syn- and  
 297 post-depositional basinal cycles, which are: a) NW-SE subgroup ( $N = 499$ ; Fig. 5A); b)  
 298 WNW-ESE subgroup ( $N = 272$ ; Fig. 5B); c) NNE-SSW subgroup ( $N = 269$ ; Fig. 5D); d)  
 299 ENE-WSW subgroup ( $N = 233$ ; Fig. 5C); e) E-W subgroup ( $N = 157$ ; Fig. 5C); and f) N-S  
 300 subgroup ( $N = 147$ ; Fig. 5D).



301  
 302 Figure 4: Terrane digital shaded relief model image and regional lineaments traced in  
 303 northwestern Mozambique, with its respective length and frequency rose diagram.  
 304

305 The NW-SE (Fig. 5A) and WNW-ESE (Fig. 5B) subgroups are widely distributed  
 306 in the North, represented by deeply dissected valleys and concordant with several fluvial

307 courses, including the SE portion of the Zambezi River (Fig. 2C). They are also parallel to  
308 sub-parallel to Precambrian igneous intrusions in the northwestern sector of the area and to  
309 Middle Jurassic Karoo magmatic associations in the South. On the other hand, the E-W  
310 system (Fig. 5C) has the longest continuous lineament observed in the area and is  
311 pronounced in the southern and northern limits of the Cahora Bassa Basin (E-W segment of  
312 the Zambezi Valley, Fig. 1B and 2C), along with the ENE-WSW subgroup (Fig. 5C). Both  
313 patterns show greater distribution in Precambrian basement rocks in the eastern section of  
314 the area. The NNE-SSW and N-S subgroups (Fig. 5D) show great distribution throughout  
315 the area seem to be restricted to Precambrian rocks and are homogeneously shorter than the  
316 other patterns. They are lesser and more distinctive NE of the area, close to the N-S  
317 oriented Niassa Lake in Malawi. However, these structures cross the Karoo younger  
318 magmatic intrusions (Middle Jurassic) and probably comprise post-Karoo tectonic  
319 reactivations.



320

321 Figure 5: Structural maps of the study area with respective frequency lineaments rose  
 322 diagram. Karoo Supergroup and younger lithologies occurrences were compiled from GTK  
 323 Consortium (2006). A) 130-165° (NW-SE) subgroup; B) 100-130° (WNW-ESE) subgroup;  
 324 C) 60-100° (E-W and ENE-WSW) subgroup; D) 165-210° (N-S and NNE-SSW) subgroup.

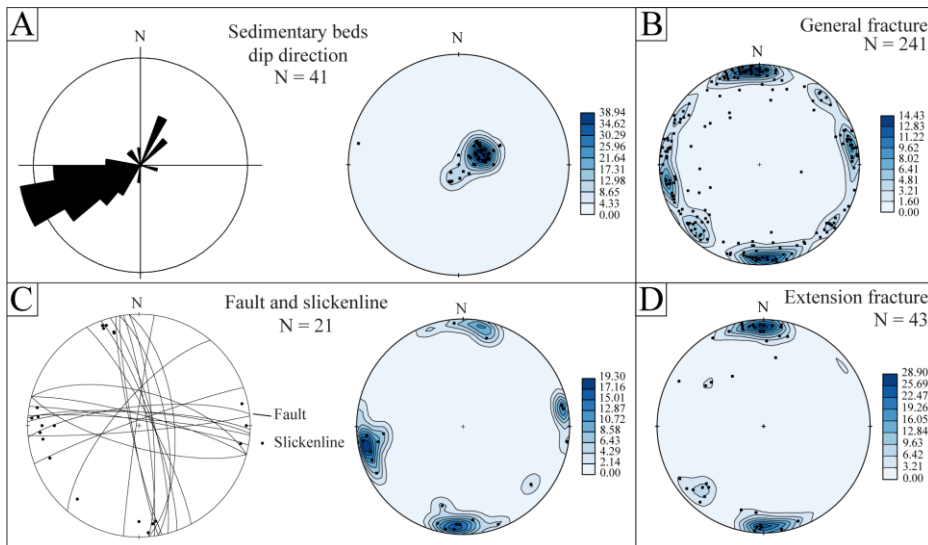
325     **4.2. Field scale structural analysis**

326         Field data provide valuable information about the structural behavior of  
327         northwestern Mozambique (see Fig. 3 for outcrop locations). Structural data were  
328         statistically analyzed from 64 measured structures with kinematic indicators and 198  
329         fractures from the Moatize-Minjova Basin covering both, the Moatize and Matinde  
330         formations. The structural behavior of the beds was analyzed from 41 measurements. The  
331         structures were collected from sedimentary assemblages of the Moatize and Matinde  
332         formations and the Karoo volcanic rocks of the latter (Middle Jurassic). These analyses  
333         provide important and relevant structural information for post-depositional basin tectonic  
334         approaches. Stereographic projections also show different layering dip patterns in the  
335         northeastern and southwestern sections of the area (Fig. 3 and Fig. 6). Layers from the  
336         Moatize and Matinde formations mostly have a gentle dip of 14° degrees, N25°W, close to  
337         the northeastern fault edge of the basin (Fig. 3 and Fig. 6A). On the other hand,  
338         southwestern beds indicate an opposite behavior dipping preferably to SW and W, oriented  
339         southwest to the fault edge of the basin (southeastern section of the Mzarabani Shear Zone).  
340         Dips are not so gentle as the former, between 6° and 22° in central section of the graben  
341         and from 15° to 24° degrees SW of the area (Fig. 3). These patterns seem to be compatible  
342         with a fault-controlled basin, limited by listric faults (NW-SE oriented) and beds dip follow  
343         post-depositional reactivations, leading to vertical block rotation.

344         The analysis of fractures and faults led to definition of two important structural  
345         patterns: a) E-W and b) NNW-SSE to N-S (Figs. 6B and 6C). Those were identified as  
346         fractures and faults. Both groups are compatible with NNE-SSW, N-S (Fig. 5D) and E-W  
347         (Fig. 5C) lineament subgroups from the regional analysis. This is an interesting aspect,  
348         since these subgroups are not the most representative patterns, although the E-W subgroup

349 has great influence over the Cahora Bassa Basin development and infilling. The kinematic  
 350 indicators (silicate-filled faults and fractures) observed in the Moatize and Matinde  
 351 formations rocks mainly characterize these faults as transcurrent, dextral and normal.

352 In general, the field structures are shallow and constantly filled by late silicate  
 353 solutions. The lack of growing faults and sedimentary disturbance associated with this  
 354 pattern indicates its post-depositional age. Slickenlines are present in transcurrent faults, as  
 355 well as polished planes. However, steps or other kinematic indicators were absent in most  
 356 cases, making it difficult to determine the sense of fault slip in several occasions. Most  
 357 faults and fractures are vertical to subvertical (dipping mostly greater than 80°) indicating  
 358 that kinematics must be preferably extensional or directional. Right-handed faults  
 359 predominate, along with filled fractures with the same orientation, postulating a  
 360 transtensional stress regime (Fig 6).



361  
 362 Figure 6: Structural diagrams from field work data. A) Observed sedimentary beds dip  
 363 directions, showed in rose diagram and stereographic projection; B) All fractures measured  
 364 in field (with tension fractures); C) Faults and slickenlines; D) Extension fracture.  
 365

366 Extensional fractures (2-20 mm wide) are filled by silicate solutions and show a  
367 preferable E-W and NNW-SSE trend (Fig. 6D). Both patterns are accompanied by  
368 transcurrent shear faults (principal structures), commonly showing anastomosing shape.  
369 The relative timing of these structural patterns could not be clearly deduced from our data  
370 set since very few cross-cutting relationships were found. We identify three transcurrent  
371 dextral faults, following N20°-28°W and N80W directions with high angles, whereas other  
372 transcurrent faults (N=12) present E-W, N80°-75°W and N10°-5°W major directions.  
373 Slickenlines from these faults indicate N18°-20°W directions with dips of 5° to 10° and E-  
374 W oriented with dip of 25°. Only one structure shows a NNW-SSE direction and dip of 84°  
375 with slickenlines oriented N15°W and dip of 14°. Slickenlines from transcurrent faults  
376 show dip angles between 4° e 16° degrees and directions parallel and sub parallel to the  
377 fault plane.

378

### 379 **4.3 Facies and Facies associations**

380 The Permian deposits of KS in northwestern Mozambique are composed of mostly  
381 interbedded coal and coarse- to fine-grained clastic deposits (Tab. 1). In this study, we have  
382 distinguished facies that comprises the Moatize and Matinde formations, composed of  
383 alluvial sequences deposited in relatively cool and humid climate (Smith et al., 1993), after  
384 Late Carboniferous glaciations, but close to transition to hotter climatic conditions  
385 (Matinde Formation), as indicated by the lack of coal and presence of commonly coarser  
386 red sequences topwards.

387 The Moatize and Matinde contact is very limited in outcrop in the Moatize-Minjova  
388 Basin, mostly because of the gentle dip of the beds (5° to 25°, Fig. 6D). This local  
389 structural characteristic does not allow great natural exposures, as they are commonly

390 associated with faulting and folding areas or in road cuts, making it difficult to obtain a  
391 proper lateral correlation for this stratigraphic contact.

392

### 393 **4.3.2 Moatize Formation**

#### 394 *Flood plain deposits with peat*

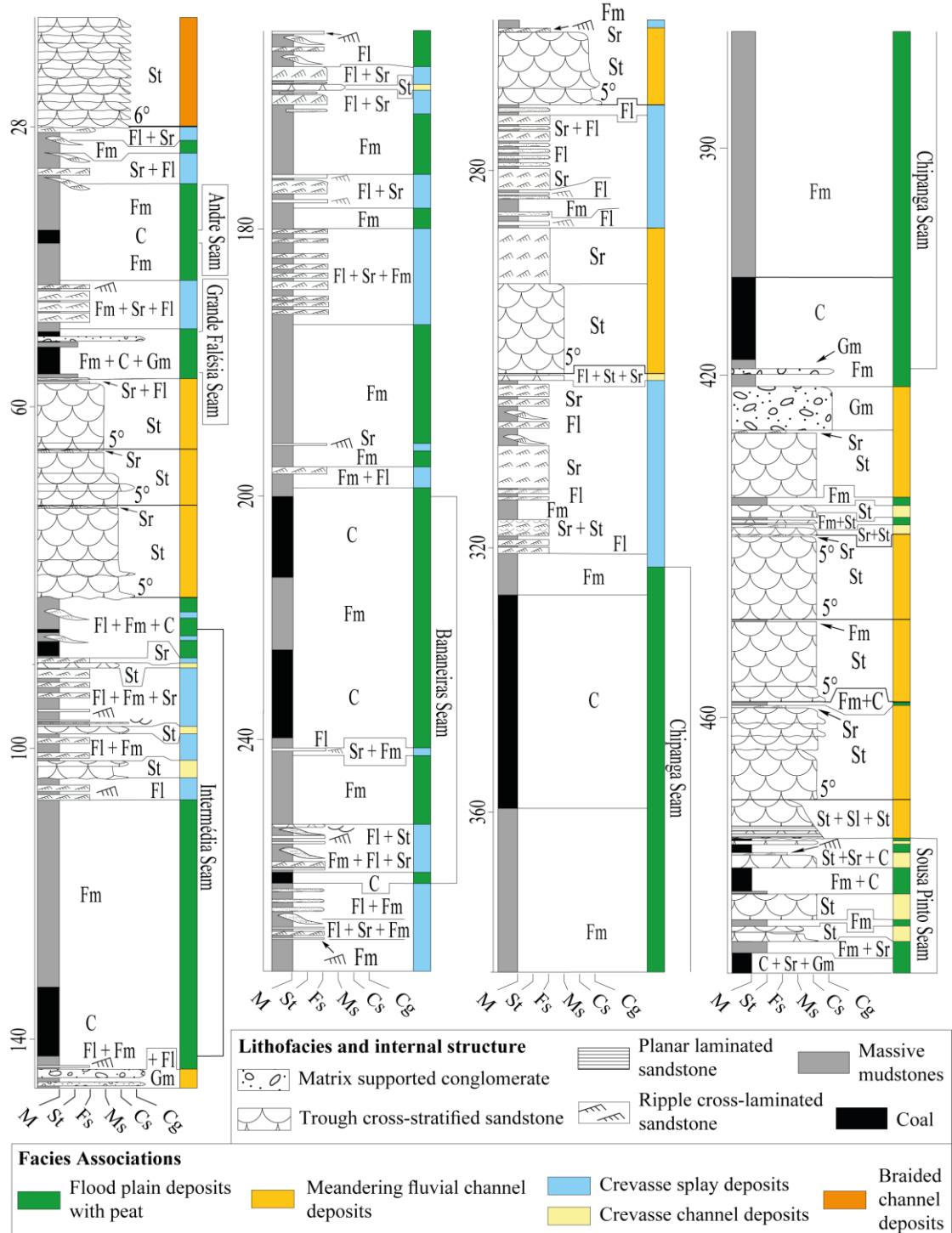
395 This association is composed of massive carbonaceous mudstones, <0.5 cm thick,  
396 interbedded with very fine to fine sandstones with ripple cross-lamination (Fm), defining  
397 linsen and wavy bedding. The heterolithic bedding is interbedded with coal (C) (Fig. 7 and  
398 Fig. 8). Sometimes, the black horizontal laminated coal beds (C) are interbedded with gray  
399 laminated (bituminous) siltstones/mudstones sequences (Fl) (Fig. 9A, 9B and 9C).  
400 Cairncross (2001) and Lakshminarayana (2015) indicate that the Moatize Formation  
401 consists of a coarsening upward sequence, mostly composed by interbedded coal,  
402 carbonaceous mudstones, mudstones, siltstones and feldspathic sandstones (Fig. 3 and Fig.  
403 9D, 9E and 9F; MB-130 outcrop). These are interbedded with crevasse splay deposits.

404

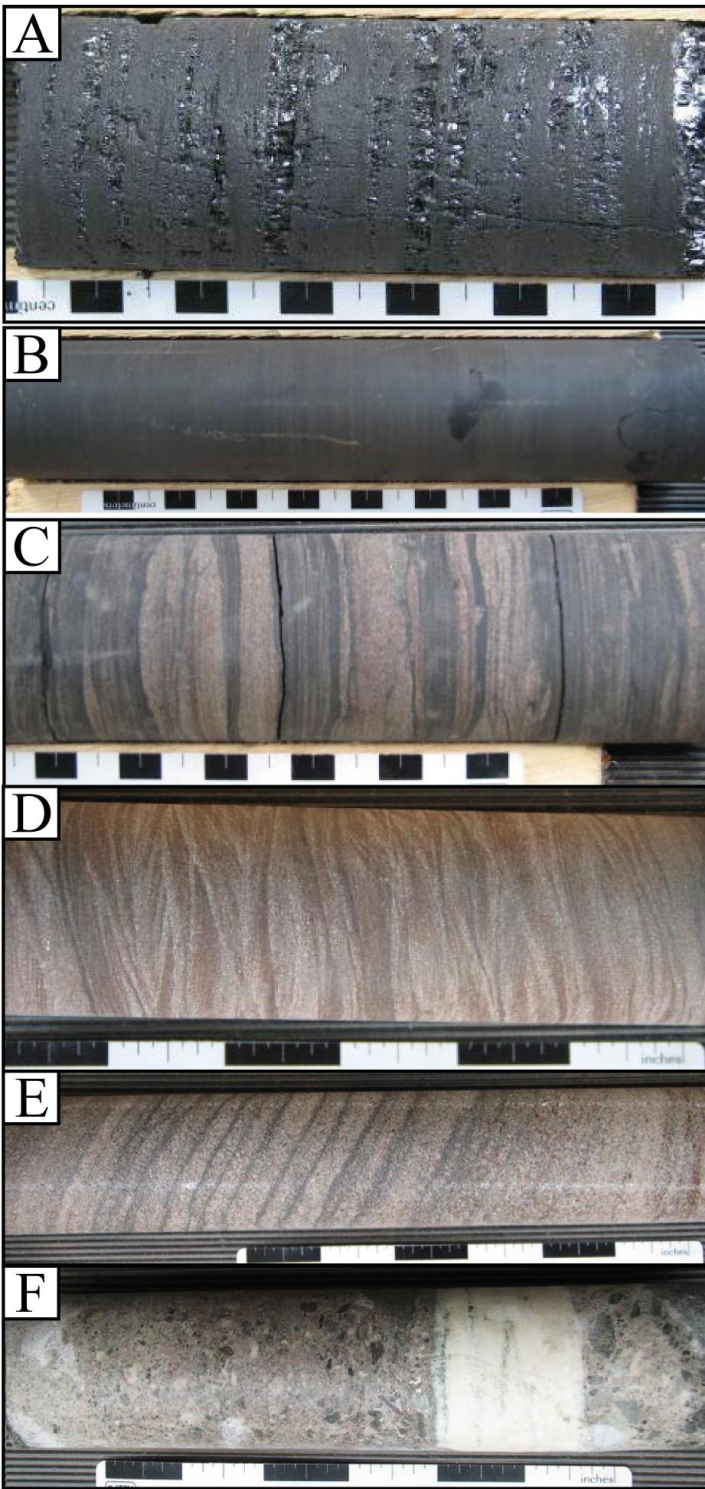
#### 405 *Fluvial channel deposits*

406 This association comprises lithofacies with fining upwards cycles (between 2 to 15  
407 m thick). From bottom to top, the cycles comprise coarse to very coarse-sandstones with  
408 tangential cross-stratification (St) and rarely low angle cross-stratification in micaceous  
409 (muscovite) medium to coarse-sandstone, sometimes conglomeratic, poorly to moderately  
410 sorted (Sl). Sometimes they occur interbedded with massive matrix supported  
411 conglomerates (Gm). They are superimposed by fine sandstones, 0.2 to 4 m thick,  
412 composed of sets of ripple cross-lamination (Sr). The latter consist of micaceous

413 (muscovite) very fine to fine-sandstone, moderately to well sorted, with critical to  
 414 subcritical ripple cross-lamination, 0.5 to 2 cm thick (Tab. 1; Fig. 7 and Fig. 8).

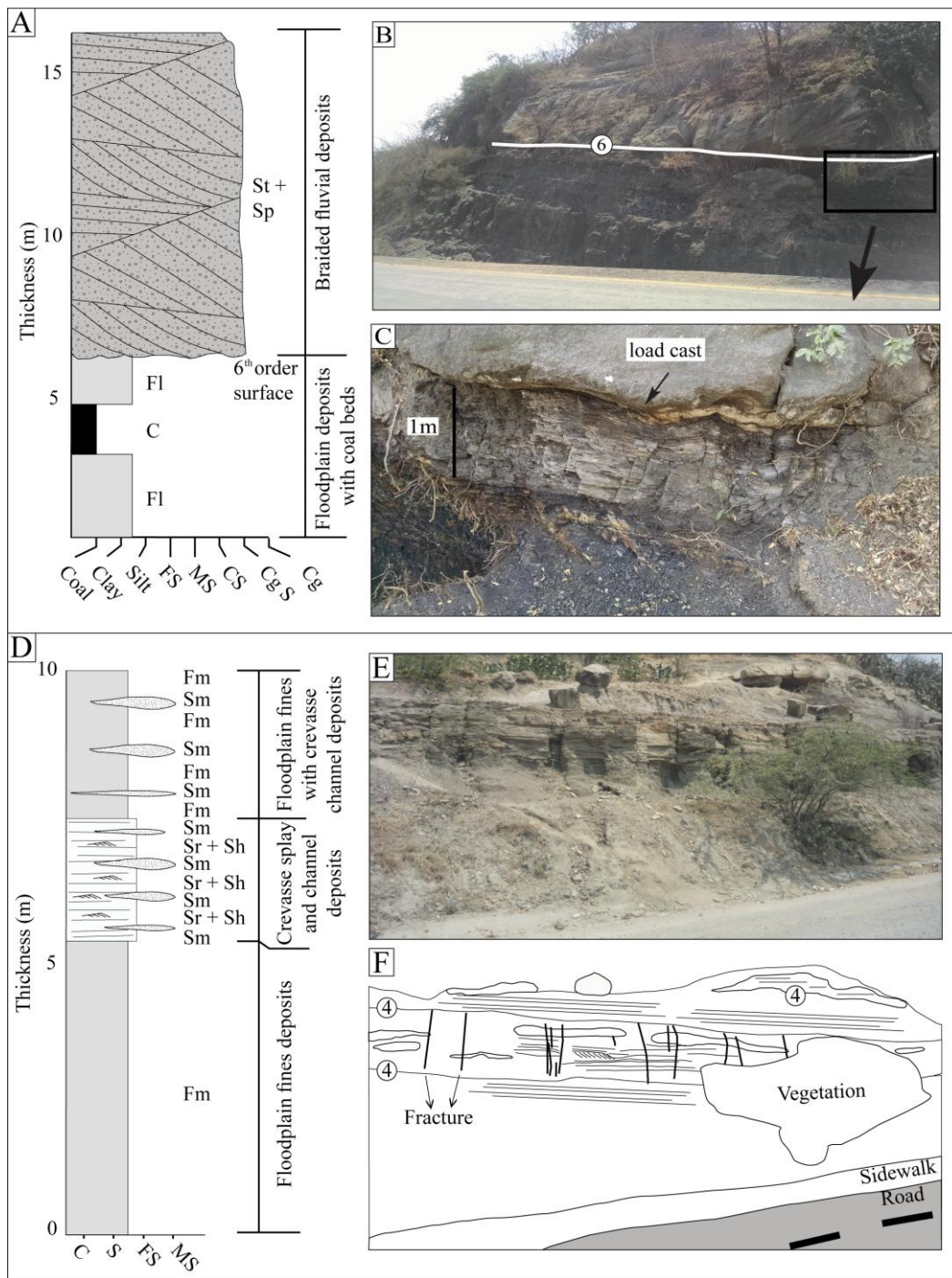


415  
 416 Figure 7: CS-006 borehole (ca. 500 m) schematic profile, showing lithofacies variations and  
 417 lithofacies assemblages.



418

419 Figure 8: CS-006 borehole main lithofacies. A) C (133,2 m); B) Fm (393 m); C) Fl (147.3  
420 m); D) Sr (282 m); E) St (294.6 m); F) Gm (424, 61 m).



421

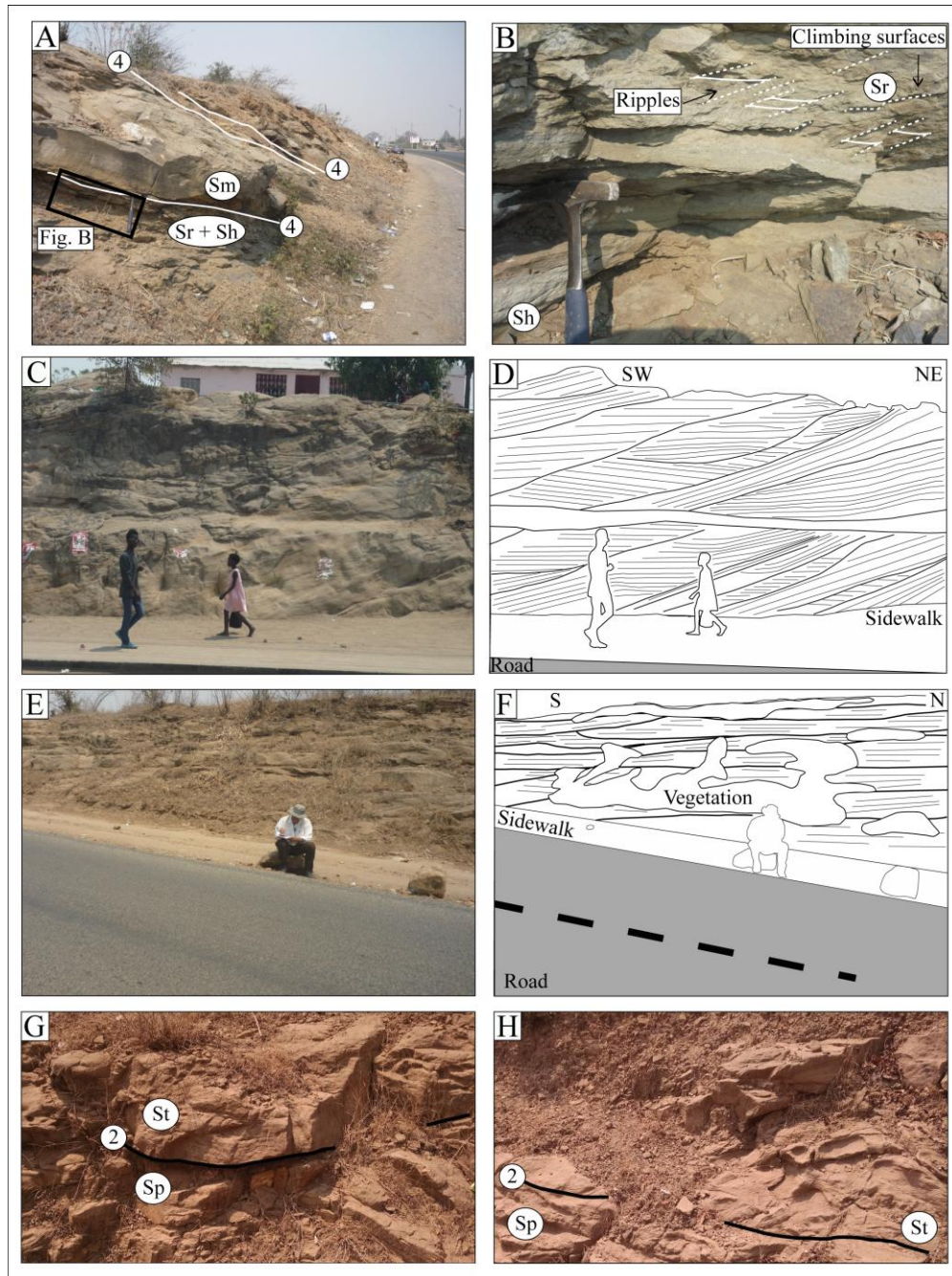
422 Figure 9: A) Schematic profile of the Moatize/Matinde Formations progradational  
 423 transition; B) Outcrop type-section of the 6<sup>th</sup> order transition; C) Detail of load casts marks  
 424 found within the unconformity. D) Schematic profile illustrating overbank lithofacies  
 425 associations; E) Relationship between the floodplain fines, crevasse splay and crevasse  
 426 channel associations; F) Schematic cross-section of Fig. E pointing out the distribution of  
 427 lithofacies association and their relationship with each other.

428 *Crevasse splay and crevasse channel deposits*

429 Deposition of facies with coarsening and thickening upwards sequence (between 0.5  
430 to 8 m thick) dominates these sedimentary deposits. From bottom to top, the succession  
431 comprise massive carbonaceous mudstones (Fm), <0.5 cm thick, of very fine to fine  
432 sandstone linsen bedding with ripple cross-lamination (Fm), superimposed on mudstones  
433 with very fine to fine-sandstone wavy/linsen bedding 0.3 to 5 cm thick, with ripple cross-  
434 lamination (Fl). These heterolithic successions are overlaid by micaceous (muscovite), very  
435 fine-grained sandstone, with 1-2 cm ripple (sometimes climbing) cross-lamination (Sr) that  
436 turning upwards to a medium to coarse-sandstone, occasionally conglomeratic, poorly to  
437 moderately sorted, with 5 to 50 cm thick sets of trough cross-stratification (St). Foresets are  
438 commonly marked by intraclasts (Fig. 3; MB-125 outcrop; Fig. 10A and 10B; MB-130  
439 outcrop; Fig. 9D, 9E and 9F).

440 In this facies association we also identified medium to coarse sandstone beds,  
441 mostly 0.5 to 2 m thick, with erosive base, showing tangential cross-stratified sets that were  
442 interpreted as crevasse channel deposits. They mostly occur (Fig. 10A and 10B) associated  
443 with massive to poorly horizontally laminated tabular fine to medium sandstone (Sh).  
444 Channels are commonly <1 meter thick. This scenario implies a sporadic change between  
445 lower and upper flow regime conditions (Allen, 2014; Fielding, 2006). Massive to poorly  
446 horizontally laminated medium-grained sandstone beds (Sm) also interpreted as crevasse  
447 channel occur as lenticular bodies inside floodplain facies association deposits (Fig. 9D,  
448 Fig. 9E and Fig. 9F).

449



450

451 Figure 10: A) Crevasse splay and crevasse channel deposits; B) Detail of very fine  
 452 sandstone with climbing ripples cross-lamination (Sr) interbedded with horizontal  
 453 laminated sandstones (Sh); C) Coarse cross-bedded sandstones (Sp and St) from the  
 454 Matinde Formation braided fluvial system (longitudinal bars); and D) Sketch of Fig. B  
 455 illustrating the internal structural pattern of beds (W to NW paleoflow); E to H)  
 456 Lithofacies (Sp and St) from a poorly confined channel, with low angle lateral accretion  
 457 pattern and main westward paleoflow.

458 **4.3.3 Matinde Formation**459 ***Fluvial channel deposits***

460 These facies associations are 3 to 5-meter thick, bounded by high-relief basal  
461 erosion surface. Internally, the sand bodies are composed mostly by metric sets of  
462 brownish, coarse to conglomeratic sandstone with planar (Sp) and tangential cross-  
463 stratification (St) (Fig. 9A, 9B and 9C; Fig. 3; MB-126 and MB-129 outcrops) (Fig. 10C  
464 and 10D). Paleoflow measurements indicate NW to NE preferential migration trends (Fig.  
465 3).

466

467 ***Poorly confined fluvial channel***

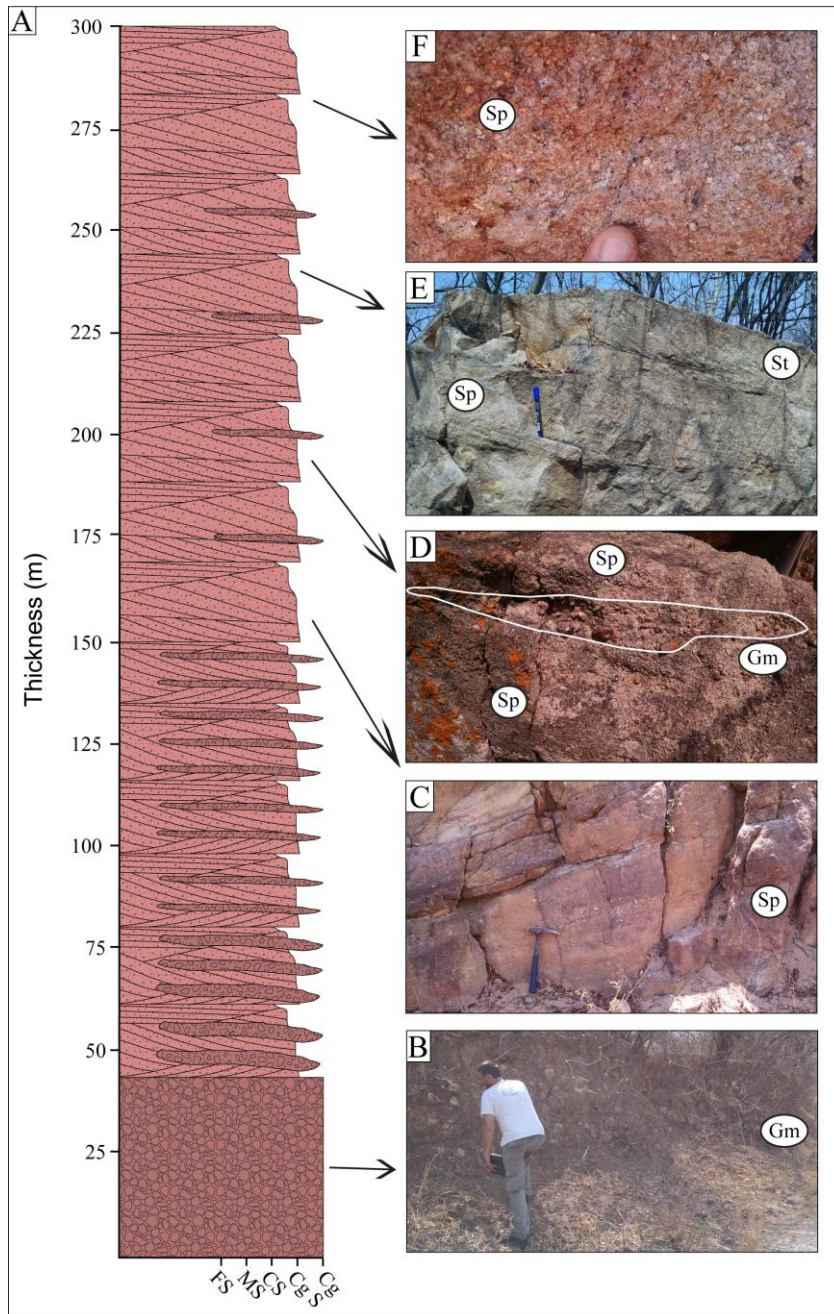
468 This lithofacies assemblage is 3 m thick, of amalgamated sandbodies, bounded by  
469 planar to a low-relief erosive surface. The sandbodies are mainly composed of brownish,  
470 medium to coarse-grained sandstones with horizontal (Sh), low-angle cross-stratification  
471 (Sl), and rarely planar (Sp) and trough cross-stratification (St). The individual sets are 20-  
472 30 cm thick. This facies association mainly outcrops north of the study area (Fig. 3; MB-  
473 128 and MB-127 outcrops), close to the faulted basin boundary with Precambrian rocks  
474 (Fig. 10E, 10F, 10G and 10H). Western and southwestern paleoflow directions are  
475 suggested from field measurements on cross-bedded strata.

476

477 ***Fluvial channel and reworked alluvial fan deposits***

478 Upwards in the profile, lithofacies assemblages attributed by us to later depositional  
479 sequences of the Matinde Formation, were observed in the southwest section of the graben  
480 (Fig. 3; MB-117 to 124 outcrops) and consists of a ~300 m thick succession of fining-  
481 upward sequences of coarse-grained to conglomeratic sandstones (Figs. 11A to 11E). These

482 facies associations show a gradual reduction of conglomeratic lithofacies. Matrix-supported  
483 conglomerates (Gm) (Fig. 11A and Fig. 11B), with clasts of about 20 cm in size of mainly  
484 moderate rounded to subangular granitic rocks, approximately 40 meters thick, occur at the  
485 base of the sequence. Upwards there is a prominent occurrence of coarse to pebbly  
486 sandstone with planar (Sp) and trough cross-stratification (St) (Fig. 11C, 11D, 11E and F)  
487 with lenses of conglomeratic sandstones, organized in 0.5 to 1 m thick sets (Fig. 11D).  
488 Clasts are dominantly composed of rounded to subangular granitic and quartz fragments of  
489 <5 centimeters in size and commonly parallel to the cross-bed stratification. Intraclasts  
490 where not observed, but several elongated clasts shape casts, commonly oriented with the  
491 whole sequence were observed, suggesting that intrabasinal clasts may have been dissolved  
492 or loosened within post-depositional processes. In a few locations there are several  
493 occurrences of iron concretions, mostly associated with faults and fractures providing a  
494 grayish color to the sediments. Immaturity, large size and composition of the clasts and  
495 sediments reflect the proximity of this package of the border fault (Fig. 3). Paleocurrent  
496 measurements from this package indicate a NW to NE paleoflow.  
497



499 Figure 11: A) Schematic profile of coarse lithofacies (Gm, Sp and St) from a fluvial  
500 channel (coarse to conglomeratic grained bars) near southwestern basin faulted margin; B)  
501 Detail of basal Gm lithofacies; C) Coarse to conglomeratic sandstone with planar cross  
502 stratification (Sp); D) Detail of Sp irregularly interbedded with Gm; E) Interbedded Sp and  
503 St (tangential) lithofacies; F) Interbedded very coarse and coarse Sp lithofacies in the top of  
504 the sequence as a result of variability in the transport energy.

505

506 **5. Discussion**

507 Structures and sedimentation in northwestern Mozambique followed important  
508 stages of intraplate brittle reactivation of large crustal structures within Gondwana  
509 Supercontinent, as marked by the overlap of very coarse lithofacies association of Matinde  
510 Formation over the floodplains of Moatize Formation, which is cross-cut by several  
511 transtensive syn-depositional structures. NW-oriented structures such as growth faults, drag  
512 folds and folds axial planes, produced by regional tectonic activity, have exposed buried  
513 coal beds in the northeast area of Cahora Bassa Basin, which is positioned north-northwest  
514 of the Moatize-Minjova Basin (Fig. 2C), with the same sedimentation pattern of the latter.  
515 The entire sequence shows a distinct regional coarsening upwards signature, which  
516 compounds a large fluvial plane during Permian in the northwestern Mozambique basins.

517 Brittle faults and fractures measurements collected from the Moatize and Matinde  
518 formations point to preponderant post-Karoo depositional tectonic reactivations, probably  
519 related to the Pangea breakup event and beginning of the East African Rift System  
520 inception. Below we provide a discussion about integration of structural reactivation  
521 mechanisms and depositional environments.

522

523 **5.1. Permian Tectonics and Basin Subsidence**

524 A complex structural web was identified in northwestern Mozambique, produced by  
525 Phanerozoic brittle reactivation of inherited basement Precambrian ductile deformation  
526 zones, mostly from Pan-African orogenic cycle. NW-SE oriented structures tightly  
527 dominate the Moatize-Minjova Basin during deposition and subsidence phases of Karoo  
528 Supergroup sequences in northwestern Mozambique. The large distribution of the

529 lineament patterns all over the region reflects the Mozambican position within the Pan-  
530 African assembly, between the interface of the Zambezi and Mozambique Orogenies.

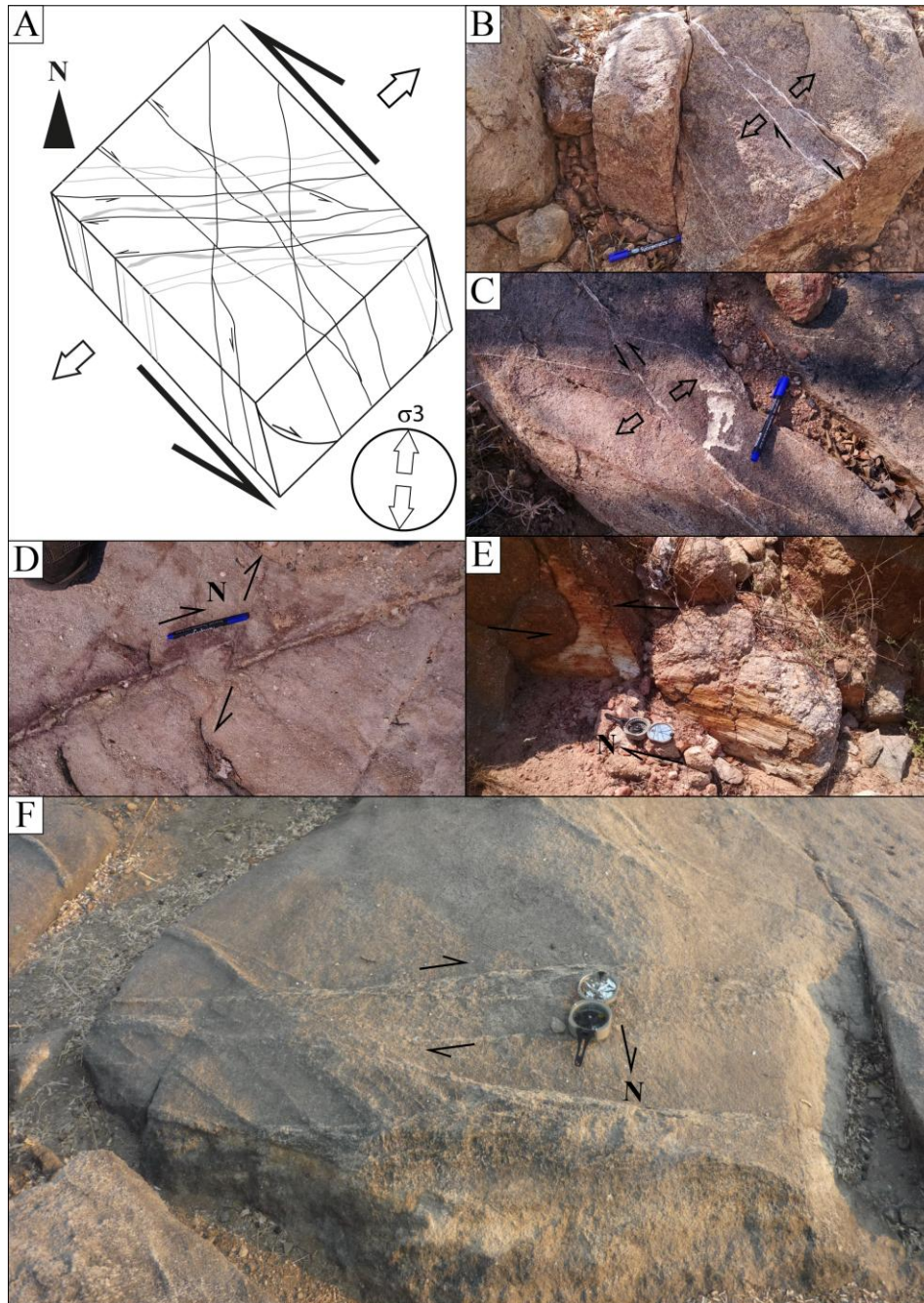
531 The NW-SE pattern is concordant with the southeastern segment of the Mzarabani  
532 Shear Zone and Mwanza and Estima Faults (Fig. 2) which are the main fault systems  
533 responsible for basin subsidence. The WNW-ESE subgroup is probably a subordinate  
534 (Riedell shear) pattern generated from the NW-SE system. On the other hand, the E-W  
535 transtension system represents the southern and northern boundary of the greater Cahora  
536 Bassa Basin, while the ENE-WSW and NNE-SSW fault systems represent the Riedell  
537 shear. Shoko and Gwavava (1999) identify similar structures in the basement below Cahora  
538 Bassa Basin from geophysical data and assigned those as the main structural pattern  
539 responsible to control subsidence control within the basin, since its earliest stages.  
540 However, NE-trending fault zones show greater importance in the Moatize-Minjova Basin,  
541 near the northeastern edge of Mozambique with Malawi, where several Jurassic dikes are  
542 aligned with this trend (Casting, 1991). Our studies from granitic and metamorphic rocks  
543 in Cahora Bassa and Tete regions showed that basement ductile structures are marked by  
544 NW-SE oriented magmatic fabric and high temperature shear zones (Philipp et al., 2014).  
545 Additionally, NW-SE and NE-SW are the main Pan-African ductile shear-zones patterns,  
546 well established in northern Malawi (Ring et al., 2002), active until Ordovician times.  
547 These considerations imply that the basement fabric heritage within northern Mozambique  
548 has played an important role during basin inception and infilling.

549 Apparently, NW-SE, WNW-ESE, and ENE-WSW fault system subgroups appear to  
550 affect more intensively the KS sequences and the Post-Karoo sequences less (Fig. 5),  
551 comprising some of the longest continuous lineaments observed as indicative of its basin-  
552 forming character. Igneous rocks from Karoo are strongly aligned and sectioned by the

553 NW-SE subgroup. We interpreted these data as probable pathways for magmatic rise  
554 through the crust at the end of the Karoo basinal cycle (beginning of Gondwana Breakup),  
555 controlling regional subsidence during Karoo and Post-Karoo sedimentation. Similar  
556 descriptions could be adopted for the WNW-ESE, and ENE-WSW subgroups, which are  
557 also well recorded in the Karoo sequences; but these two subgroups host only small  
558 intrusions and are probably shallower in the crust.

559           The less pronounced N-S and NNE-SSW fault system scarcely affect the basins,  
560 comprising smaller lengths, and hence are probably shallower fault zones resembling  
561 subsidiary structures associated with the greater patterns. Otherwise, they intercept the  
562 Later Karoo volcanic intrusions in the southern region, constraining its post-Karoo tectonic  
563 age.

564           A dynamic analysis based on field scale data suggests a local NNE-SSW  
565 extensional regime to generate such structural pattern (Fig. 12). Since they post-date Karoo  
566 sedimentation, due to its large occurrence all over the basin and great fit with the N-S  
567 trending East African Rift structure (Lake Niassa), this extensional component is probably  
568 related to an N-S transtensional regime produced during the Gondwana dispersal in the  
569 eastern African margin.



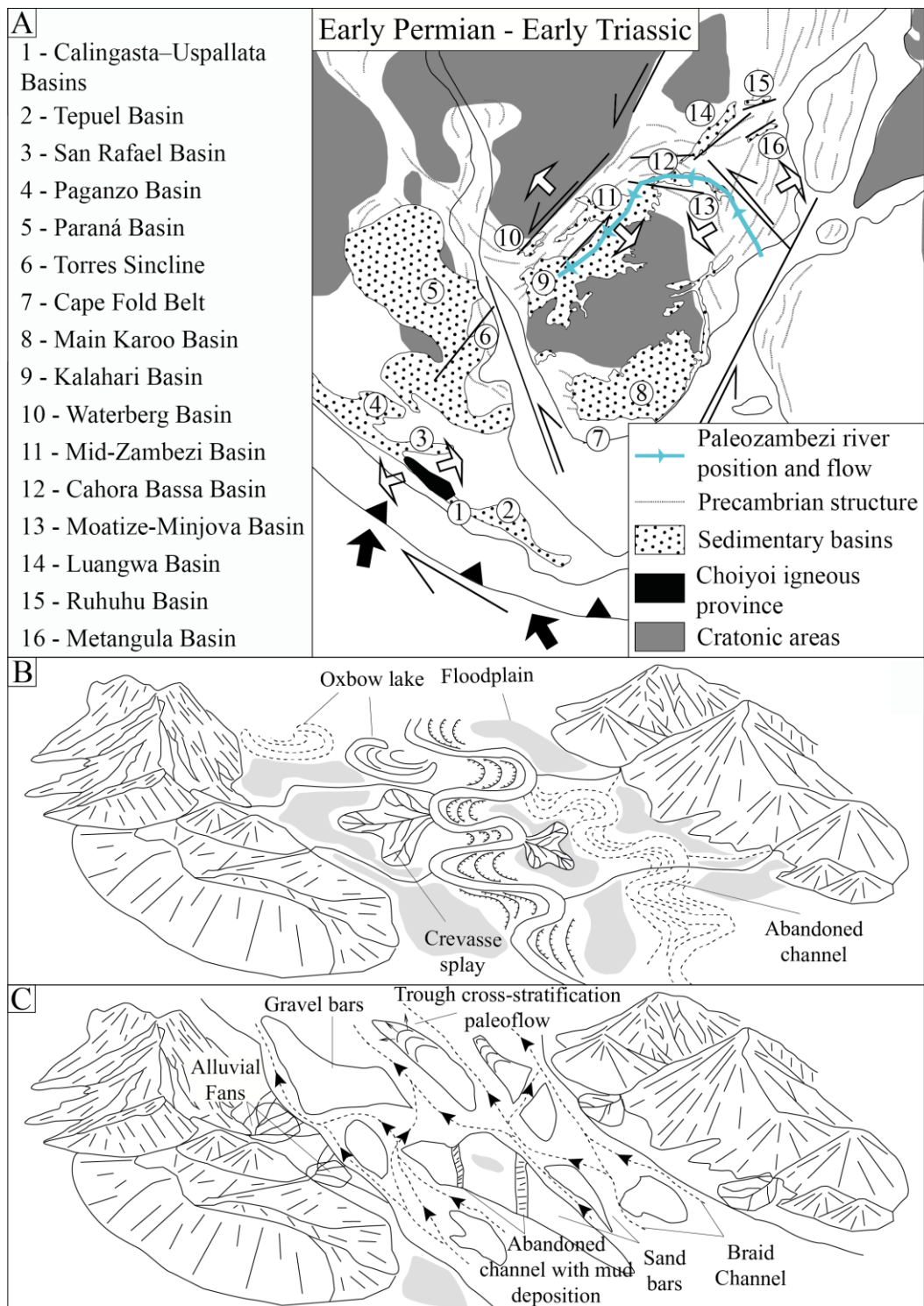
570

571 Figure 12: A) Sketch of main structural pattern determined from field measurements data; B)  
 572 Top-most coarse to conglomeratic lithofacies preserving structures filled by silicate  
 573 solutions; C) Sinistral transtractive fault system with silicate solution, which marks the  
 574 shear direction; D) NW-SE dextral strike-slip fault dislocating N-S shear fault with  
 575 sediment fill (post-depositional); E) N-S trend sinistral strike-slip fault with slickenlines  
 576 and shear direction indicators (steps); and F) E-W dextral fault with silicate solutions in  
 577 sandstones from Moatize Formation.

578 In a regional context, Permian times were a period of large tectonic activity along  
579 Gondwana, such as the Pangea assembly (Variscan Orogeny) in northern Africa (Torsvik &  
580 Cocks, 2013; Linol et al., 2015) and ongoing subduction of Panthalassan oceanic crust  
581 (Gondwanides Orogeny, ca. 305–230 Ma) in the southwestern Gondwana/Pangea margin  
582 (Cawood & Buchan, 2007). Both tectonic processes may have acted as a trigger for  
583 regional inland subsidence that took place in several basins within Gondwana. This period  
584 accomplished the Cape Fold Belt Orogeny, which comprises a large deformation structural  
585 pattern with major N-S (Craddock et al., 2007) to NE-SW stress fields acting on the  
586 Gondwana margin (Tankard et al., 2009; Hansma et al., 2015), which deformed earlier  
587 glaciogenic deposits of KS in South Africa (Craddock et al., 2007; Hansma et al., 2015).  
588 Additionally, Smith et al. (1993), Cadle et al. (1993), Johnson et al. (1996), Catuneanu et  
589 al. (2005) and references therein indicate that glaciogenic deposits commonly rest non-  
590 conformably or with a slightly angular unconformity over low relief pre-Karoo landscape.  
591 These evidences suggests that it starts after the main glacial period, probably during Early  
592 Permian as constrained by Ar-Ar deformational ages of ca. 280-245 Ma within the Cape  
593 Fold Belt (Hansma et al., 2015), prior to the onset of coal-bearing layers deposition of  
594 Moatize Formation, which recorded large syn-depositional faulting and folding in its  
595 stratigraphic record (Vasconcelos et al., 2014; Lakshminarayana, 2015). Basin inversion  
596 and basement uplift during this period have also been documented by Holz et al. (2006) in  
597 the southern section of the Paraná Basin in South America, improving the influence of  
598 southern Gondwana margin tectonics inland.

599 In this context, we understand that the Moatize-Minjova Basin was developed by a  
600 NW-trending structural system, with sinistral transtensive regime, related to N-S/NE-SW  
601 oriented stress field from the Gondwana southern margin during the early times of the Cape

602 Orogeny evolution. Stress propagated along the first order, NE to NNE oriented,  
603 Precambrian Mozambique Ocean Suture and converged inland through the NW Zambezi  
604 Pre-Transform System as a synthetic Riedell shear of the main structure (Fig. 13A).  
605 Subsidence was achieved from a NE-SW extension, produced by crustal readjustment. On  
606 the other hand, episodic subsidence in Mid-Zambezi, Mana Pools, Luangwa, Metangula,  
607 Ruhuhu and Waterberg basins, that are NE-SW-trending, are related to readjustments  
608 produced by the Damara-Katanga Belt, between Kalahari and Congo/Tanzania cratonic  
609 areas (Fig. 13A).



610

611 Figure 13: A) Schematic geodynamic conditions throughout Gondwana south-southwestern  
 612 margin during Permian sedimentation period; B and C) Schematic depositional  
 613 environment of Early-Late Permian meandering (B) and Late Permian - Early Triassic  
 614 braided (C) lithofacies associations.

615     **5.2 Stratigraphic and Depositional Implications**

616         Fluvial channels or poorly confined channels, bars and overbanks are the main  
617         depositional elements identified in the area, composed by facies and facies associations  
618         characterizing individual bodies where the internal geometry and external form can be  
619         differentiated. These elements led us to identify meandering (Moatize Formation) and  
620         braided (Matinde Formation) fluvial systems.

621         The facies description and facies associations of well CS\_006A have shown that the  
622         Moatize Formation was deposited in a continental environment dominated by meandering  
623         river systems. Coals may have been deposited in peat associated with floodplains and  
624         probably in oxbow lakes (abandoned meandering channel; Fig. 13B). Thus, lateral  
625         migration of fluvial channels may have played an important role in the matter of coal  
626         seams preservation. The study of the vertical lithofacies succession showed that coal is  
627         interbedded with thin layers of siltstone and fine sandstones, marking its cyclic deposition  
628         pattern. This sedimentary change within coal-bearing layers controls the quality of coal and  
629         is directly related to the deposition of crevasse splay successions.

630         The stratigraphic sections demonstrated that the Chipanga seam, composed by  
631         interbedded flood fines and coal beds, occur near the base of the sequence (Fig. 7) and  
632         brings important subsidence implications with it. The great thickness of these floodplain  
633         fines deposits implies a high subsidence regime in the basin, with low fluvial channel  
634         amalgamation. This suggests an Early Permian depositional age, right after glacial retreat  
635         and consequent isostatic rebound which lead to high subsidence rates. This was followed by  
636         tectonically active periods throughout the Permian (as demonstrated earlier), due to the  
637         ongoing Panthalassa subduction along southern the Gondwana margin and the beginning of  
638         Cape Fold Belt deformation. Early Permian tectonic activity is recorded in basins on the

639 eastern margin, such as Ruhuhu Basin, near the Tanzanian margin (Fig. 1B), an important  
640 tectonic event around Artinskian times (Middle - Early Permian), which led to braided  
641 stream deposition in the base of the Moatize correlatable sequence (Wopfner, 2002).  
642 Therefore, the entire sequence is interpreted as a great fluvial plain, with large floodplain  
643 succession with thick peat seams accumulation in cold and wet swamps in the overbank  
644 areas.

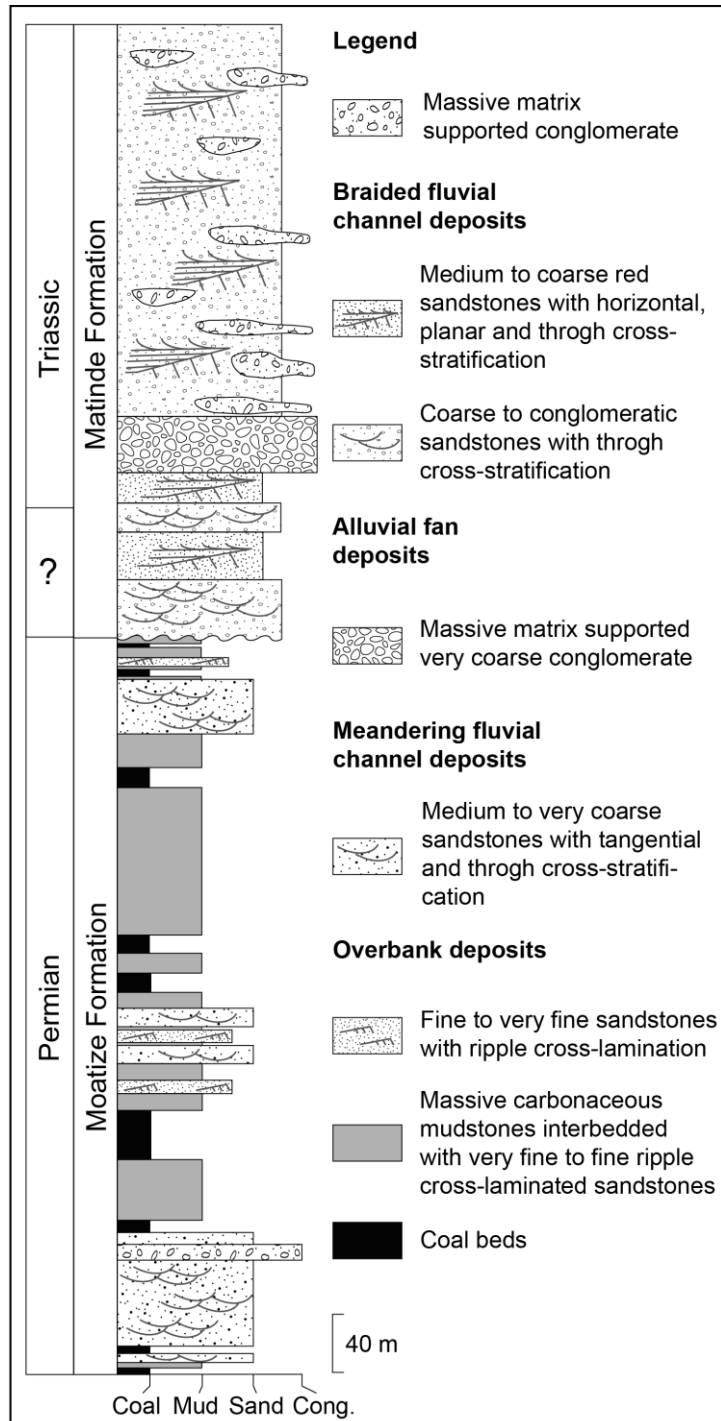
645 The stratigraphic analysis allowed the identification of a likely six-order sequence  
646 boundary on the uppermost portion of stratigraphic well CS\_006A (depth of 28 m). It  
647 comprises an irregular surface marking the contact between the Moatize (Fig. 13B) and  
648 Matinde (Fig. 13C) formations, where load casts indicate an overlap of a coarse braided  
649 fluvial system over a meandering floodplain. However, these marks suggest that the hiatus  
650 between these two formations must not be great. This results in a very low probability of  
651 large peatland development with deposition of organic matter and coal formation in this  
652 range. Field analysis indicates a multiple-story channel fill and sandstone sheet complexes.  
653 Vasconcelos (2000) also pointed out that in some areas of northern Mozambique these two  
654 formations show some contemporarily as indicated by load casts in the contact between  
655 them. The overlap of coarse sandy to conglomeratic braided fluvial deposits implies in a  
656 change of the local geomorphology, associated with rift shoulders uplift during the Moatize  
657 Formation deposition, attributed to the earlier Gondwanides tectonic activity. The  
658 Gondwanides Orogeny was also responsible for coal seams deformation in its later stages.  
659 This tectonic activity led to distinct sedimentation patterns on different Karoo basins within  
660 Southern Africa and in South America basins. Changes in depositional style, as supported  
661 by lithofacies association through these basins, indicates plate readjustments and  
662 rejuvenation of local structural patterns.

663       The basin depocenter was probably located towards the southwestern limit of the  
664   basin, based on structural and coarsening upward sedimentary patterns and controlled by  
665   the Mzarabani Fault Zone, preserving a thick and more complete section of Matinde  
666   Formation. A southwestern depocenter position is also corroborated by geophysical data for  
667   the Cahora Bassa region presented by Orpen et al. (1989) and Shoko & Gwavava (1999),  
668   showing that the Mzarabani Shear Zone probably controlled basin subsidence  
669   southeastwards. These arguments are in agreement with GTK Consortium (2006) mapping,  
670   which show that these lithofacies transitioned to the Cádzi Formation (Fig. 3).

671       The upper conglomeratic sequences can be interpreted in two ways. Basal matrix  
672   supported (Gm) conglomerates can represent alluvial fans deposits from the faulted margin.  
673   Finning upwards pattern, clasts organization and internal structures indicate main fluvial  
674   depositional control with northwards paleoflow. These elements may represent a coarser  
675   lithofacies association from the braided fluvial system (migration of longitudinal and/or  
676   accretion macroforms) or they can mark the transition to the upper Cadzi Formation, which  
677   may have occurred near Middle Triassic times, since the Matinde Formation is probably  
678   younger than Late Permian as determined by Pereira et al. (2016) (Fig. 14).

679       This latter model counterpoints the GTK Consortium (2006) which interpreted these  
680   lithofacies as part of the Matinde Formation, which is the one we follow in this paper, due  
681   to the large distribution of geological mapping of these authors and to lateral stratigraphic  
682   relationships and depositional environments determined by us. Another strong aspect is the  
683   important tectonic period that commonly marks the Permian-Triassic transition in the  
684   Paraná Basin and other basins in South America and Africa (Zerfass et al., 2003; Zerfass et  
685   al., 2004; Zerfass et al., 2005; Catuneanu et al., 2005) and left an hiatus that can be

686 observed throughout the Tanzanian Karoo basins and in Mozambique (Catuneanu et al.,  
 687 2005).



688

689 Figure 14: Schematic stratigraphic profile of the Moatize and Matinde formations.

690

691           The transition between the Moatize and Matinde formations probably approximates  
692       the Late Permian - Early Triassic period, based on palynological date presented earlier  
693       (Daber, 1984; Pereira et al., 2016) and other coal bearing seams deposits elsewhere in the  
694       Karoo basins (Catuneanu et al., 2005), although not all show clear tectonic implications.  
695       The Mid-Zambezi basin coal-bearing beds, correlatable to facies of the Moatize Formation,  
696       change to mostly mudstones with subordinate siltstones and sandstones of a lacustrine  
697       deposit (Nyambe & Utting, 1997). This suggests that high subsidence rates took place  
698       westwards from northern Mozambique, controlled by NE-SW crustal faults (Fig 13A), but  
699       produced for the same regional tectonic regime. This also improves the model proposed by  
700       Key et al. (2015) were a proto-Zambezi river with a western paleoflow since Early Permian  
701       times has influenced deposition in Central-Eastern Africa with thick proximal coarser  
702       lithofacies near the Precambrian orogenic belt and finer distal lithofacies inland towards the  
703       Mid-Zambezi and Kalahari Basins.

704

## 705       **6. Conclusions**

706       In summary, northwestern Mozambique basins were affected by NE-SW and NW-  
707       SE transtensive trends, along the African eastern cratonic margin, which led to crustal  
708       readjustments of Precambrian structures and inland subsidence. Tectonic reactivation was  
709       produced by far-field stress transferred from the Gondwanides Orogeny and recorded in the  
710       sedimentary records of the Karoo basins in Mozambique and Southern Africa and also in  
711       South America basins. Identification of the same structural pattern of the basement units in  
712       the Karoo Supergroup and the latest coverage underscores the importance of tectonic  
713       reactivation of the same weakness zones in the depositional control of Paleozoic and  
714       Cenozoic units.

715        Permian sequences in the Moatize-Minjova Basin comprise mainly meandering and  
716        braided fluvial plane deposits. The former comprise floodplain, crevasse splay and fluvial  
717        channel main lithofacies associations. This sequence was prograded by a multiple-story  
718        braided fluvial plane in the Matinde Formation. Lithofacies associations and their  
719        relationship with each other suggest deposition within a fluvial confined to poorly confined  
720        channel system with longitudinal and low-angle lateral accretion macroforms. The top of  
721        the stratigraphic sequence comprises sediment gravity flow, channel and downstream  
722        macroform accretion facies associations. Conglomerates with boulders dominate near the  
723        southwestern fault bounded graben boundary, indicating an increase in the fluvial transport  
724        energy towards the top of the sequence, due to high relief geomorphologic depositional  
725        environment, which may have started during the end of the Moatize Formation depositional  
726        cycle. Northwestward paleoflow from Matinde lithofacies suggest that the Zambezi River  
727        flow was inverted during Permian sedimentation in northern Mozambique, with its  
728        headwaters located in the southeastern highland areas, inherited from the Pan-African  
729        orogeny.

730        For further studies, we recommend conducting a stratigraphic detail study in the  
731        area to better understand the factors that controlled the deposition of the studied sediments.  
732        A more detailed stratigraphic model to describe the Triassic deposits in the region and  
733        Vúzi, Moatize and Matinde Formations elsewhere in northwestern Mozambique would  
734        improve tectonic and stratigraphic understanding in the area.

735

## 736      **7. Acknowledgements**

737        This study is part of the doctoral thesis of the first author at Programa de Pós-  
738        Graduação em Geociências of Universidade Federal do Rio Grande do Sul. We thank the

739 National Council for Scientific and Technological Development (Conselho Nacional do  
740 Desenvolvimento Científico e Tecnológico - CNPq) of Brazil, for scholarship number  
741 [141240/2013-0](#) of the first author. We also would like to thank Professor Dr. Léo Afraneo  
742 Hartmann, Paulo Fernandes and an anonymous reviewer for the English review and general  
743 improvements to the paper. We are grateful to the undergraduate student Andre Santos, of  
744 the same university, for great cooperation in map compilation and for the geology field  
745 assistance of Mr. Antonio Rizzo Alface. Finally, we thank Vale Mozambique S.A. for  
746 providing the borehole profile presented in this paper.

747

## 748 **8. References**

749 Allen, J.P., Fielding, C.R., Gibling, M.R., Rygel, M.C., 2014. Recognizing products of  
750 palaeoclimate fluctuation in the fluvial stratigraphic record: An example from the  
751 Pennsylvanian to Lower Permian of Cape Breton Island, Nova Scotia. *Sedimentology* 61,  
752 1332–1381.

753

754 Alessandretti, L., Philipp, R.P., Chemale Jr, F., Brückmann, M.P., Zvirtes, G., Matté, V.,  
755 Ramos V.A., 2013. Provenance, volcanic record, and tectonic setting of the Paleozoic  
756 Ventania Fold Belt and the Claromecó Foreland Basin: Implications on sedimentation and  
757 volcanism along the southwestern Gondwana margin. *Journal of South American Earth  
758 Sciences* 47, 12-31.

759

760 Alessandretti, L., Warren, L.V., Machado, R. Novello, V.F., Sayeg, I.J., 2015. Septarian  
761 carbonate concretions in the Permian Rio do Rasto Formation: Birth, growth and

- 762 implications for the early diagenetic history of southwestern Gondwana succession.
- 763 *Sedimentary Geology* 326, 1–15.
- 764
- 765 Angelier, J. 1994. Fault slip analysis and palaeostress reconstruction. In: P. L. Hancock,
- 766 (eds) *Continental Deformation*. Pergamon Press, Oxford, 53-100.
- 767
- 768 Bangert, B., Stollhofen, H., Lorenz, V., Armstrong, R., 1999. The geochronology and
- 769 significance of ash-fall tuffs in the glaciogenic Carboniferous-Permian Dwyka Group of
- 770 Namibia and South Africa. *Journal of African Earth Sciences* 29, 33–49.
- 771
- 772 Barton, C.M., Carney, J.N., Crow, M.J., Dunkley, P.N., Simango, S., 1991. The Geology of
- 773 the Country around Rushinga and Nyamapanda. *Zimbabwe Geological Survey Bulletin*, 92.
- 774
- 775 Barton, C.M., Carney, J.N., Crow, M.J., Evans, J.A., Simango, S., 1993. Geological and
- 776 structural framework of the Zambezi Belt, northeastern Zimbabwe. In: Findla, R. H.,
- 777 Unrug, R., Banks, M. R., Vevers, J. J. (eds) *Gondwana Eight: Assembly, Evolution and*
- 778 *Dispersal*. Balkema, Rotterdam, 55-68.
- 779
- 780 Linol, B., de Wit, M. J., Milani, E. J., Guillocheau, F., Scherer, C. M., 2015. New Regional
- 781 Correlations Between the Congo, Paraná and Cape-Karoo Basins of Southwest Gondwana.
- 782 In: De Wit, M. J. (eds) *Geology and Resource Potential of the Congo Basin. Regional*
- 783 *Geology Reviews*, 245-268.
- 784

- 785 Bumby, A.J., Guiraud, R., 2005. The geodynamic setting of the Phanerozoic basins of  
786 Africa. *Journal of African Earth Sciences* 43, 1-12.
- 787
- 788 Cadle, A.B., Cairncross, B., Christie, A.D.M., Roberts, D.L., 1993. The Karoo Basin of  
789 South Africa: type basin for the coal bearing deposits of Southern Africa. *International*  
790 *Journal Coal Geology* 23, 117–157.
- 791
- 792 Cairncross, B., 2001. An overview of Permian (Karoo) coal deposits of Southern Africa.  
793 *Journal of African Earth Sciences* 33, 529–562.
- 794
- 795 Casting, C., 1991. Post-Pan-African tectonic evolution of South Malawi in relation to the  
796 Karroo and Recent East African Rift Systems. *Tectonophysics* 191, 55-73.
- 797
- 798 Catuneanu, O., 2004. Basement control on flexural profiles and the distribution of foreland  
799 facies: the Dwyka Group of the Karoo Basin, South Africa. *Geology* 32 (6), 517–520.
- 800
- 801 Catuneanu, O., Wopfner, H., Eriksson, P.G., Cairncross, B., Rubidge, B.S., Smith R.M.H.,  
802 Hancox, P.J., 2005. The Karoo basins of south-central Africa. *Journal of African Earth*  
803 *Sciences* 43, 211–253.
- 804
- 805 Cawood, P.A., Buchan, C., 2007. Linking accretionary orogenesis with supercontinent  
806 assembly. *Earth-Science Reviews* 82, 217–256.
- 807

- 808 Cordani, U.G., Pimentel, M.M., Araújo, C. E.G., Fuck, R.A., 2013. The significance of the  
809 Transbrasiliano-Kandi tectonic corridor for the amalgamation of West Gondwana. Brazilian  
810 Journal of Geology 43(3), 583-597.
- 811
- 812 Craddock, J.P., McKiernan, A.W., Maarten J. de Wit, M.J., 2007. Calcite twin analysis in  
813 syntectonic calcite, Cape Fold Belt, South Africa: Implications for fold and cleavage  
814 formation within a shallow thrust front. Journal of Structural Geology 29, 1100-1113.
- 815
- 816 Daber, R., 1984. Plantas fósseis de Moçambique, 9. Ciência e Tecnologia, Maputo, pp. 77-  
817 81.
- 818
- 819 Du Toit, A. L., 1927. A geological comparison of South America with South Africa. The  
820 Carnegie Institution, Washington, Publication 381.
- 821
- 822 Fernandes, P., Cogné, N., Chew, D.M., Bruno Rodrigues, B., Jorge, R.C.G.S., Marques, J.,  
823 Jamal, D., Vasconcelos, L., 2015. The thermal history of the Karoo Moatize-Minjova  
824 Basin, Tete Province, Mozambique: An integrated vitrinite reflectance and apatite fission  
825 track thermochronology study. Journal of African Earth Sciences 112, 55-72.
- 826
- 827 Fielding, C.R., 2006. Upper flow regime sheets, lenses and scour fills: extending the range  
828 of architectural elements for fluvial sediment bodies. Sedimentary Geology 190, 227–240.
- 829
- 830 Fritz, H., Abdelsalam, M., Ali, K.A., Bingen, B., Collins, A.S., Fowler, A.R., Ghebreab,  
831 W., Hauzenberger, C.A., Johnson P.R., Kusky, T.M., Macey, P., Muhongo, S., Stern, R. J.,

- 832 Viola, G., 2013. Orogen styles in the East African Orogen: A review of the Neoproterozoic  
833 to Cambrian tectonic evolution. *Journal of African Earth Sciences* 86, 65–106.
- 834
- 835 Gray, D.R., Foster, D.A., Maas, R., Spaggiari, C.V., Gregory, R.T., Goscombe, B.D.,  
836 Hoffmann, K. H., 2007. Continental growth and recycling by accretion of deformed  
837 turbidite fans and remnant ocean basins: Examples from Neoproterozoic and Phanerozoic  
838 orogens. In: Hatcher, R.D. Jr, Carlson, M. P., McBride, J.H., Martinez  
839 Catalan, J. R. (eds) *The 4D Framework of Continental Crust*. Geological Society of  
840 America Memoirs 200, 63–92.
- 841
- 842 GTK Consortium, 2006. Explanation of geological maps of sheets: Songo (1532),  
843 Cazula/Zóbuè (1533-1534), Mecumbura/Chioco (1631-1632), Tete (1633) and Tambara  
844 (1634). Ministério dos Recursos Minerais, Direcção Nacional de Geologia, Maputo.
- 845
- 846 Hansma, J., Tohver, E., Schrank, C., Jourdan, F., Adams, D., 2015. The timing of the Cape  
847 Orogeny: New  $^{40}\text{Ar}/^{39}\text{Ar}$  age constraints on deformation and cooling of the Cape Fold Belt,  
848 South Africa. *Gondwana Research*, article in press.
- 849
- 850 Hanson, R.E., 2003. Proterozoic geochronology and tectonic evolution of southern Africa.  
851 Geological Society, Special Publications 206, 427-463.
- 852
- 853 Hanson, R.E., Wilson, T.J., Munyanyiwa, H., 1994. Geologic evolution of the  
854 Neoproterozoic Zambezi orogenic belt in Zambia. *Journal of African Earth Sciences* 18,  
855 135-150.

- 856
- 857 Hargrove, U.S., Hanson, R.E., Martin, M.W., Blenkinsop, T.G., Bowring, S.A., Walker, N.,  
858 Munyanyiwa, H., 2003. Tectonic evolution of the Zambezi orogenic belt: geochronological,  
859 structural, and petrological constraints from northern Zimbabwe. *Precambrian Research*  
860 123, 159–186.
- 861
- 862 Holz, M., Küchle, J., Philipp, R.P., Bischoff, A.P., Arima, N., 2006. Hierarchy of tectonic  
863 control on stratigraphic signatures: Base-level changes during the Early  
864 Permian in the Paraná Basin, southernmost Brazil. *Journal of South American Earth  
865 Sciences* 22, 185–204.
- 866
- 867 Johnson, M.R., Van Vuuren, C.J., Hegenberger, W.F., Key, R., Shoko, U., 1996.  
868 Stratigraphy of the Karoo Supergroup in southern Africa—an overview. *Journal of African  
869 Earth Sciences* 23, 3-15.
- 870
- 871 Key, R.M., Cotterill, F.P.D., Moore, A.E., 2015. The Zambezi River: An Archive of  
872 Tectonic Events Linked to the Amalgamation and Disruption of Gondwana and Subsequent  
873 Evolution of the African Plate. *South African Journal of Geology* 118(4), 425-438.
- 874
- 875 Lakshminarayana, G., 2015. Geology of Barcode type coking coal seams, Mecondezi sub-  
876 basin, Moatize Coalfield, Mozambique. *International Journal of Coal Geology* 146, 1–13.
- 877

- 878 Lopes, G., Pereira, Z., Fernandes, P., Marques, J., 2014. Datação Palinológica dos  
879 Sedimentos Glaciogénicos da Formação (Tilítica) de Vúzi, sondagem ETA 65, Bacia  
880 Carbonífera de Moatize-Minjova, Moçambique-Resultados Preliminares. In: Actas do IX  
881 Congresso Nacional de Geologia/2. Congresso de Geologia dos Países de Língua  
882 Portuguesa, Porto, Portugal, p. 7.
- 883
- 884 Macey, P.H., Miller, J.A., Rowe, C.D., Grantham, G.H., Siegfried, P., Armstrong, R.A.,  
885 Kemp, J., Bacalau, J., 2013. Geology of the Monapo Klippe, NE Mozambique and its  
886 significance for assembly of central Gondwana. Precambrian Research 233, 259– 281.
- 887
- 888 Meert, J.G., 2003. A synopsis of events related to the assembly of eastern Gondwana.  
889 Tectonophysics 362, 1–40.
- 890
- 891 Miall, A.D., 1978. Fluvial Sedimentology. Canadian Society of Petroleum Geologists, 859  
892 pp.
- 893
- 894 Miall, A.D., 1992. Alluvial deposits. In: Walker. R.G. James, N.P. (eds), Facies Models:  
895 Response to sea-level change. InGeoL Association, Canada, Saint john's Newfoundland,  
896 119-142 pp.
- 897
- 898 Miall, A.D., 1996. The Geology of Fluvial Deposits. Sedimentary Facies, Basin Analysis,  
899 and Petroleum Geology. Springer, Berlin, 582 pp.
- 900

- 901 Milani, E.J., 1997. Evolução tectono-estratigráfica da Bacia do Paraná e seu relacionamento  
902 com a geodinâmica fanerozóica do Gondwana sul-ocidental. DSc thesis, Universidade  
903 Federal do Rio Grande do Sul.
- 904
- 905 Milani, E.J., Ramos, V.A., 1998. Orogenias paleozóicas no domínio sul-ocidental do  
906 Gondwana e os ciclos de subsidência da Bacia do Paraná. Revista Brasileira de Geociências  
907 28, 473–484.
- 908
- 909 Milani, E.J., de Wit, M.J., 2008. Correlations between the classic Paraná and Cape- Karoo  
910 sequences of South America and southern Africa and their basin infills flanking the  
911 Gondwanides: du Toit revisited. Geological Society, London, Special Publications, 294,  
912 319–342.
- 913
- 914 Nyambe, I., Utting, J., 1997. Stratigraphy and palynostratigraphy, Karoo Supergroup  
915 (Permian and Triassic), mid-Zambezi Valley, southern Zambia. Journal of African Earth  
916 Sciences 24, 563-583.
- 917
- 918 Orpen, J.L., Swain, C.J., Nugent, C., Zhou, P.P., 1989. Wrench faulting and half graben  
919 tectonics in the development of the Paleozoic Zambezi Karoo basins in Zimbabwe—the  
920 Lower and Mid Zambezi basins respectively—and regional implications. Journal of African  
921 Earth Sciences 8, 215–229.
- 922
- 923 Pereira, Z., Lopes, G., Fernandes, P., Marques, J., 2014. Palinoestratigrafia da Sondagem  
924 ETA 72 da Bacia Carbonífera de Moatize-Minjova, Província de Tete, Moçambique. In:

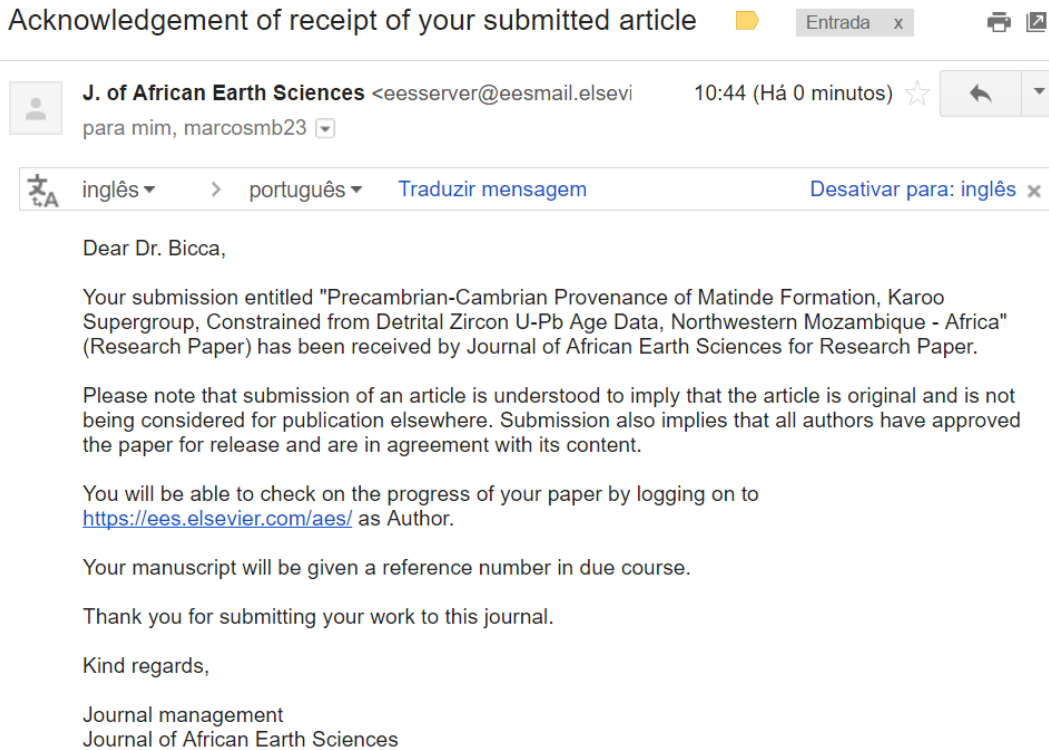
- 925 Vasconcelos, L. (Ed.), Livro de Resumos, 2 Congresso Nacional de Geologia e 12  
926 Congresso de Geoquímica dos Países de Língua Portuguesa, Maputo, Moçambique, pp. 67–  
927 71.
- 928
- 929 Pereira, Z., Fernandes, P., Lopes, G., Marques, J., Vasconcelos, L., 2016. The Permian–  
930 Triassic transition in the Moatize–Minjova Basin, Karoo Supergroup, Mozambique: A  
931 palynological perspective. *Review of Palaeobotany and Palynology* 226, 1–19.
- 932
- 933 Philipp, R.P., Machado, R., Jamal, D.L., Samburane, E., Juliani, C., Cordani, U.G.,  
934 Tassinari, C.G., 2014. Petrologia da sequencia estratiforme gabro-anortosítica da Suíte  
935 Tete, centro-norte de Moçambique. Congresso de Geologia de Moçambique, 2o. Livro de  
936 Resumos, p.38.41.
- 937
- 938 Rapela, C.W., Verdecchia, S.O., Casquet C., Pankhurst, R.J., Baldo, E.G., Galindo, C.,  
939 Murra, J.A., Dahlquist, J.A., Fanning, C.M., 2015. Identifying Laurentian and SW  
940 Gondwana sources in the Neoproterozoic to Early Paleozoic metasedimentary rocks of the  
941 Sierras Pampeanas: Paleogeographic and tectonic implications. *Gondwana Research*, article  
942 in press.
- 943
- 944 Ring, U., Kröner, A., Buchwaldt, R., Toulkeridis, T., Layer, P.W., 2002. Shear-zone  
945 patterns and eclogite-facies metamorphism in the Mozambique belt of northern Malawi,  
946 east-central Africa: implications for the assembly of Gondwana. *Precambrian Research*  
947 116, 19–56.
- 948

- 949 Shackleton, R.M., 1996. The final collision between East and West Gondwana: where is it?
- 950 Journal of African Earth Sciences 23, 271–287.
- 951
- 952 Shoko, D.S.M., Gwavava, O., 1999. Is magmatic underplating the cause of post-rift uplift
- 953 and erosion within the Cabora Bassa Basin, Zambezi Rift, Zimbabwe? Journal of African
- 954 Earth Sciences 28 (2), 465-486.
- 955
- 956 Smith, R.M.H., Eriksson, P.G., Botha, W.J., 1993. A review of the stratigraphy and
- 957 sedimentary environments of the Karoo-aged basins of Southern Africa. Journal of African
- 958 Earth Sciences 16, 143–169.
- 959
- 960 Stern, R.J., 1994. Arc assembly and continental collision in the Neoproterozoic East
- 961 African orogen: implications for the consolidation of Gondwanaland. Annual Reviews of
- 962 Earth and Planetary Sciences 22, 319-351.
- 963
- 964 Tankard, A., Welsink, H., Aukes, P., Newton, R., Stettler, E., 2009. Tectonic evolution of
- 965 the Cape and Karoo basins of South Africa. Marine and Petroleum Geology 26, 1379–
- 966 1412.
- 967
- 968 Torsvik, T.H., Cocks, L.R.M., 2013. Gondwana from top to base in space and time.
- 969 Gondwana Research 24, 999–1030.
- 970

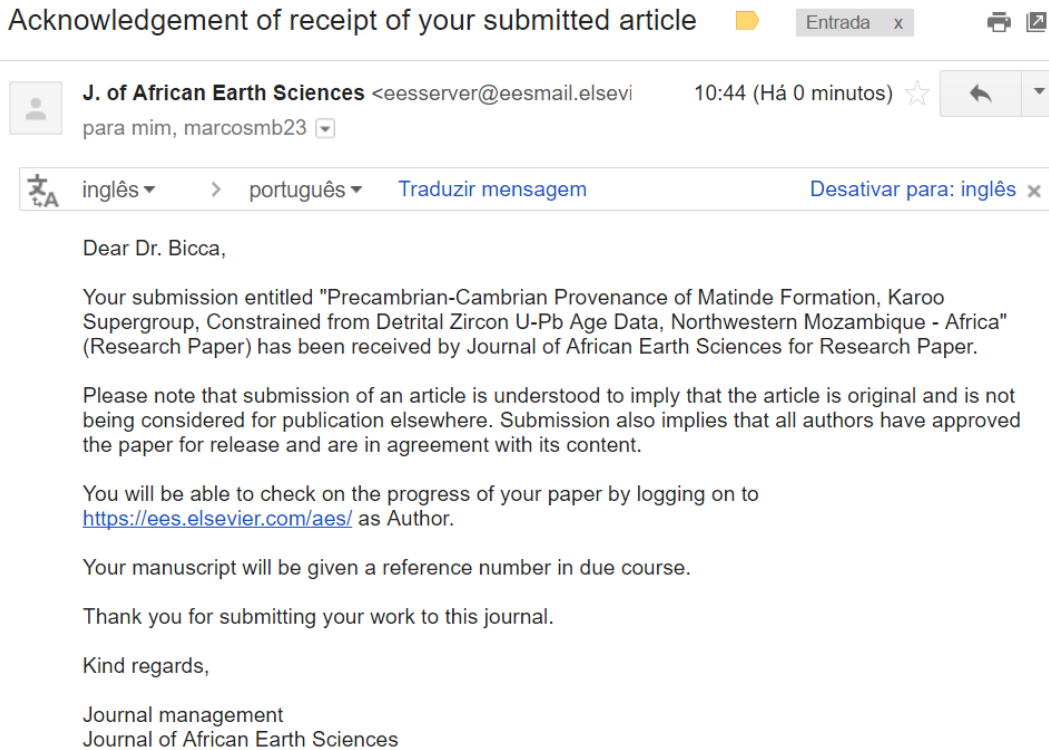
- 971 Trouw, R.A. J. and De Wit, M. J., 1999. Relation between the Gondwanide Orogen and  
972 contemporaneous intracratonic deformation. *Journal of African Earth Sciences* 28, 203–  
973 213.
- 974
- 975 Vasconcelos, L., 2000. Overview of the Moatize Coal Basin geology, Tete Province,  
976 Republic of Mozambique. *Chron. Rech. Minière (Orléans)*, vol. 538, pp. 47–58.
- 977
- 978 Vasconcelos, L., Chafy, A., Xerinda, L., 2014. Determination of the limit of oxidation in  
979 zones of sub-outcropping Chipanga Coal Seam, Moatize Coal Basin, Mozambique. *Journal*  
980 *of African Earth Sciences* 99, 554–567.
- 981
- 982 Weiss, R.H., Wopfner, H., 1997. Palynology and palaeoecology of Late Palaeozoic  
983 glacigenic Idusi Formation of southern Tanzania. *Geologisches Institut, Universität Köln,*  
984 *Sonderveröffentlichungen* 114 (Festschrift E. Kempf), 535–559.
- 985
- 986 Wopfner, H., 2002. Tectonic and climatic events controlling deposition in Tanzanian Karoo  
987 basins. *Journal of African Earth Sciences* 34, 167–177.
- 988
- 989 Wopfner, H., Kreuser, T., 1986. Evidence for Late Palaeozoic glaciation in southern  
990 Tanzania. *Palaeogeography, Palaeoclimatology, Palaeoecology* 56, 259–275.
- 991
- 992 Zerfass, H., Lavina, E.L., Schultz, C.L., Garcia, A.J.V., Faccini, U.F., Chemale Jr., F.,  
993 2003. Sequence-stratigraphy of continental strata of Southernmost Brazil: a contribution to

- 994 Southwestern Gondwana palaeogeography and palaeoclimate. *Sedimentary Geology* 161,  
995 85– 105.
- 996
- 997 Zerfass, H., Chemale Jr., F., Schultz, C.L., Lavina, E.L., 2004. Tectonics and sedimentation  
998 in Southern South America during Triassic. *Sedimentary Geology* 166, 265–292.
- 999
- 1000 Zerfass, H., Chemale Jr., F., Lavina, E.L., 2005. Tectonic control of the Triassic Santa  
1001 Maria units of the Paraná Basin, Southernmost Brazil, and its correlation to the Waterberg  
1002 Basin, Namibia. *Gondwana Research* 8 (2), 163–176.
- 1003
- 1004

### 3. ARTIGO SUBMETIDO À REVISTA JOURNAL OF AFRICAN EARTH SCIENCES

Acknowledgement of receipt of your submitted article 

J. of African Earth Sciences <eesserver@eesmail.elsevier.com> 10:44 (Há 0 minutos) 

para mim, marcosmb23 

 inglês ▾ > português ▾ Traduzir mensagem Desativar para: inglês 

Dear Dr. Bicca,

Your submission entitled "Precambrian-Cambrian Provenance of Matinde Formation, Karoo Supergroup, Constrained from Detrital Zircon U-Pb Age Data, Northwestern Mozambique - Africa" (Research Paper) has been received by Journal of African Earth Sciences for Research Paper.

Please note that submission of an article is understood to imply that the article is original and is not being considered for publication elsewhere. Submission also implies that all authors have approved the paper for release and are in agreement with its content.

You will be able to check on the progress of your paper by logging on to <https://ees.elsevier.com/aes/> as Author.

Your manuscript will be given a reference number in due course.

Thank you for submitting your work to this journal.

Kind regards,

Journal management  
Journal of African Earth Sciences

1   **Precambrian-Cambrian Provenance of Matinde Formation, Karoo Supergroup,**  
2   **Constrained from Detrital Zircon U-Pb Age Data, Northwestern Mozambique -**  
3   **Africa**

4

5   Marcos Müller Bicca<sup>a\*</sup>

6   Andrea Ritter Jelinek<sup>a</sup>

7   Ruy Paulo Philipp<sup>a</sup>

8

9   \* Corresponding author

10   E-mail addresses: [marcos.mb83@gmail.com](mailto:marcos.mb83@gmail.com) (M.M. Bicca); [andrea.jelinek@ufrgs.br](mailto:andrea.jelinek@ufrgs.br)  
11   (A.R. Jelinek); [ruy.philipp@ufrgs.br](mailto:ruy.philipp@ufrgs.br) (R.P. Philipp).

12

13   <sup>a</sup>Instituto de Geociências – Universidade Federal do Rio Grande do Sul, Campus do  
14   Vale. Av. Bento Gonçalves, 9500, Porto Alegre, Rio Grande do Sul, CEP 91509-900,  
15   Brazil.

16

17   **Highlights**

18

19       Detrital zircon dating provided Mesoproterozoic to Cambrian provenance;

20

21       Neoproterozoic ages indicate an south-southwestern provenance;

22

23       Guro Suite and SW Nampula Complex are the main source regions;

24

25       Headwaters of Permian-Triassic fluvial systems were positioned southwards;

26     **Abstract**

27                 Permian-Triassic times were a period of high sedimentation rates into the  
28     intracontinental Karoo rift basin of northwestern Mozambique reflecting high  
29     exhumation rates in the underlying high grounded Precambrian-Cambrian basement  
30     assemblages. The U-Pb dating of detrital zircons from Permian-Triassic Matinde  
31     Formation of Karoo Supergroup proved to be a reliable proxy to map denudation  
32     patterns of source regions.

33

34                 The analytical data allow discriminate two main age populations of Late  
35     Mesoproterozoic - Early Neoproterozoic (*ca.* 1100-950 Ma) and a Late Neoproterozoic  
36     - Early Cambrian (*ca.* 550-490 Ma). The former resembles to the late stages of Rodinia  
37     Supercontinent geotectonic activity mostly represented by magmatic and less  
38     metamorphic rocks, which are present everywhere in the northern Mozambique  
39     basement. The latter register large metamorphic overprint from Pan-African Orogeny on  
40     the older Mesoproterozoic basement, although with magmatic activity related to crustal  
41     reworking.

42                 The less pronounced populations between *ca.* 850-560 Ma together with  
43     paleoflow measurements allowed restricting the source areas when compared to a  
44     gathering of individual zircon age populations of the underlying basement. The older  
45     component refer to the bimodal magmatism related to the breakup phase of Rodinia  
46     Supercontinent registered in the Guro Suite which marks the western limit of the  
47     Moatize-Minjova rift basin. The ages between 630-560 compound the individual zircon  
48     ages of Guro Suite and SW Nampula although they are not attributed to a specific  
49     magmatic or metamorphic event.

50           The SW and NE Nampula Complexes must have been a unique geotectonic  
51       entity since Late Mesoproterozoic, reworked during Pan-African Orogeny. This allied to  
52       the N-NW paleoflow of Proto-Zambezi river and provenance data suggests that  
53       Nampula Complex was a probable high ground source area for fluvial sediments.  
54       Permian-Triassic rifting induced by far stress fields transferred from Gondwana margin  
55       have disrupted the Nampula Complex reactivating Precambrian structures and fabrics  
56       and the Jurassic-Cretaceous Gondwana breakup led to its actual morphology and  
57       configuration.

58

59       **Keywords:** Precambrian-Cambrian basement, Pan-African Orogeny, Karoo  
60       Supergroup, Provenance

61

## 62       **1. Introduction**

63       U-Pb geochronology applied in detrital zircon grains is a powerful tool to  
64       understand provenance patterns in sedimentary basins (Fedo et al., 2003; Hartmann et  
65       al., 2008; Hawkesworth et al., 2010; Cawood, 2012; Bicca et al., 2013; Oliveira et al.,  
66       2014; Bahlburg and Berndt, 2016). The age spectra constrained by this analysis reflect  
67       the tectonic setting of the basin in which the zircons are deposited (Cawood, 2012),  
68       assuming that the measured age distribution observed comprise an unbiased  
69       representation of the true age distribution in the sample and sedimentary unit it  
70       represents (Gehrels, 2014).

71       Because zircon is resistant to abrasion and chemical alteration during  
72       sedimentary processes, the determination of the ages of detrital zircons indicates the  
73       timing of events in the source regions (Hartmann et al., 2008). An additional bias in

74 provenance studies is the variable abundance of zircons in source terrains (Moecher and  
75 Samson, 2006).

76 The use of U-Pb dating by LA-ICP-MS technique to determine the ages of  
77 geological processes that formed the host rocks is a modern and common procedure in  
78 provenance investigation of sedimentary rocks (Hartmann et al., 2008; Guadagnin et al.,  
79 2010; Thomas et al., 2010; Cawood, 2012; Bicca et al., 2013; Oliveira et al., 2014).

80 In this paper we present a provenance analysis based on LA-ICPMS U-Pb ages  
81 of detrital zircon grains from a key immature coarse-sandstone of Matinde Formation  
82 from Karoo Supergroup, with specific focus on determine the denudation patterns of the  
83 Precambrian-Cambrian basement of northern Mozambique. The Late Carboniferous to  
84 Middle Jurassic volcano-sedimentary successions of the Karoo Supergroup (Smith,  
85 1993; Catuneanu et al., 2005) are widely distributed throughout south and central Africa  
86 hosted in marginal and intracontinental basins preserving one of the largest registers of  
87 Gondwana evolution. In northwestern Mozambique they are represented by rift basin  
88 relying over the Precambrian basement rocks that were formed over a very long time  
89 span covering the Archean, Paleoproterozoic, Mesoproterozoic and Neoproterozoic, as  
90 the result of juvenile generation of crust, terrain accretion and crustal reworking during  
91 several orogenic cycles (Stern, 1994; Hanson, 2003; Meert, 2003; GTK Consortium,  
92 2006; Fritz et al., 2013; Macey et al., 2013; Grantham et al., 2013). A complex range of  
93 igneous and metamorphic ages, Th/U rates and zircon morphology suggest that main  
94 suturing, klippening and magmatism, related to the different stages of the protracted  
95 Pan-African orogenic cycle, controlled river catchment and provenance during Permian-  
96 Triassic sedimentation.

97

98

99      **2. Geological Settings**

100        The sedimentary basins of northwestern Mozambique comprise intracontinental  
101      rift basins filled by continental sediments and volcanic rocks from Karoo Supergroup  
102      and younger sequences. This basin relies over an important crustal structure, which  
103      correspond to an eastern extension of the Damara-Lufilian-Zambezi structure (Fig. 1).

104        Crystalline basement of northwestern Mozambique is made of a very complex  
105      assemblage of igneous and low to high-grade metamorphic rocks, from distinct crustal  
106      levels, spanning from Mesoproterozoic to Neoproterozoic-Early Paleozoic in age  
107      (Hanson, 2003; Macey et al., 2013). Most Late Mesoproterozoic rocks have been  
108      reworked by the protracted Pan-African Orogeny in the later Neoproterozoic during  
109      Gondwana-assembly (Pinna et al., 1993; Sacchi et al., 2000), which occur in two main  
110      episodes at ca. 550 Ma and ca. 500 Ma (Ueda et al., 2012). Several studies developed in  
111      the north of Mozambique allow the definition of distinct crustal entities (Fig. 1),  
112      although, the geotectonic model still a matter of discussion (Pinna et al., 1993; Jacobs et  
113      al., 2008; Viola et al., 2008; Bingen et al., 2009; Ueda et al., 2012; Fritz et al., 2013;  
114      Macey et al., 2013).

115        The north of Mozambique can be divided into two major Mesoproterozoic  
116      domains separated by the prominent Neoproterozoic–early Paleozoic Lurio Belt (Fig. 1)  
117      (Viola et al., 2008). This belt comprises a series of NE-anastomosing shear zones and is  
118      mostly represented by the granulite Ocua Complex, which occur mostly in the NE of  
119      Mozambique, while the SW segment of the Lurio Belt is partially undercovered (Fig. 1).

120        U–Pb SIMS ages from selected latest-tectonic units in the Nampula Complex and the  
121      Lurio Belt give ages between  $518 \pm 2$  and  $514 \pm 5$  Ma, coeval with migmatisation and  
122      granitoid plutonism in the Nampula Complex (Ueda et al., 2012). The significance of  
123      the Lurio Belt is controversial. Some authors believe it represents a major suture zone

124 connecting with the Damara-Lufilian-Zambezi Belt (Sacchi et al., 2000; Grantham et  
125 al., 2003). Others suggest it is an accommodation zone, especially because of the  
126 similarities between metamorphic complexes north of the Lurio Belt with those of the  
127 Nampula Complex to the south (Viola et al., 2008; Bingen et al., 2009), an because of  
128 an apparent decrease in strain along the belt from NE to SW.

129 The two domains north and south of the Lurio Belt share a similar  
130 Mesoproterozoic crustal growth history, although their evolution was diachronous. The  
131 Nampula Complex south of the belt developed between 1125 and 1035 Ma while the  
132 Unango and Marrupa Complexes to the north were between 1062 and 946 Ma. The  
133 maximum crustal thickening produced by Pan-African Orogeny in northeastern  
134 Mozambique occurred between *ca.* 570 and 530 Ma and later in the Nampula Complex  
135 (550–500 Ma) (Bingen et al., 2009; Macey et al., 2010; Thomas et al., 2010).

136 The Unango and Marrupa Complexes are crustal domains made of large  
137 volumes of orthogneisses related to a continental arc setting (Bingen et al., 2009) and a  
138 minor magmatic phase at *ca.* 799 Ma registered in the Unango Complex. These  
139 complexes were overthrust at *ca.* 550 Ma by an assemblage of Neoproterozoic  
140 granulites of the Cabo Delgado nappes (including the Xixano, M'Sawize, Muaquia and  
141 Lalamo complexes), forming a stack of west vergent nappes (Viola et al., 2008; Bingen  
142 et al., 2009; Boyd et al., 2010; Macey et al., 2013).

143 In northwestern Mozambique the Unango Complex overlies the small fault-  
144 bounded Ponta Messuli Complex (Viola et al., 2008; Bingen et al., 2009), which  
145 contains Paleoproterozoic metasediments affected by migmatitization at around 1950  
146 Ma and intruded by granitic rocks at 1056 Ma. This complex is also overlain by the  
147 Neoproterozoic Txitonga Group which comprises a volcano-sedimentary complex with  
148 bimodal magmatism (Jacob et al., 2008). Westwards the Southern Irumide Belt is a

149 structurally and metamorphically complex region of mainly Mesoproterozoic igneous  
150 rocks related to a voluminous 1090–1040 Ma continental arc-related magmatic rocks,  
151 accompanied by high-temperature/low-pressure metamorphism (Fritz et al., 2013).

152 Southern of the Lurio belt the Nampula Complex forms a large contiguous  
153 crustal block which consists of 1150–1030 Ma orthogneisses and metasedimentary  
154 rocks with high grade metamorphism around 1090–1030 Ma (Bingen et al., 2009;  
155 Macey et al., 2010). The ortogneisses from SW segment of the Nampula Complex (Fig.  
156 1) are interpreted as remnants of Mesoproterozoic continental magmatic arch (*ca.* 1100  
157 Ma; Chaúque, 2012). Over the Nampula Complex there are the tectonic emplaced  
158 Monapo and Mugeba granulite facies klippen that are assumed as equivalents of the  
159 Cabo Delgado nappes (Macey et al., 2007), considered to be erosional remnants of a  
160 larger and widespread nappe structure (Viola et al., 2008; Macey et al., 2013), which is  
161 improved by the absence of granulite-facies rocks in the underlying Nampula Complex.  
162 The Monapo Klippe consists dominantly of a mélange of granulite gneiss, deformed at  
163 634 ± 8 Ma and intruded by ultramafic and mafic gneisses and alkaline granitic rocks  
164 (637 ± 5 Ma; Macey et al., 2013).

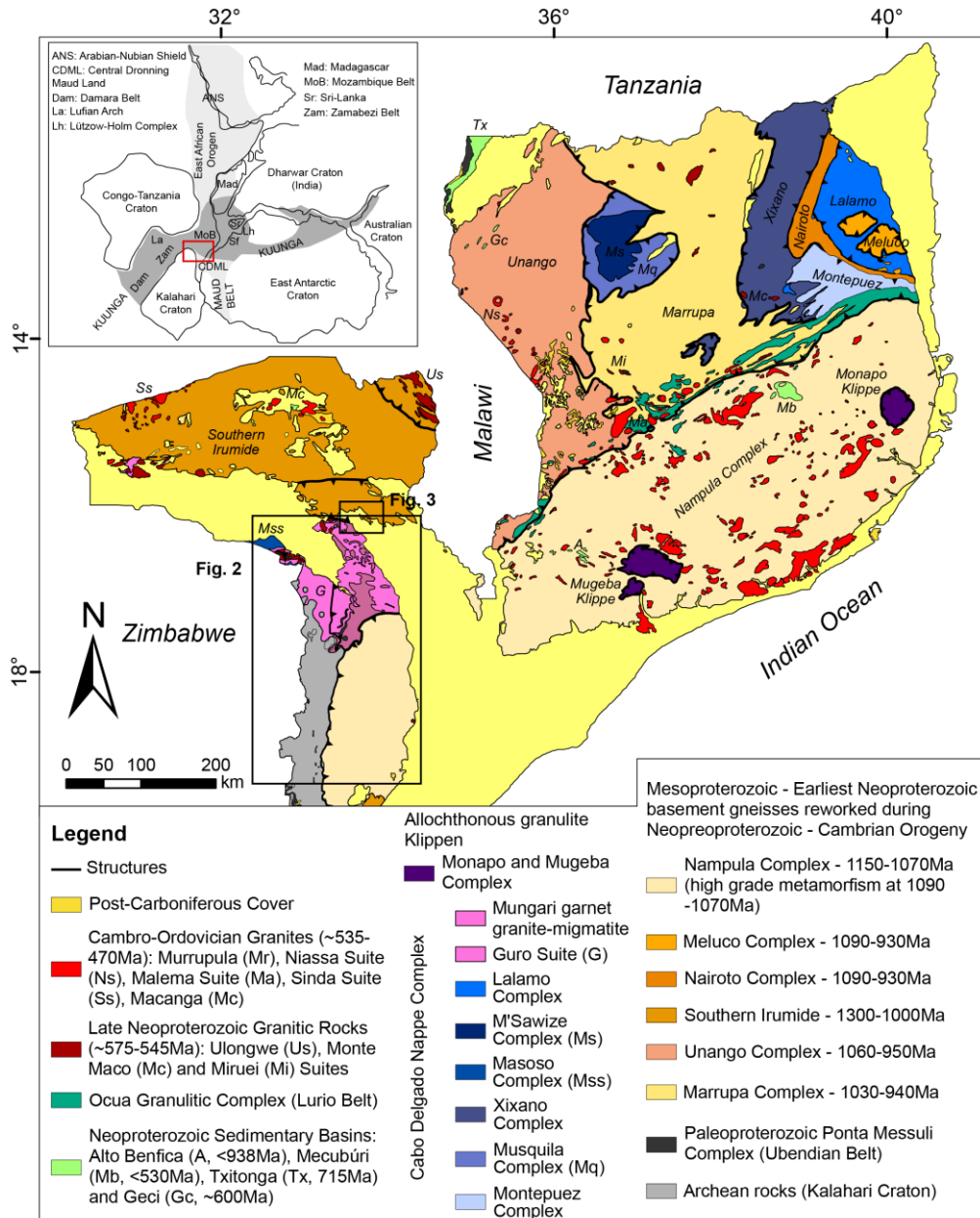
165 These rocks are overlain by isolated Neoproterozoic metamorphosed molasse  
166 sediments (Fig. 1; Thomas et al., 2010; Chaúque, 2012). In the northeast section of NC  
167 the Mecubúri and Alto Benfica Groups are considered to be an autochthonous Cambrian  
168 meta-sedimentary cover of the Nampula Complex (Thomas et al., 2010). U–Pb analyses  
169 of detrital zircons from samples of the Mecubúri Group constrain a maximum  
170 deposition age of 530 ± 18 Ma, with zircon rims and metamorphic monazite grains  
171 dated at *ca.* 500 ± 10 and 499 ± 15 Ma respectively. Dating of detrital zircons from  
172 the Mecuburi Group indicate source rocks with ages peaking between *ca.* 1100–950 Ma,

173 750–800 Ma and 700–530 Ma, similar to the crystallisation ages in the Unango and  
174 Marrupa Complexes (Thomas et al., 2010).

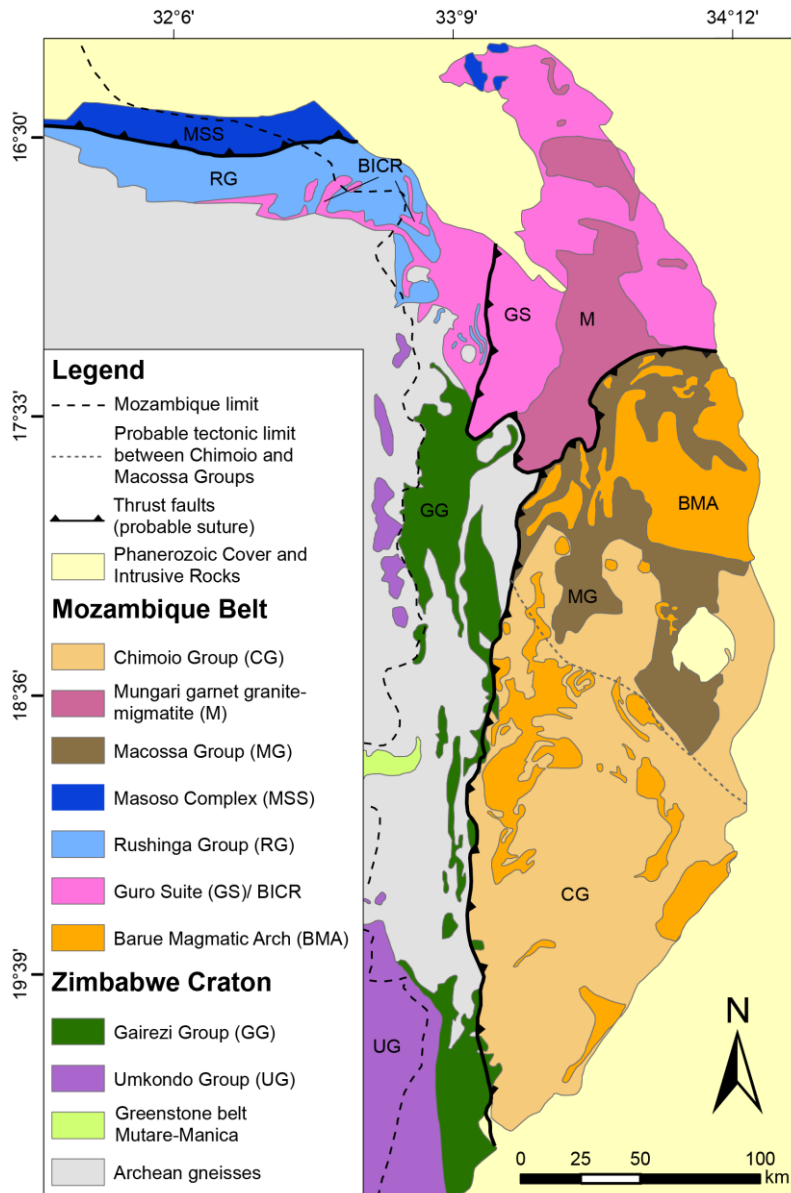
175 The southwest Nampula Complex (Fig. 2) is attributed to the frontal nappes of  
176 Chimoio-Macossa and Mungari Groups (Chaúque, 2012), consisting of low- to high-  
177 grade paragneisses. The first is associated with the Barue magmatic arc represented by  
178 orthomagmatic rocks (*ca.* 1100 Ma; Fig. 2). These are in direct tectonic contact with the  
179 Kalahari cratonic rocks. The Mungari nappe includes the Guro Suite associations, which  
180 comprise abundant Neoproterozoic bimodal intrusive association (Fig. 2), characterize  
181 the east-dipping outer rim of the craton margin in the north (Chaúque et al., 2017). The  
182 felsic component dominantly consists of foliated aplitic granites, while the mafic one  
183 corresponds to metagabbro, locally deformed into mafic gneiss or schist with intruding  
184 pegmatite. Zircon grains from Granitic rocks indicate a magmatic crystallization age of  
185  $867 \pm 15$  Ma. Dating of the nucleus of metamorphic zircons show recrystallization ages  
186 at *ca.* 850 – 839 Ma, related to extensional faulting, while the metamorphic rims  
187 provided an age of  $512 \pm 4$  Ma related to the Pan-African Orogeny (GTK Consortium  
188 2006). At the northeastern margin of the cratonic area occur the low to medium grade  
189 metasedimentary and felsic metavolcanic (*ca.* 800 Ma) rocks of the Rushinga Group  
190 which may represent a passive margin of Neoproterozoic age (Barton et al., 1991;  
191 Hargrove et al., 2003; GTK Consortium 2006; Chaúque, 2012).

192 Protracted collisional orogenesis was followed by the intrusion of late- to post  
193 tectonic Late Neoproterozoic granites (ca. 575–545 Ma) and Cambrian-Ordovician K-  
194 granites (ca. 530–495 Ma) (Macey et al., 2007; Jacobs et al., 2008; Ueda et al., 2012;  
195 Macey et al., 2013; Grantham et al., 2013). The latter is pronounced in the eastern  
196 Nampula Complex (Fig. 1) due to crustal delamination process that led to protract  
197 cooling history during Cambrian-Ordovician Times (Jacob et al., 2008; Emmel et al.,

198 2014). These Precambrian-Cambrian basement rocks were partially covered by the  
 199 Phanerozoic volcano-sedimentary deposits of the Karoo Supergroup and younger  
 200 sequences (GTK Consortium, 2006).



201  
 202 Figure 1: Simplified geological map of north Mozambique modified from Macey et al.  
 203 (2013) showing the main lithostratigraphic units. In top is shown the reconstruction of  
 204 Gondwana during the Cambrian after Meert (2003), with the locations of the East  
 205 African Orogen and Kuunga Orogen and in the bottom the location of the geological  
 206 map presented in the southern of Africa.



207  
208 Figure 2: Geological and tectonic map of the SW section of the Nampula Complex in  
209 the contact with the cratonic margin (after GTK Consortium 2006 and Chaúque et al.,  
210 2017). BICR = Basal Intrusive Complex of de Rushinga.

211

212 **2.1 Geology of the Matinde Formation**

213 The Matinde Formation generally comprises continental sedimentation during  
214 Permian-Triassic (mostly Triassic; Pereira et al., 2016) and represents one of the Karoo  
215 Supergroup deposits of northern Mozambique. This sequence is host in an NW-striking  
216 intracontinental rift basin, locally called as Moatize-Minjova Basin (Fig. 3). The rift

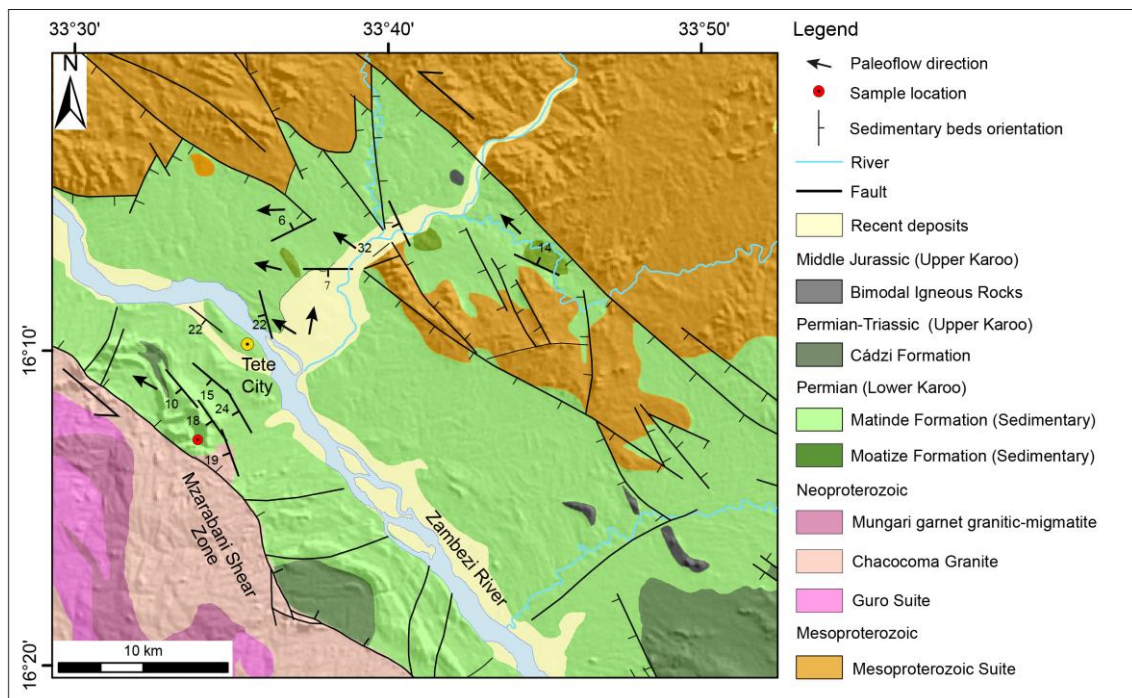
217 is limited by Precambrian structures and basin evolution follows distinct reactivation  
218 periods occurred in Phanerozoic times (Castaing, 1991; GTK Consortium, 2006;  
219 Fernandes et al., 2015; Bicca et al., 2017), under a transtensional stress regime  
220 associated with the NW-SE sinistral Zambezi pre-transform fault system (Castaing,  
221 1991; Bicca et al., 2017). The structural control over sedimentation is evidenced by  
222 depositional cycles of the Moatize and Matinde Formations.

223 The Moatize Formation is made of interbedded carbonaceous mudstones,  
224 mudstones, rhythmites, sandstones and cyclic coal deposits (Cairncross, 2001;  
225 Lakshminarayana, 2015; Bicca et al., 2017) and its lithofacies assemblages are  
226 interpreted as a meandering fluvial system (Bicca et al., 2017). The coal beds represents  
227 thick peat deposits (ca. < 40m) interbedded with very thick flood plain fines sequences  
228 (ca. < 100m) (Fig. 4; Bicca et al., 2017). The absolute age of these coal-bearing  
229 formation is not well constrained and most comes from palynological record which  
230 suggests a Lower to Middle Permian age for the top part of the Moatize Formation  
231 (Daber, 1984). Although, Pereira et al. (2014) founded a Kungurian/Roadian age  
232 (Lower – Middle Permian) for the basal sequences of the Moatize Formation,  
233 positioning its depositional cycle throughout the Early-Late Permian.

234 Overlaying the Moatize Formation there are mostly cross-bedded coarse-grained  
235 alluvial deposits from the Matinde, its being assumed a depositional age close to the  
236 Permian-Triassic boundary but most of the depositional cycle relies in the Triassic  
237 period (Pereira et al., 2016). This formation is attributed to a braided fluvial plain  
238 system mostly represented by coarse to conglomeratic red sandstones (Fig. 4). Planar  
239 and through-cross bedding are the most common structures, separated in sets of ca. 0.5  
240 to 2 meters by planar surfaces (GTK Consortium, 2006; Bicca et al., 2017). Lithofacies  
241 associations and its internal relationship suggest deposition of poorly channelized

242 braided alluvial plain in which downstream and probably lateral accretion macroforms  
 243 alternates with gravity flow deposits (Bicca et al., 2017). Northwestwards paleoflow  
 244 from Moatize and Matinde lithofacies suggest that the Zambezi River flow was inverted  
 245 during Permian sedimentation in northern Mozambique, with its headwaters located in  
 246 the southeastern highland areas, inherited from the Pan-African Orogeny (Key et al.,  
 247 2015; Bicca et al., 2017).

248



249

250 Figure 3: Simplified geological and structural map of the Moatize-Minjova Basin and  
 251 sample location (modified from Bicca et al., 2017).

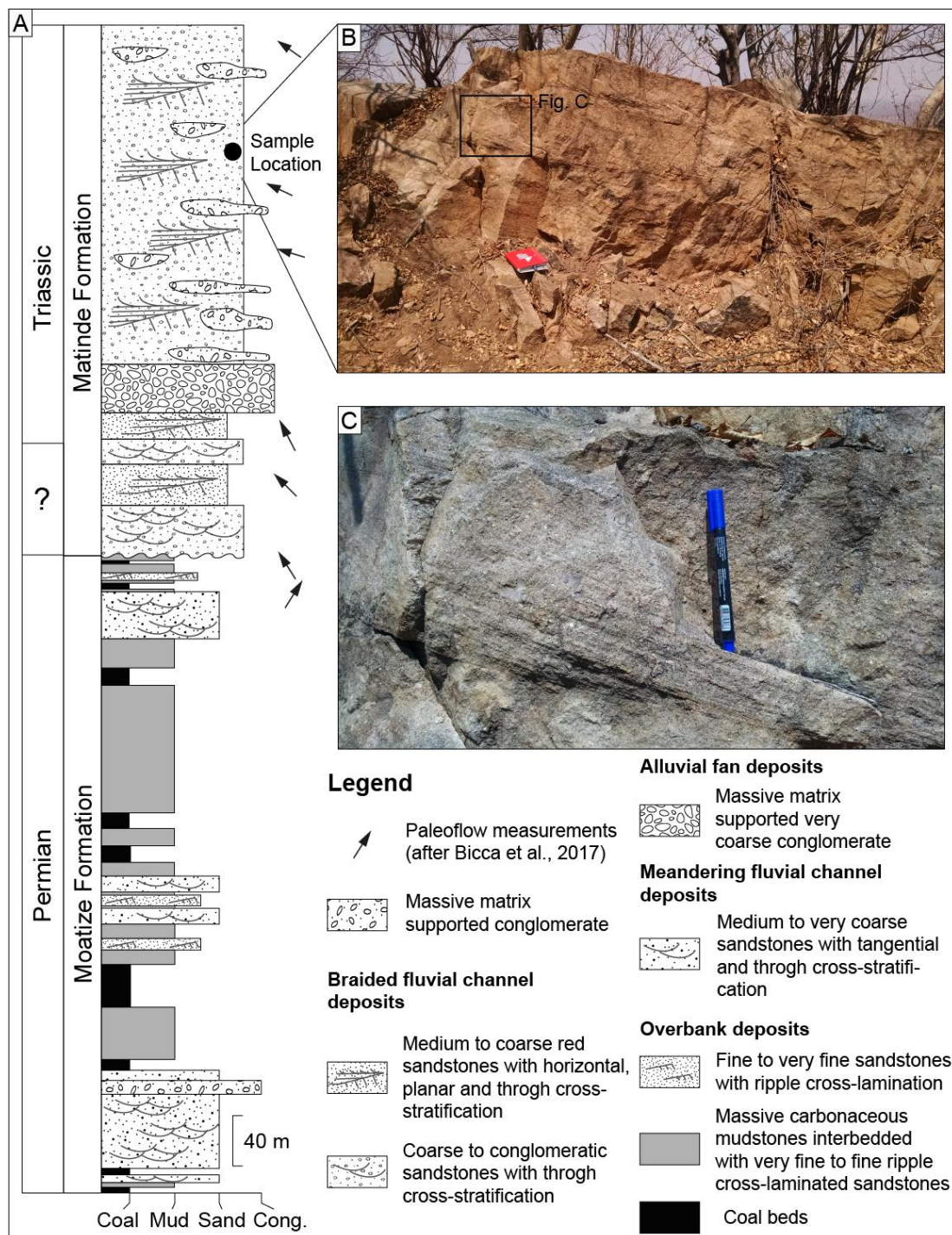
252

253

254

255

256



258 Figure 4: A) Schematic profile of the Moatize and Matinde Formations; B) Through and  
259 planar cross-bedded coarse sandstones from where we took the sample; C) detail of the  
260 coarse sandstone with quartz clasts (modified from Bicca et al., 2017).

261

262

263

264     **3. Methods**

265       We collected one sample from a coarse-sandstone of Matinde Formation  
266       exposed in the study area at coordinates 16°12'22.57"S and 33°34'5.09"E (Fig. 3 and  
267       Fig. 4). The outcrop is the top of a 300 m high profile that has thick (1–2 m) sets of  
268       coarse-sandstones and conglomerates with a fining upward pattern. This sequence  
269       marks an important process of rejuvenation in the source area, as indicated by the  
270       Permian-Triassic depositional pattern (Fig. 4) and show excellent levels of outcrop  
271       preservation in terms of weathering, tectonic and any hydrothermal processes, difficult  
272       to find in the region. In addition, more mature sandstones tend to does not preserve  
273       metamorphic overgrowths due to abrasion during transport (Hartmann and Santos,  
274       2004).

275       Mineral separation was carried out at Rio Grande do Sul Federal University,  
276       using standard procedures of crushing the rock, milling and sieving. Zircons were  
277       separated using conventional heavy liquids and magnetic procedures, hand-picked and  
278       mounted on an epoxy disc, together with CZ3 (564 Ma) zircon standards and polished  
279       to expose their internal surfaces.

280       U-Pb analysis was performed with laser-ablation multi-collector inductively  
281       coupled plasma mass spectrometry (LA-MC-ICP-MS) at São Paulo University. All  
282       grains used for zircon dating were imaged with cathodoluminescence to determine their  
283       internal structures and crystallization phases (to support spot location and age  
284       interpretation). Only zircon grains free of imperfections such as fractures and mineral  
285       inclusions were selected for analysis (Fig. 5). The analytical conditions and data  
286       reduction for the LA-MC-ICPMS method were identical to those described by Chemale  
287       Jr. et al. (2011). Isoplot 3 software (Ludwig, 2003) was used to generate the concordia  
288       diagrams and histograms. For the concordia age calculations and frequency histograms,

289 only the analysis with  $100 \pm 10\%$  of concordance was included. The U-Pb detrital  
290 zircon analytical data are show in Table 1. Corrections for common Pb were made using  
291 measured  $^{204}\text{Pb}$  and the Pb isotopic composition. Results with more than 1% common  
292 Pb correction were not use to calculate the ages. Confidence limits (90%) were  
293 compiled for pooled ages and one sigma limits for individual zircons. Ages older than  
294 1.5 Ga are express as weighed mean  $^{207}\text{Pb}/^{206}\text{Pb}$  age values, and younger ages are  
295 weighed mean  $^{204}\text{Pb}/^{235}\text{U}$  values. The analytical results were compared with the  
296 geological, isotopic, and geochronological data available in the literature (Macey et al.,  
297 2010; Thomas et al., 2010; Manjate, 2011; Chaúque, 2012; Manjate, 2015; Chaúque et  
298 al., 2017).

299

300

301

302

303

304

305

306

307

308

309

310

311

312

313

314 Table 1: U/Pb data of Matinde Formation

| Spot | RATIOS  |        |         |         |               |         |         |         |         |         |         |          | AGES |      |                      |            |                      |            |                      |         |     |     | Conc. | Conc. |
|------|---------|--------|---------|---------|---------------|---------|---------|---------|---------|---------|---------|----------|------|------|----------------------|------------|----------------------|------------|----------------------|---------|-----|-----|-------|-------|
|      | 207/235 | 1sigma | 206/238 | 1 sigma | coef.<br>corr | 238/206 | 1 sigma | 207/206 | 1 sigma | 208/206 | 1 sigma | Pb total | U    | Th/U | T <sub>206/238</sub> | 1<br>sigma | T <sub>207/235</sub> | 1<br>sigma | T <sub>207/206</sub> | 1 sigma |     |     |       |       |
|      |         |        |         |         |               |         |         |         |         |         |         | comum    | ppm  | %    |                      |            |                      |            |                      |         |     |     |       |       |
| 10.1 | 0.6295  | 0.0185 | 0.0794  | 0.0008  | 0.60          | 12.5913 | 0.1275  | 0.0575  | 0.0017  | 0.2035  | 0.0038  | 0.16     | 582  | 0.57 | 0.493                | 0.005      | 0.496                | 0.011      | 0.510                | 0.065   | 99  | 96  |       |       |
| 26.1 | 0.6363  | 0.0201 | 0.0795  | 0.0014  | 0.26          | 12.5722 | 0.2254  | 0.0580  | 0.0020  | 0.1055  | 0.0038  | 0.86     | 431  | 0.27 | 0.493                | 0.009      | 0.500                | 0.013      | 0.530                | 0.078   | 98  | 93  |       |       |
| 2.1  | 0.6239  | 0.0360 | 0.0797  | 0.0012  | 0.68          | 12.5430 | 0.1863  | 0.0568  | 0.0035  | 0.1386  | 0.0127  | 0.29     | 160  | 0.43 | 0.494                | 0.007      | 0.492                | 0.023      | 0.482                | 0.139   | 100 | 102 |       |       |
| 38.1 | 0.6404  | 0.0223 | 0.0810  | 0.0014  | 0.35          | 12.3513 | 0.2140  | 0.0574  | 0.0022  | 0.1803  | 0.0067  | 0.58     | 279  | 0.54 | 0.502                | 0.008      | 0.503                | 0.014      | 0.506                | 0.081   | 99  | 99  |       |       |
| 18.1 | 0.6429  | 0.0177 | 0.0811  | 0.0014  | 0.85          | 12.3291 | 0.2130  | 0.0575  | 0.0017  | 0.0692  | 0.0026  | 0.78     | 541  | 0.37 | 0.503                | 0.008      | 0.504                | 0.011      | 0.510                | 0.065   | 99  | 98  |       |       |
| 43.1 | 0.6592  | 0.0229 | 0.0820  | 0.0009  | 0.64          | 12.2003 | 0.1330  | 0.0583  | 0.0021  | 0.0467  | 0.0041  | 0.79     | 468  | 0.11 | 0.508                | 0.005      | 0.514                | 0.014      | 0.542                | 0.080   | 98  | 93  |       |       |
| 3.1  | 0.6695  | 0.0246 | 0.0833  | 0.0010  | 0.01          | 12.0082 | 0.1373  | 0.0583  | 0.0022  | 0.1090  | 0.0060  | 0.24     | 363  | 0.37 | 0.516                | 0.006      | 0.520                | 0.015      | 0.541                | 0.084   | 99  | 95  |       |       |
| 48.1 | 0.7159  | 0.0813 | 0.0869  | 0.0021  | 0.56          | 11.5019 | 0.2841  | 0.0597  | 0.0074  | 0.3552  | 0.0258  | 1.10     | 90   | 0.98 | 0.537                | 0.013      | 0.548                | 0.048      | 0.593                | 0.273   | 98  | 90  |       |       |
| 4.1  | 0.7180  | 0.0575 | 0.0889  | 0.0017  | 0.10          | 11.2453 | 0.2132  | 0.0586  | 0.0051  | 0.1304  | 0.0157  | 0.89     | 88   | 0.37 | 0.549                | 0.010      | 0.549                | 0.034      | 0.551                | 0.190   | 99  | 99  |       |       |
| 24.1 | 0.7374  | 0.0552 | 0.0913  | 0.0025  | 0.45          | 10.9587 | 0.3032  | 0.0586  | 0.0051  | 0.1226  | 0.0174  | 2.33     | 110  | 0.29 | 0.563                | 0.015      | 0.561                | 0.031      | 0.553                | 0.175   | 100 | 101 |       |       |
| 61.1 | 0.7512  | 0.0919 | 0.0912  | 0.0028  | 0.50          | 10.9672 | 0.3412  | 0.0598  | 0.0086  | 0.2056  | 0.0206  | 0.82     | 59   | 0.49 | 0.563                | 0.017      | 0.569                | 0.056      | 0.595                | 0.343   | 98  | 94  |       |       |
| 39.1 | 0.7609  | 0.0403 | 0.0919  | 0.0020  | 0.03          | 10.8827 | 0.2349  | 0.0601  | 0.0035  | 0.4045  | 0.0181  | 0.41     | 103  | 1.12 | 0.567                | 0.012      | 0.575                | 0.023      | 0.606                | 0.126   | 98  | 93  |       |       |
| 20.1 | 0.7574  | 0.0420 | 0.0922  | 0.0022  | 0.23          | 10.8506 | 0.2607  | 0.0596  | 0.0038  | 0.0217  | 0.0132  | 0.74     | 123  | 0.07 | 0.568                | 0.013      | 0.573                | 0.024      | 0.589                | 0.145   | 99  | 96  |       |       |
| 4.1  | 0.7812  | 0.0479 | 0.0965  | 0.0017  | 0.51          | 10.3590 | 0.1871  | 0.0587  | 0.0041  | 0.1464  | 0.0185  | 0.76     | 102  | 0.32 | 0.594                | 0.010      | 0.586                | 0.027      | 0.556                | 0.144   | 101 | 106 |       |       |
| 22.1 | 0.7790  | 0.0583 | 0.0966  | 0.0024  | 0.47          | 10.3558 | 0.2587  | 0.0585  | 0.0053  | 0.0863  | 0.0201  | 0.78     | 65   | 0.21 | 0.594                | 0.014      | 0.585                | 0.032      | 0.549                | 0.182   | 101 | 108 |       |       |
| 3.1  | 0.8077  | 0.0300 | 0.0977  | 0.0012  | 0.01          | 10.2398 | 0.1293  | 0.0600  | 0.0024  | 0.0365  | 0.0082  | 0.81     | 176  | 0.09 | 0.601                | 0.007      | 0.601                | 0.017      | 0.603                | 0.087   | 99  | 99  |       |       |
| 14.1 | 0.8353  | 0.0430 | 0.0992  | 0.0019  | 0.28          | 10.0815 | 0.1920  | 0.0611  | 0.0036  | 0.1100  | 0.0094  | 0.69     | 112  | 0.27 | 0.610                | 0.011      | 0.617                | 0.023      | 0.642                | 0.127   | 98  | 94  |       |       |
| 2.1  | 0.8201  | 0.0400 | 0.0994  | 0.0015  | 0.15          | 10.0562 | 0.1553  | 0.0598  | 0.0033  | 0.0981  | 0.0116  | 0.48     | 108  | 0.25 | 0.611                | 0.009      | 0.608                | 0.023      | 0.597                | 0.125   | 100 | 102 |       |       |
| 19.1 | 0.8399  | 0.0627 | 0.0994  | 0.0026  | 0.24          | 10.0605 | 0.2620  | 0.0613  | 0.0053  | 0.1099  | 0.0210  | 0.98     | 61   | 0.28 | 0.611                | 0.015      | 0.619                | 0.034      | 0.649                | 0.185   | 98  | 94  |       |       |
| 11.1 | 0.8281  | 0.0725 | 0.0999  | 0.0029  | 0.01          | 10.0060 | 0.2914  | 0.0601  | 0.0067  | 0.1275  | 0.0161  | 1.15     | 49   | 0.34 | 0.614                | 0.017      | 0.613                | 0.039      | 0.607                | 0.223   | 100 | 101 |       |       |
| 5.1  | 0.8876  | 0.0368 | 0.1039  | 0.0014  | 0.38          | 9.6246  | 0.1331  | 0.0620  | 0.0029  | 0.0919  | 0.0079  | 0.42     | 124  | 0.23 | 0.637                | 0.008      | 0.645                | 0.020      | 0.673                | 0.099   | 98  | 94  |       |       |
| 32.1 | 1.7145  | 0.0550 | 0.1687  | 0.0030  | 0.17          | 5.9278  | 0.1054  | 0.0737  | 0.0025  | 0.0977  | 0.0058  | 0.34     | 121  | 0.28 | 1.005                | 0.017      | 1.014                | 0.021      | 1.034                | 0.069   | 99  | 97  |       |       |
| 15.1 | 1.7167  | 0.0653 | 0.1694  | 0.0035  | 0.27          | 5.9019  | 0.1233  | 0.0735  | 0.0032  | 0.1125  | 0.0076  | 0.90     | 104  | 0.30 | 1.009                | 0.020      | 1.015                | 0.025      | 1.027                | 0.088   | 99  | 98  |       |       |
| 8.1  | 1.8024  | 0.0873 | 0.1721  | 0.0026  | 0.61          | 5.8089  | 0.0875  | 0.0759  | 0.0040  | 0.1626  | 0.0100  | 0.56     | 74   | 0.44 | 1.024                | 0.014      | 1.046                | 0.031      | 1.093                | 0.102   | 97  | 93  |       |       |
| 58.1 | 1.8008  | 0.1107 | 0.1729  | 0.0037  | 0.58          | 5.7848  | 0.1248  | 0.0756  | 0.0053  | 0.1673  | 0.0188  | 0.24     | 78   | 0.39 | 1.028                | 0.020      | 1.046                | 0.041      | 1.083                | 0.146   | 98  | 94  |       |       |
| 9.1  | 1.7779  | 0.0629 | 0.1736  | 0.0021  | 0.35          | 5.7613  | 0.0698  | 0.0743  | 0.0028  | 0.0937  | 0.0061  | 0.38     | 123  | 0.27 | 1.032                | 0.012      | 1.037                | 0.023      | 1.049                | 0.075   | 99  | 98  |       |       |
| 57.1 | 1.7523  | 0.0649 | 0.1739  | 0.0027  | 0.86          | 5.7502  | 0.0886  | 0.0731  | 0.0031  | 0.0796  | 0.0097  | 1.02     | 110  | 0.21 | 1.034                | 0.015      | 1.028                | 0.024      | 1.016                | 0.085   | 100 | 101 |       |       |

|      |        |        |        |        |      |         |        |        |        |        |        |       |     |      |       |       |       |       |       |       |     |     |
|------|--------|--------|--------|--------|------|---------|--------|--------|--------|--------|--------|-------|-----|------|-------|-------|-------|-------|-------|-------|-----|-----|
| 6.1  | 1.8105 | 0.0680 | 0.1763 | 0.0022 | 0.39 | 5.6726  | 0.0704 | 0.0745 | 0.0030 | 0.1645 | 0.0079 | 1.05  | 120 | 0.48 | 1.047 | 0.012 | 1.049 | 0.024 | 1.055 | 0.077 | 99  | 99  |
| 7.1  | 1.8444 | 0.0507 | 0.1773 | 0.0018 | 0.87 | 5.6397  | 0.0582 | 0.0754 | 0.0021 | 0.0687 | 0.0030 | 0.34  | 245 | 0.20 | 1.052 | 0.010 | 1.061 | 0.018 | 1.080 | 0.055 | 99  | 97  |
| 62.1 | 1.8698 | 0.2047 | 0.1776 | 0.0059 | 0.17 | 5.6315  | 0.1872 | 0.0764 | 0.0103 | 0.1020 | 0.0439 | 1.24  | 21  | 0.19 | 1.054 | 0.032 | 1.070 | 0.073 | 1.105 | 0.267 | 98  | 95  |
| 50.1 | 1.8397 | 0.0510 | 0.1780 | 0.0024 | 0.65 | 5.6189  | 0.0752 | 0.0750 | 0.0022 | 0.0334 | 0.0051 | 0.23  | 181 | 0.09 | 1.056 | 0.013 | 1.060 | 0.018 | 1.068 | 0.059 | 99  | 98  |
| 19.1 | 1.8481 | 0.0736 | 0.1796 | 0.0039 | 0.19 | 5.5687  | 0.1203 | 0.0746 | 0.0034 | 0.1615 | 0.0129 | 0.21  | 116 | 0.46 | 1.065 | 0.021 | 1.063 | 0.026 | 1.059 | 0.090 | 100 | 100 |
| 29.1 | 1.8922 | 0.0622 | 0.1796 | 0.0033 | 0.83 | 5.5674  | 0.1014 | 0.0764 | 0.0027 | 0.1804 | 0.0089 | 0.75  | 93  | 0.48 | 1.065 | 0.018 | 1.078 | 0.022 | 1.106 | 0.069 | 98  | 96  |
| 14.1 | 1.9051 | 0.0462 | 0.1822 | 0.0031 | 0.67 | 5.4895  | 0.0922 | 0.0759 | 0.0020 | 0.2022 | 0.0222 | 0.22  | 356 | 0.46 | 1.079 | 0.017 | 1.083 | 0.016 | 1.091 | 0.053 | 99  | 98  |
| 49.1 | 1.9065 | 0.1046 | 0.1821 | 0.0030 | 0.53 | 5.4906  | 0.0915 | 0.0759 | 0.0044 | 0.1387 | 0.0163 | 0.51  | 71  | 0.32 | 1.079 | 0.016 | 1.083 | 0.036 | 1.093 | 0.117 | 99  | 98  |
| 16.1 | 1.9308 | 0.0516 | 0.1836 | 0.0032 | 0.78 | 5.4460  | 0.0956 | 0.0763 | 0.0023 | 0.5575 | 0.0116 | 0.22  | 222 | 1.57 | 1.087 | 0.018 | 1.092 | 0.018 | 1.102 | 0.059 | 99  | 98  |
| 56.1 | 2.0298 | 0.1413 | 0.1860 | 0.0045 | 0.26 | 5.3754  | 0.1303 | 0.0791 | 0.0063 | 0.1846 | 0.0214 | 1.81  | 34  | 0.48 | 1.100 | 0.024 | 1.126 | 0.048 | 1.175 | 0.166 | 97  | 93  |
| 13.1 | 2.0193 | 0.1078 | 0.1867 | 0.0031 | 0.33 | 5.3561  | 0.0894 | 0.0784 | 0.0045 | 0.2491 | 0.0248 | 0.87  | 66  | 0.79 | 1.103 | 0.017 | 1.122 | 0.036 | 1.158 | 0.114 | 98  | 95  |
| 37.1 | 1.9935 | 0.0725 | 0.1916 | 0.0037 | 0.07 | 5.2193  | 0.1001 | 0.0755 | 0.0030 | 0.2283 | 0.0138 | 0.56  | 79  | 0.66 | 1.130 | 0.020 | 1.113 | 0.025 | 1.081 | 0.082 | 101 | 104 |
| 17.1 | 1.6549 | 0.0399 | 0.1642 | 0.0027 | 0.81 | 6.0887  | 0.1005 | 0.0731 | 0.0019 | 0.1231 | 0.0026 | 0.14  | 338 | 0.33 | 0.980 | 0.015 | 0.991 | 0.016 | 1.016 | 0.054 | 98  | 96  |
| 27.1 | 2.0292 | 0.0633 | 0.1906 | 0.0034 | 0.58 | 5.2472  | 0.0930 | 0.0772 | 0.0025 | 0.1854 | 0.0091 | 0.42  | 120 | 0.48 | 1.125 | 0.018 | 1.125 | 0.021 | 1.127 | 0.065 | 99  | 99  |
| 1.1  | 1.7282 | 0.0472 | 0.1688 | 0.0017 | 0.72 | 5.9229  | 0.0606 | 0.0742 | 0.0021 | 0.0788 | 0.0070 | 0.15  | 266 | 0.23 | 1.006 | 0.010 | 1.019 | 0.018 | 1.048 | 0.056 | 98  | 95  |
| 12.1 | 1.5501 | 0.2015 | 0.1584 | 0.0051 | 0.62 | 6.3144  | 0.2042 | 0.0710 | 0.0107 | 0.1344 | 0.0343 | 2.98  | 38  | 0.33 | 0.948 | 0.029 | 0.951 | 0.079 | 0.957 | 0.289 | 99  | 99  |
| 52.1 | 1.6287 | 0.0665 | 0.1614 | 0.0027 | 0.55 | 6.1942  | 0.1024 | 0.0732 | 0.0033 | 0.0648 | 0.0092 | 0.99  | 88  | 0.20 | 0.965 | 0.015 | 0.981 | 0.026 | 1.019 | 0.093 | 98  | 94  |
| 25.1 | 0.8448 | 0.0515 | 0.0994 | 0.0026 | 0.21 | 10.0585 | 0.2581 | 0.0616 | 0.0043 | 0.1136 | 0.0127 | 0.54  | 105 | 0.32 | 0.611 | 0.015 | 0.622 | 0.028 | 0.661 | 0.149 | 98  | 92  |
| 40.1 | 1.1581 | 0.0709 | 0.1279 | 0.0021 | 0.95 | 7.8210  | 0.1285 | 0.0657 | 0.0042 | 0.1028 | 0.0323 | 2.33  | 115 | 0.15 | 0.776 | 0.012 | 0.781 | 0.032 | 0.796 | 0.128 | 99  | 97  |
| 23.1 | 1.2064 | 0.1164 | 0.1321 | 0.0047 | 0.15 | 7.5683  | 0.2718 | 0.0662 | 0.0077 | 0.1982 | 0.0381 | 1.72  | 35  | 0.49 | 0.800 | 0.027 | 0.804 | 0.054 | 0.813 | 0.241 | 99  | 98  |
| 5.1  | 1.3690 | 0.0657 | 0.1425 | 0.0020 | 0.66 | 7.0161  | 0.0998 | 0.0697 | 0.0038 | 0.3083 | 0.0160 | 0.59  | 117 | 0.99 | 0.859 | 0.011 | 0.876 | 0.028 | 0.918 | 0.105 | 98  | 93  |
| 28.1 | 1.5429 | 0.0430 | 0.1556 | 0.0026 | 0.89 | 6.4265  | 0.1055 | 0.0719 | 0.0021 | 0.1365 | 0.0060 | 1.22  | 237 | 0.38 | 0.932 | 0.014 | 0.948 | 0.017 | 0.983 | 0.058 | 98  | 94  |
| 1.1  | 0.6319 | 0.0381 | 0.0787 | 0.0014 | 0.13 | 12.7088 | 0.2261 | 0.0582 | 0.0040 | 0.1765 | 0.0166 | 2.14  | 104 | 0.43 | 0.488 | 0.008 | 0.497 | 0.024 | 0.539 | 0.152 | 98  | 90  |
| 23.1 | 0.7111 | 0.0210 | 0.0886 | 0.0011 | 0.87 | 11.2915 | 0.1374 | 0.0582 | 0.0020 | 0.0882 | 0.0201 | 0.00  | 321 | 0.27 | 0.547 | 0.006 | 0.545 | 0.012 | 0.539 | 0.074 | 100 | 101 |
| 13.1 | 1.3414 | 0.1158 | 0.1403 | 0.0047 | 0.50 | 7.1285  | 0.2386 | 0.0693 | 0.0066 | 0.0565 | 0.0529 | 1.08  | 41  | 0.09 | 0.846 | 0.026 | 0.864 | 0.049 | 0.909 | 0.220 | 97  | 93  |
| 17.1 | 1.6238 | 0.0421 | 0.1599 | 0.0019 | 0.25 | 6.2524  | 0.0757 | 0.0736 | 0.0022 | 0.0955 | 0.0089 | 0.41  | 202 | 0.20 | 0.956 | 0.011 | 0.979 | 0.017 | 1.031 | 0.063 | 97  | 92  |
| 6.1  | 1.7018 | 0.0513 | 0.1688 | 0.0020 | 0.10 | 5.9225  | 0.0705 | 0.0731 | 0.0024 | 0.0992 | 0.0043 | 0.67  | 124 | 0.25 | 1.006 | 0.011 | 1.009 | 0.019 | 1.017 | 0.066 | 99  | 98  |
| 18.1 | 1.7540 | 0.1503 | 0.1748 | 0.0059 | 0.61 | 5.7213  | 0.1947 | 0.0728 | 0.0080 | 0.4657 | 0.0297 | 0.71  | 22  | 1.15 | 1.038 | 0.033 | 1.029 | 0.058 | 1.008 | 0.248 | 100 | 103 |
| 35.1 | 0.6166 | 0.0196 | 0.0784 | 0.0013 | 0.78 | 12.7473 | 0.2134 | 0.0570 | 0.0019 | 0.0988 | 0.0115 | 19.39 | 295 | 0.24 | 0.487 | 0.008 | 0.488 | 0.012 | 0.492 | 0.073 | 99  | 99  |
| 45.1 | 0.7426 | 0.1325 | 0.0889 | 0.0032 | 0.40 | 11.2456 | 0.4036 | 0.0606 | 0.0125 | 0.3608 | 0.0446 | 1.02  | 47  | 0.80 | 0.549 | 0.019 | 0.564 | 0.080 | 0.624 | 0.421 | 97  | 88  |
| 41.1 | 0.8053 | 0.1805 | 0.0951 | 0.0042 | 0.35 | 10.5179 | 0.4657 | 0.0614 | 0.0159 | 0.0603 | 0.0479 | 7.86  | 30  | 0.16 | 0.585 | 0.025 | 0.600 | 0.104 | 0.654 | 0.479 | 97  | 89  |
| 54.1 | 1.1280 | 0.1580 | 0.1222 | 0.0046 | 0.41 | 8.1854  | 0.3049 | 0.0670 | 0.0107 | 0.1429 | 0.0384 | 1.06  | 29  | 0.35 | 0.743 | 0.026 | 0.767 | 0.074 | 0.837 | 0.343 | 96  | 88  |
| 30.1 | 1.4999 | 0.2657 | 0.1515 | 0.0087 | 0.13 | 6.5997  | 0.3811 | 0.0718 | 0.0156 | 0.1374 | 0.0695 | 7.37  | 11  | 0.24 | 0.909 | 0.049 | 0.930 | 0.110 | 0.980 | 0.449 | 97  | 92  |
| 36.1 | 1.4758 | 0.2043 | 0.1588 | 0.0071 | 0.73 | 6.2978  | 0.2805 | 0.0674 | 0.0130 | 0.1269 | 0.0700 | 3.35  | 18  | 0.10 | 0.950 | 0.040 | 0.921 | 0.083 | 0.850 | 0.393 | 103 | 111 |

|      |        |        |        |        |      |        |        |        |        |        |        |      |    |      |       |       |       |       |       |       |     |     |
|------|--------|--------|--------|--------|------|--------|--------|--------|--------|--------|--------|------|----|------|-------|-------|-------|-------|-------|-------|-----|-----|
| 31.1 | 1.7561 | 0.0742 | 0.1664 | 0.0035 | 0.33 | 6.0102 | 0.1281 | 0.0765 | 0.0036 | 0.1645 | 0.0139 | 0.94 | 65 | 0.48 | 0.992 | 0.020 | 1.029 | 0.028 | 1.109 | 0.099 | 96  | 89  |
| 60.1 | 1.7743 | 0.2101 | 0.1798 | 0.0060 | 0.10 | 5.5615 | 0.1866 | 0.0716 | 0.0103 | 0.1238 | 0.0348 | 6.30 | 19 | 0.38 | 1.066 | 0.033 | 1.036 | 0.077 | 0.974 | 0.281 | 102 | 109 |
| 21.1 | 1.1320 | 0.2825 | 0.1239 | 0.0095 | 0.63 | 8.0688 | 0.6181 | 0.0662 | 0.0210 | 0.1929 | 0.0937 | 3.09 | 18 | 0.53 | 0.753 | 0.055 | 0.769 | 0.128 | 0.814 | 0.501 | 97  | 92  |

315 4. Results

Cathodoluminescence (CL) imaging of 64 zircon crystals (Fig. 6) indicate size variation from 100 to 300  $\mu\text{m}$ , but most crystals are 100–200  $\mu\text{m}$ . Some crystals show rounded hedges, but many have irregular shapes; this is consistent with the immature nature of the coarse-sandstone. Rounding of the crystals was attributed to two processes: i) sedimentary abrasion during transport, and ii) preserved metamorphic rims and overgrowths (Fig. 5). The internal textures of the crystals is very complex, with cores often showing oscillatory zoning, surrounded by one or more metamorphic rims or recrystallized zoned patterns. Sector-zoned, relatively homogeneous grains as well as grains with more complex textures also occur. Chaotic textures are common trends in zircons from granulite facies rocks. Concentric zoning, when present, is rather irregular and resembles only weakly the parallel or regular geometry of zoned magmatic zircon. Distinct age populations could be identifying in the core and in metamorphic rims ranging from Late Mesoproterozoic to Cambrian times (Tab. 1 and Fig. 5).

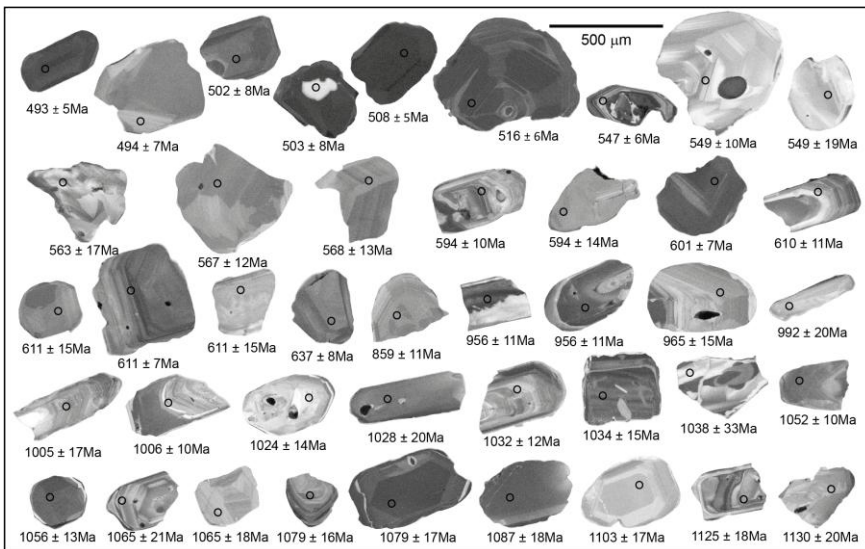


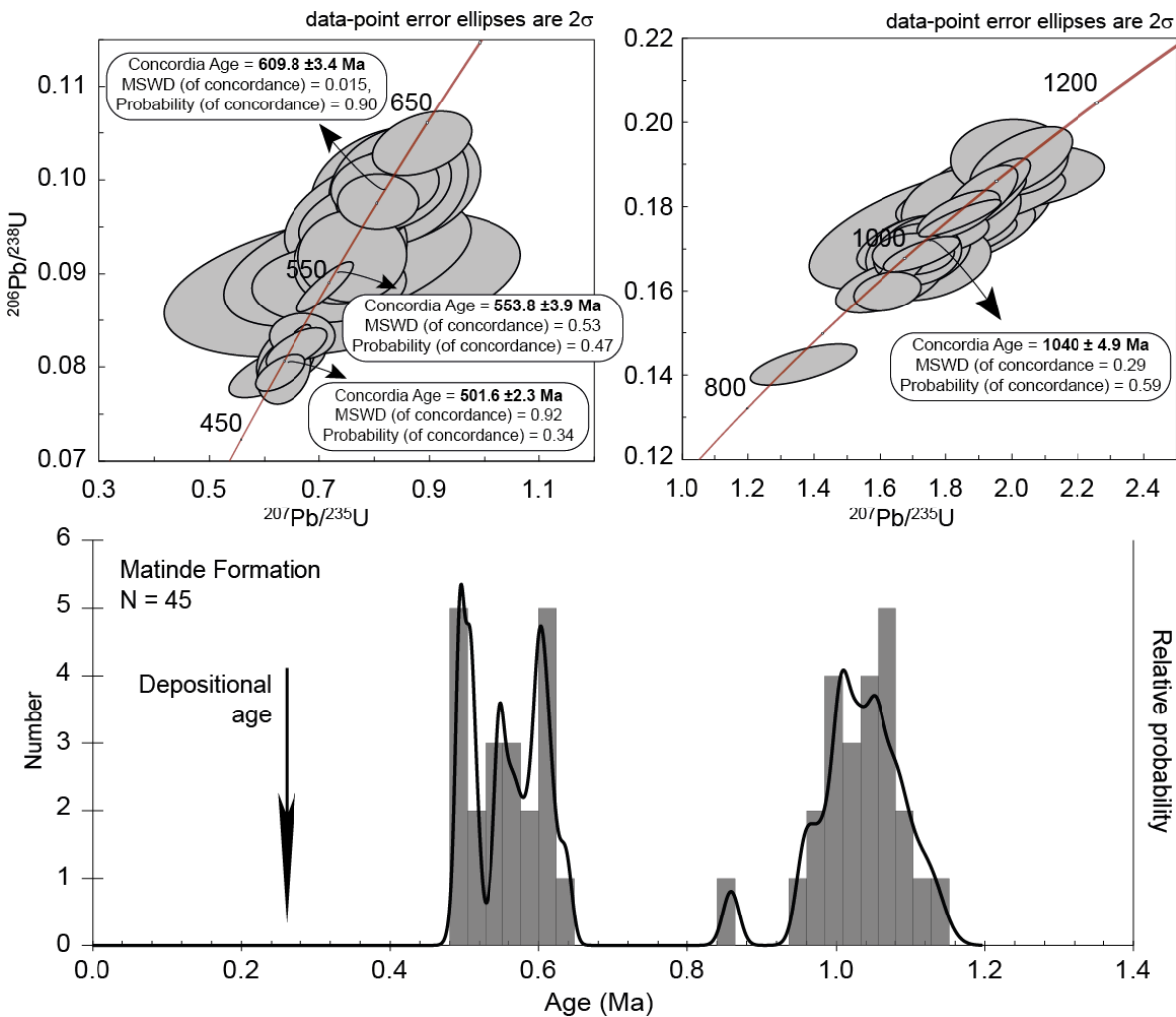
Figure 5: Cathodoluminescence image of some zircon grains that are representative of the analytical results using LA-ICP-MS. The spots and measured U-Pb ages (Ma) are indicated.

332           The older age component is represented by 19 zircon grains providing Late  
333    Mesoproterozoic ages ( $1,005 \pm 17$  Ma to  $1,130 \pm 20$  Ma) with a concordant age of  $1040 \pm$   
334    4.9 Ma ( $N = 7$ ) (Fig. 6). Th/U ratios of these grains are very distinct ranging from 0.09 to  
335    1.57, which is related to the U content of each zircon grain varying from 22 to 356 ppm  
336    (Tab. 1), being the highest Th/U ratios related to an increasing in the U and Th  
337    concentrations. The zircons of this population are commonly rounded fragments of crystal,  
338    but some preserve part of its prismatic form (Fig. 5). Well-developed thin oscillatory  
339    zoning occur in several grains, sometimes surrounding earlier crystallization phases with no  
340    internal texture. Homogeneous metamorphic rims are also preserved in a few grains.

341           A second population of zircon ages constraining the Early-Middle Neoproterozoic  
342    times ( $859 \pm 11$  Ma to  $992 \pm 20$  Ma) were identified from 5 zircon grains (Fig. 7), but did  
343    not allow to define a concordia age. These grains show distinct internal textures indicating  
344    well developed magmatic oscillatory growth in two crystals (Fig. 5). One crystal is  
345    prismatic, but with no evident internal texture and one fragment of zircon showing sector-  
346    zoning with two clear compositionally distinct areas, probably derived from a high-grade  
347    metamorphic rocks (Fig. 5). A last zircon show two homogeneous recrystallization zones  
348    around a elongated lighted nucleus evidencing a probable heritage zircon core. Th-U ratios  
349    are between 0.20 to 0.99, while the U content range from 65 to 338 ppm (Tab. 1), which we  
350    interpreted as magmatic ages, assuming the premises described above.

351           The younger age component from our data comprises the Late Neoproterozoic –  
352    Cambrian ages, from  $637 \pm 8$  Ma to  $493 \pm 5$  Ma. This age population is registered in 21  
353    zircon grains that show oscillatory growing and less metamorphic rims.  
354    Cathodoluminescence imaging reveals both sector-zoned cores with thin overgrowths and  
355    oscillatory zoned cores (Fig. 5). Local zircon resorption and reprecipitation, patchy zoning

356 and fractures disrupting original zoning and filled by zircon with low-trace elements  
357 composition (Corfu et al., 2003; Fig. 5) are also observed. Three main peak ages could be  
358 distinguished from this age component: (1) from 8 zircon grains we determine a magmatic  
359 concordia age of  $609.8 \pm 3.4$  Ma; (2) Six grains define a concordia age of  $553.8 \pm 3.9$  Ma  
360 referring to zircons with oscillatory growth; (3) An younger concordant age of  $501.6 \pm 2.3$   
361 Ma constrained from seven zircon grains mark the late high grade metamorphism of the  
362 Pan-African Orogeny (Fig. 6). Th-U ratios are between 0.07 to 1.12 while the U content  
363 ranges from 47 to 582 ppm (Tab. 1). These concentrations suggest that the ages obtained  
364 are mostly magmatic, but a few grains that present Th/U ratios around 0.1, could be related  
365 to metamorphic processes involved into their generation (Hartmann and Santos, 2004).



366

367 Figure 6: A) Concordia plots ( $^{206}\text{Pb}/^{238}\text{U}$  -  $^{207}\text{Pb}/^{235}\text{U}$ ) of all Late Neoproterozoic ages, with  
 368 the position of three determined concordant ages:  $501 \pm 2.3$  Ma (N = 7);  $553.8 \pm 3.9$  Ma (N  
 369 = 6);  $609.8 \pm 3.4$  Ma (N = 8). B) Concordia plots ( $^{206}\text{Pb}/^{238}\text{U}$  -  $^{207}\text{Pb}/^{235}\text{U}$ ) of all Late  
 370 Mesoproterozoic - Early Neoproterozoic ages with the position of one determined  
 371 concordant ages of  $1040 \pm 4.9$  Ma (N = 7). C) Histogram and relative density plot of all  
 372 detrital ages obtained in this work.

373

## 374 5. Interpretation

375 The detrital zircon age spectra observed in the sample showed only older age's with  
 376 respect to the depositional age that reflect the history of the underlying basement as  
 377 expected in intracratonic settings (Cawood et al., 2012). Zircon morphology, internal

378 textures and ages provide insights into the geotectonic history of the underlying basement,  
379 allowing the definition of four main age groups: i) 1,130-1,005 Ma; ii) 992-859 Ma; iii)  
380 637-563 Ma; and iv) 549-493 Ma. The former and the latter are the most prominent  
381 provenances of the Karoo sediments, highlighting two important events of crustal  
382 generation, consumption and deformation of Rodinia and Gondwana (Pan-African  
383 Orogeny) Supercontinents.

384 Paleocurrent measurements indicate an N-NW paleoflow for the fluvial sequences  
385 of the Matinde Formation (Bicca et al., 2017). Since we collected immature sandstone, the  
386 probable source areas are located somewhere in the south of the Moatize-Minjova Basin,  
387 less than *ca.*200km (Hartmann et al., 2004) due to the preservation of the metamorphic  
388 rims.

389 The first and older age group reflects the greater crustal component in the north of  
390 Mozambique. They mostly reflect magmatic crystallization ages as evidenced by  
391 oscillatory grown in the zircon grains, which are a common feature in this population. Late  
392 Mesoproterozoic was an important moment of crustal generation everywhere in the distinct  
393 terrenes of northern Mozambique. These age spectrum falls in the age range of the Barue  
394 Magmatic Arch (SW Nampula; Fig. 7), as also, in the provenance record of the Chimoio-  
395 Macossa (SW Nampula) and Mungari nappes, which in turn received sediments from the  
396 Báruè Magmatic Arch (Chaúque, 2012).

397 The ages between *ca.* 950 and 550 Ma do not present very wide distribution and  
398 correspond to important periods of crustal geotectonic evolution in the north of  
399 Mozambique. Manjate (2011) reports an U-Pb metamorphic age at  $956 \pm 38$  Ma (MSWD =  
400 0.39) for the orthogneisses of SW Nampula and Grantham et al. (2011) found an age of  
401 996.8 Ma  $\pm$  3.4 Ma (MSWD = 2.3) for a migmatitic vain of the Chimoio Group

402 (paragneisses of SW Nampula). Similar ages are observed as metamorphic ages around *ca.*  
403 940 Ma in the Unango and Marrupa Complexes (Bingen et al., 2009). Nevertheless, the  
404 zircon ages clusters the data of Manjate (2015) for the Guro Suite/Mungari Garnet Granite  
405 Migmatite/Chacocoma Granite zircon dating (Fig. 7). These suggests that Early  
406 Neoproterozoic population ages probably represents a late magmatic and metamorphic  
407 event associated to Rodinia amalgamation processes present in the Mesoproterozoic  
408 basement rocks (Jacobs et al., 2008; Macey et al., 2013). On the other hand, the  
409 crystallization ages around *ca.* 860 and 820 Ma (GTK Consortium, 2006; Chaúque, 2012;  
410 Manjate, 2015) are positioned near a extension tectonic period and emplacement of the  
411 protoliths of the Guro Suite, which possess a positive ε<sub>ND</sub> suggesting a strong mantle  
412 contribution (Chaúque, 2012) and are related to the breakup of Rodinia Supercontinent. The  
413 Mozambique Ocean closed during a protracted period of island-arc and microcontinent  
414 accretion between *ca.* 850 and 620 Ma (Fritz et al., 2013).

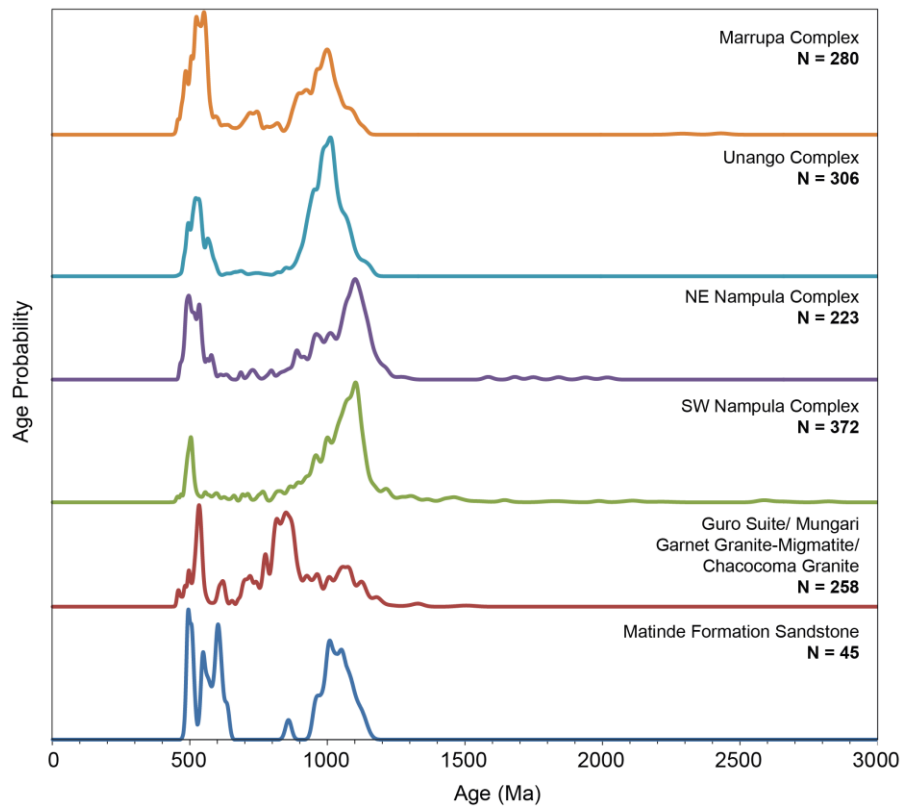
415 The ages around *ca.* 630 and 560 Ma refers to distinct events of deformation and  
416 magmatism along the north of Mozambique basement. They are registered in the Monapo  
417 Klippe (*ca.* 635 Ma), and interpreted as a major episode of granulite-facies metamorphism  
418 and crust generation (Macey et al., 2013). SHRIMP zircon data from samples from alkaline  
419 intrusions and mafic granulites in the same complex yield crystallization and metamorphic  
420 ages of *ca.* 635 Ma and 570-590 Ma, respectively (Grantham et al., 2013).

421 The Cabo Delgado Nappe Complex (north of the Lurio Belt) was an extended crust  
422 that formed adjacent to the Mozambique Ocean and experienced a *ca.* 650–620 Ma  
423 granulite-facies metamorphism (Fritz et al., 2013). They are also found in the Ocua  
424 Complex, which contains high-P granulite boudins dated at  $557 \pm 16$  Ma, evidence for  
425 deformation at least until  $532 \pm 13$  Ma and abundant on  $612 \pm 6$  to  $504 \pm 11$  Ma felsic

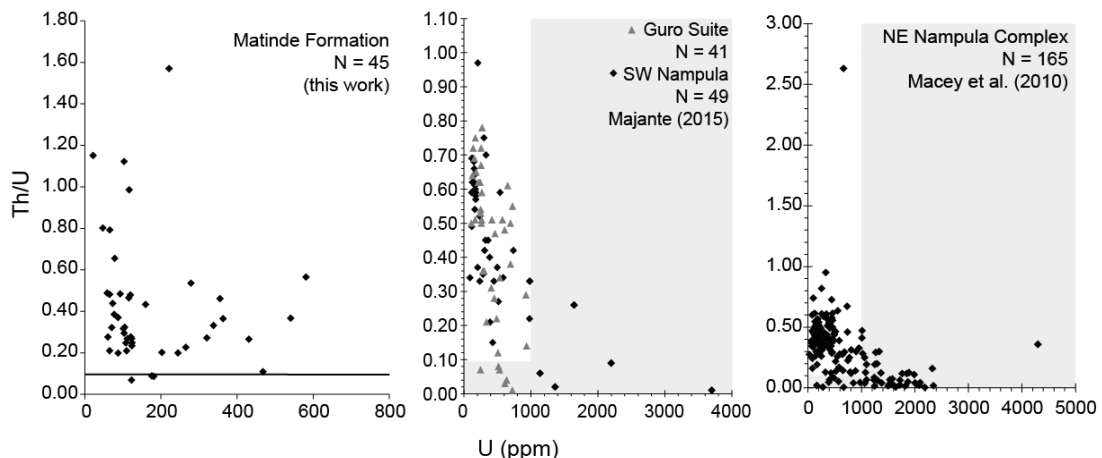
426 plutons (Norconsult Consortium, 2007). Evidence of the closure of the Mozambique Ocean  
427 is present on data from other sections of the East Africa Orogen indicated by accretion of  
428 various volcanic arc and microcontinent fragments onto the margin of the Congo-Tanzania  
429 Craton between 655 and 610 Ma (Meert, 2003; Collins and Pisarevsky, 2005; Jöns and  
430 Schenk, 2008; Bingen et al., 2007). This age population is not strongly impressed in the  
431 SW Nampula Complex and Guro Suite/Mungari Garnet Granite Migmatite/Chacocoma  
432 Granite although they are present in the individual zircon ages presented by Chaúque  
433 (2012) and Manjate (2015), but enough to correlate with our data. Additionally, the  
434 provenance analyzes in the Alto-Benfica and Mecuburi Neoproterozoic-Cambrian basins in  
435 detrital zircons using the U-Pb method (NE Mozambique, Thomas et al., 2010) indicated a  
436 strong contribution of the northern Marrupa and Unango Complexes. The Mecuburi Group  
437 present a high contribution of zircon dated at *ca.* 600 Ma however, they are practically  
438 absent from Alto-Benfica age populations. The latter, show some ages > 1200 Ma (Thomas  
439 et al., 2010), suggesting that the Moatize-Minjova Basin has a distinct provenance, since  
440 these ages were not verified in their zircons.

441 After the events of crustal thickening and klippening resulting from the Pan-African  
442 Orogeny (*ca.* 550-480 Ma), the southern region of the Moatize-Minjova Basin probably  
443 formed a topographic high along with the entire NE portion of Mozambique. These sites  
444 have probably originated the headwaters of the rivers and tributaries that bathed the Proto-  
445 Zambezi basin, as suggested by Key et al. (2015) and Bicca et al. (2017). The ages  
446 contained between *ca.* 550 and 480 Ma are attributed to magmatic and metamorphic events  
447 common in the region due to high-grade metamorphism produced by Pan-African Orogeny  
448 and therefore are not good markers for determining sedimentary provenance (Fig. 7).

449 The concentrations and rates of Th/U of our data compared with a few available  
 450 data from underlying assemblages interpreted as the main source region for the sediments  
 451 allow defining some correlations. The NE Nampula Th/U rates are comparable to ours, but  
 452 Th/U rates of < 0.1 were attribute to a metamorphic origin (Hartmann and Santos, 2004) as  
 453 also the very high U concentrations (> 1000 ppm) which are reasonable common in that  
 454 area and were not observed in the zircons from Matinde Formation (Fig. 8). This  
 455 comparison strengthens the correlation of Matinde Formation sediments with SW Nampula  
 456 Complex rocks, which has compositional characteristics close to those obtained in the  
 457 Moatize-Minjova Basin zircons (Fig. 8).



458  
 459 Figure 7: Comparative age graphics of our sandstone sample from the Moatize-Minjova  
 460 Basin with its probable source area. The data presented in the two below graphic comprise  
 461 U-Pb dating of zircon grains (LA-ICP-MS and SHRIMP) from the surrounding basement of  
 462 the basin and were compiled from Chaúque (2012) and Manjate (2015).



463

464 Figure 8: Relationship between U content and Th/U rates for the NE and NW Nampula  
 465 complexes and of the Guro Suite. The dark line highlights the 0.1 limit of Th/U rates and  
 466 light gray areas represent the less pronounced concentrations U concentrations in our data.

467

## 468 6. Conclusion

469 Provenance data from U-Pb LA-ICPMS dating of detrital zircon crystals showed to  
 470 be as a reliable analytical technique to map sediment source regions from ancient fold and  
 471 thrust belts underlying sedimentary basin. This information unveils to be relevant to  
 472 reestablish the paleogeography allowing identifying the probable configuration of basement  
 473 relief near this intracontinental rift. The choice of the sample in relation to the sand  
 474 granulometry and tectono-stratigraphic relevance, allow obtaining a more comprehensive  
 475 information of the magmatic and metamorphic processes in the northern Mozambique. A  
 476 detailed and systematic analysis of zircon morphology and internal textures, U-Pb ages and  
 477 Th/U rates allows defining the SW Nampula and the Guro Suite/Mungari Garnet Granite  
 478 Migmatite/Chacocoma Granite (W-SW of the basin) as the main source areas during  
 479 Permian Triassic sedimentation in our sample from the Moatize-Minjova Basin. The data  
 480 revealed a strong contribution of Late Mesoproterozoic ages, which constrain the greater  
 481 magmatic and metamorphic ages of the basement from northern Mozambique. A Late

482 Neoproterozoic-Cambrian age population, reflecting magmatic and high metamorphic ages,  
483 was provided by the large overprint of the Pan-African Orogeny. Nevertheless, it was the  
484 less pronounced zircon grain ages that allowed restricting a narrower source region.

485 The ages between ca. 950 Ma to 550 Ma are not prominent in northwestern  
486 Mozambique basement rocks, especially ages around ca 630-600 Ma. This moment refer to  
487 a distinct period of high-grade metamorphism and little magmatism associated with the  
488 closure of the Mozambique Ocean and mostly preserved in Cabo Delgado, Mugeba and  
489 Monapo Klippens of NE Mozambique. However, they are present as individual zircon ages  
490 in the SW Nampula Complex and Guro Suite/Mungari Garnet Granite  
491 Migmatite/Chacocoma Granite associations, which must have being the major source area  
492 for the Moatize-Minjova Basin during Permian-Triassic sedimentation. The ages between  
493 ca. 950 and 820 Ma are also well documented in the established provenance region.

494 Further investigations are needed to improve our data and map local and regional  
495 variations in provenance pattern in different stratigraphic levels and sites in all the Karoo  
496 basins from northern Mozambique. These would allow a more precise definition of  
497 paleogeomorphology evolution of the Precambrian-Cambrian basement rocks through  
498 Phanerozoic.

499

## 500 **7. Acknowledgments**

501 This study is part of the doctoral thesis of the first author at Programa de Pós-  
502 Graduação em Geociências of Universidade Federal do Rio Grande do Sul. We thanks to  
503 Conselho Nacional do Desenvolvimento Científico e Tecnológico (CNPq) of Brazil, for  
504 scholarship financially supported number [141240/2013-0](#) of the first author. We are  
505 grateful to Mr. Antonio Rizzo Alface for the geology field assistance.

- 506     **8. References**
- 507     Bahlburg, H., Jasper Berndt, J., 2016. Provenance from zircon U–Pb age distributions in  
508     crustally contaminated granitoids. *Sedimentary Geology* 336, 161–170.
- 509
- 510     Barton, C.M., Carney, J.N., Crow, M.J., Dunkley, P.N., Simango, S., 1991. The Geology of  
511     the Country around Rushinga and Nyamapanda. *Zimbabwe Geological Survey Bulletin*, 92.
- 512
- 513     Bicca, M.M., Chemale Jr., F., Jelinek, A.R., Christie Helouise Engelmann de  
514     Oliveira, C.H.E.O., Guadagnin, F., Armstrong, R., 2013. Tectonic evolution and  
515     provenance of the Santa Bárbara Group, Camaquã Mines region, Rio Grande do Sul, Brazil  
516     48, 173–192.
- 517
- 518     Bicca, M.M., Philipp, R.P., Jelinek, A.R., Ketzer, J.M.M., Scherer, C.M.S., Jamal, D.L.,  
519     Reis, A.D., 2017. Permian-Early Triassic Tectonic and Stratigraphy of the Karoo  
520     Supergroup in Northwestern Mozambique. *Journal of African Earth Sciences*. Article in  
521     press.
- 522
- 523     Bingen, B., Jacobs, J., Viola, G., Henderson, I.H.C., Skår, Ø., Boyd, R., Thomas, R.J.,  
524     Solli, A., Key, R.M., Daudi, E.X.F., 2009. Geochronology of the Precambrian crust in the  
525     Mozambique belt in NE Mozambique, and implications for Gondwana assembly.  
526     Precambrian Research 170, 231–255.
- 527
- 528     Bingen, B., Viola, G., Griffin, W.L., Jacobs, J., Boyd, R., Thomas, R.J., Daudi, E.,  
529     Henderson, I.H.C., Beyer, E., Skar, Ø., Engvik, A., Key, R.M., Solli, A., Sandstad, J.S.,

- 530 Smethurst, M., Tveten, E., Bjerkgård, T., Melezhik, V.A., Jamal, D., Smith, R., Hollick,  
531 L.M., Feito, P., 2007. Crustal architecture of the Mozambique Belt in northeastern  
532 Mozambique: perspective from U–Pb geochronology and Lu–Hf isotopes in zircon. In: 7th  
533 International Symposium on Applied Isotope Geochemistry, Stellenbosch, 10–14  
534 September.
- 535
- 536 Boyd, R., Nordgulen, Ø., Thomas, R.J., Bingen, B., Bjerkgård, T., Grenne, T., Henderson,  
537 I., Melezhik, V.A., Often, M., Sandstad, J.S., Solli, A., Tveten, E., Key, R.M., Smith, R.A.,  
538 Gonzalez, E., Hollick, L.J., Jacobs, J., Jamal, D., Motuza, G., Bauer, W., Daudi, E., Feitio,  
539 P., Manhica, V., Moniz, A., Rosse, D., 2010. The geology and geochemistry of the East  
540 African Orogen in NE Mozambique. *South African Journal of Geology* 113, 87–129.
- 541
- 542 Cairncross, B., 2001. An overview of Permian (Karoo) coal deposits of Southern Africa.  
543 *Journal of African Earth Sciences* 33, 529–562.
- 544
- 545 Castaing, C., 1991. Post-Pan-African tectonic evolution of South Malawi in relation to the  
546 Karroo and Recent East African Rift Systems. *Tectonophysics* 191, 55-73.
- 547
- 548 Catuneanu, O., Wopfner, H., Eriksson, P.G., Cairncross, B., Rubidge, B.S., Smith R.M.H.,  
549 Hancox, P.J., 2005. The Karoo basins of south-central Africa. *Journal of African Earth  
550 Sciences* 43, 211–253.
- 551

- 552 Cawood, P., Hawkesworth, C., Dhuime, B., 2012. The continental record and generation of  
553 the continental crust. Geological Society of America Bulletin 125, 14–32.
- 554
- 555 Chaúque, F. R., 2012. Contribution to the knowledge of the tectonic evolution of the  
556 Mozambique Belt, Mozambique. Thesis (Ph.D) - Institute of Geosciences, University of  
557 São Paulo, São Paulo, 187pp.
- 558
- 559 Chaúque, F. R., Cordani, U.G., Jamal, D.L., Onoe, A.T., 2017. The Zimbabwe Craton in  
560 Mozambique: A brief review of its geochronological pattern and its relation to the  
561 Mozambique Belt. Journal of African Earth Sciences. doi: 10.1016/j.jafrearsci.  
562 2017.01.021.
- 563
- 564 Chemale Jr., F., Philipp, R.P., Dussin, I.A., Formoso, M.L.L., Kawashita, K., Bertotti, A.L.,  
565 2011. Lu-Hf and U-Pb age determinations of Capivarita Anorthosite in the Dom  
566 Feliciano Belt, Brazil. Precambrian Research 186, 117-126.
- 567 Daber, R., 1984. Plantas fósseis de Moçambique, 9. Ciência e Tecnologia, Maputo, pp. 77-  
568 81.
- 569
- 570 Collins, A.S., Pisarevsky, S.A., 2005. Amalgamating eastern Gondwana: the evolution  
571 of the Circum Indian Orogen. Earth Science Reviews 71, 229–270.
- 572
- 573 Corfu, F., Hanchar, J.M., Hoskin, P.W.O., Kinny, P., 2003. Atlas of Zircon Textures In:  
574 Hanchar, J.M., Hoskin, P.W.O. (Eds.), Zircon. Reviews in Mineralogy and Geochemistry  
575 53, 469-500.

576

577 Emmel, B., Kumar, R., Jacobs, J., Ueda, K., Van Zuilen, M., Matola, R., 2014. The low  
578 temperature thermochronological record of sedimentary rocks from the central Rovuma  
579 Basin (N Mozambique) d Constraints on provenance and thermal history. *Gondwana Res.*  
580 25, 1216e1229. <http://dx.doi.org/10.1016/j.gr.2013.05.008>.

581

582 Fedo, C.M., Sircombe, K.N., Rainbird, R.H., 2003. Detrital zircon analysis of the  
583 sedimentary record. In: Hanchar, J.M., Hoskin, P.W.O. (Eds.), *Zircon. Reviews in*  
584 *Mineralogy and Geochemistry* 53, 277–303.

585

586 Fernandes, P., Cogné, N., Chew, D.M., Bruno Rodrigues, B., Jorge, R.C.G.S., Marques, J.,  
587 Jamal, D., Vasconcelos, L., 2015. The thermal history of the Karoo Moatize-Minjova  
588 Basin, Tete Province, Mozambique: An integrated vitrinite reflectance and apatite fission  
589 track thermochronology study. *Journal of African Earth Sciences* 112, 55-72.

590

591 Fritz, H., Abdelsalam, M., Ali, K.A., Bingen, B., Collins, A.S., Fowler, A.R., Ghebreab,  
592 W., Hauzenberger, C.A., Johnson P.R., Kusky, T.M., Macey, P., Muhongo, S., Stern, R. J.,  
593 Viola, G., 2013. Orogen styles in the East African Orogen: A review of the Neoproterozoic  
594 to Cambrian tectonic evolution. *Journal of African Earth Sciences* 86, 65–106.

595

596 Gehrels, G., 2014. Detrital zircon U-Pb geochronology applied to tectonics. *Annual*  
597 *Review of Earth and Planetary Sciences* 42, 127-149.

598

599 Grantham, G.H., Maboko, M., Eglington, B.M., 2003. A review of the evolution of

- 600 the Mozambique Belt and implications for the amalgamation for Rodinia and  
601 Gondwana. In: Yoshida, M., Windley, B.F., Dasgupta, S. (Eds.), Proterozoic East  
602 Gondwana: Supercontinent Assembly and Breakup. Geological Society of London,  
603 Special Publications 206, 401–426.
- 604
- 605 Grantham, G.H., Macey, P.H., Horie, K., Kawakami, T., Ishikawa, M., Satish-Kumar, M.,  
606 Tsuchiya, N., Graser, P., Azevedo, S., 2013. Comparison of the metamorphic history of the  
607 Monapo Complex, northern Mozambique and Balchenfjella and Austhameren areas, Sør  
608 Rondane, Antarctica: Implications for the Kuunga Orogeny and the amalgamation of N and  
609 S Gondwana. Precambrian Research 234, 85– 135.
- 610
- 611 Grantham, G.H., Manhica, A.D.S.T., Armstrong, R.A., Kruger, F.J., Loubser, M., 2011.  
612 New SHRIMP, Rb/Sr and Sm/Nd isotope and whole rock chemical data from central  
613 Mozambique and western Dronning Maud Land, Antarctica: implications for the nature of  
614 the eastern margin of the Kalahari Craton and the amalgamation of Gondwana. Journal of  
615 African Earth Sciences 59, 74–100.
- 616
- 617 GTK Consortium, 2006. Explanation of geological maps of sheets: Songo (1532),  
618 Cazula/Zóbuè (1533-1534), Mecumbura/Chioco (1631-1632), Tete (1633) and Tambara  
619 (1634). Ministério dos Recursos Minerais, Direcção Nacional de Geologia, Maputo.
- 620
- 621 Guadagnin, F., Chemale Jr., F., Dussin, I.A., Jelinek, A.R., Santos, M.N., Borba, M.L.,  
622 Justino, D., Bertotti,A.L.,Alessandretti, L., 2010. Depositional age and provenance of the

- 623 Itajaí Basin, Santa Catarina State, Brazil: implications for SW Gondwana correlation.
- 624 Precambrian Res. 180, 156–182.
- 625
- 626 Hanson, R.E., 2003. Proterozoic geochronology and tectonic evolution of southern Africa.
- 627 Geological Society, Special Publications 206, 427-463.
- 628
- 629 Hargrove, U.S., Hanson, R.E., Martin, M.W., Blenkinsop, T.G., Bowring, S.A., Walker, N.,
- 630 Munyanyiwa, H., 2003. Tectonic evolution of the Zambezi orogenic belt: geochronological,
- 631 structural, and petrological constraints from northern Zimbabwe. Precambrian Research
- 632 123, 159–186.
- 633
- 634 Hartmann, L. A., Santos, J. O. S., 2004. Predominance of high Th/U, magmatic zircon in
- 635 Brazilian shield sandstones. Geology 32, 73–76.
- 636
- 637 Hartman, L.A., Santos, J.O.S., McNaughton, N.J., 2008. Detrital Zircon U-Pb Age Data,
- 638 and Precambrian Provenance of the Paleozoic Guaritas Formation, Southern Brazilian
- 639 Shield. International Geology Review 50, 364–374.
- 640
- 641 Hawkesworth, C., Dhuime, B., Pietranik, A., Cawood, P., Kemp, T., and Storey, C., 2010.
- 642 The Generation and Evolution of the Continental Crust: Journal of the Geological Society
- 643 167, 229–248.
- 644
- 645 Jacobs, J., Bingen, B., Thomas, R.J., Bauer, W., Wingate, M., Feitio, P., 2008. Early
- 646 Palaeozoic orogenic collapse and voluminous late-tectonic magmatism in Dronning

- 647 Maud Land and Mozambique: insights into the partially delaminated orogenic root of the  
648 East African-Antarctic Orogen? In: Satish-Kumar, M., Motoyoshi, Y., Osanai, Y., Hiroi,  
649 Y., Shiraishi, K. (Eds.), Geodynamic Evolution of East Antarctica: A Key to the East-West  
650 Gondwana Connection. Geological Society of London, Special Publications 308, 69–90.
- 651
- 652 Jöns, N., Schenk, V., 2008. Relics of the Mozambique Ocean in the central East African  
653 Orogen: evidence from the Vohibory Block of southern Madagascar. Journal of  
654 Metamorphic Geology 26, 17–28.
- 655
- 656 Key, R.M., Cotterill, F.P.D., Moore, A.E., 2015. The Zambezi River: An Archive of  
657 Tectonic Events Linked to the Amalgamation and Disruption of Gondwana and Subsequent  
658 Evolution of the African Plate. South African Journal of Geology 118(4), 425-438.
- 659
- 660 Lakshminarayana, G., 2015. Geology of Barcode type coking coal seams, Mecondezi sub-  
661 basin, Moatize Coalfield, Mozambique. International Journal of Coal Geology 146, 1–13.
- 662
- 663 Ludwig, K. R., 2003. Isoplot/Ex version 3.00—a geochronological toolkit for Microsoft  
664 Excel: Berkeley, CA, Berkeley Geochronological Center Special Publication 4, 70p.
- 665
- 666 Macey, P.H., Ingram, B.A., Roberts, M.R., de Kock, G., Cronwright, M.S., Botha, G.A.,  
667 Grantham, G.H., Maree, L., Botha, P.M.W., Kota, M., Opperman, R., Haddon, I.G.,  
668 Rowher, M., Nolte, J.C., 2007. Map Explanation of Sheets Alto Molócuè, 1537.
- 669 Murrupula, 1538. Nampula, 1539. Mogincual, 1540. Errego, 1637. Gilé (1638)  
670 and Angoche (1639-40). National Directorate of Geology, Republic of Mozambique.

- 671
- 672 Macey, P.H., Miller, J.A., Rowe, C.D., Grantham, G.H., Siegfried, P., Armstrong, R.A.,
- 673 Kemp, J., Bacalau, J., 2013. Geology of the Monapo Klippe, NE Mozambique and its
- 674 significance for assembly of central Gondwana. *Precambrian Research* 233, 259– 281.
- 675
- 676 Manjate, V. A., 2011. Geocronologia da região de Gondola-Nhamatanda, centro de
- 677 33 Moçambique. Dissertação de Mestrado - São Paulo : IGc/USP. 82 pp. (unpubl.)
- 678
- 679 Manjate, V. A., 2015. Caracterização Geocronológica dos granitoides do Complexo de
- 680 Bárue e da Suíte de Guro, Centro-Oeste de Moçambique, e suas relações com a
- 681 metagênese. Thesis (Ph.D) - Institute of Geosciences, University of São Paulo, São Paulo,
- 682 149pp. (unpubl.)
- 683
- 684 Meert, J.G., 2003. A synopsis of events related to the assembly of eastern Gondwana.
- 685 *Tectonophysics* 362, 1–40.
- 686
- 687 Macey, P.H., Thomas, R.J., Grantham, G.H., Ingram, B.A., Jacobs, J., Armstrong, R.A.,
- 688 Roberts, M.P., Hollick, L., Bingen, B., de Kock, G., Bauer, W., Gonzales, E., Bjerksgård, T.,
- 689 Henderson, I.H.C., Cronwright, M., Harley, S., Solli, A., Nordgulen,
- 690 Ø., Viola, G., Motuza, G., Daudi, E.X.F., Manhica, V., 2010. Mesoproterozoic
- 691 geology of the Nampula Block, northern Mozambique: tracing fragments of
- 692 Mesoproterozoic crust in the heart of Gondwana. *Precambrian Research* 182,
- 693 124–148.
- 694

- 695 Moecher, D. P., and Samson, S. D., 2006. Differential zircon fertility of source terranes and  
696 natural bias in the detrital zircon record: Implications for sedimentary provenance analysis:  
697 *Earth and Planetary Science Letters* 247, 252–266.
- 698
- 699 Norconsult Consortium, 2007. Mineral Resources Management Capacity Building  
700 Project, Republic of Mozambique. Component 2: Geological Infrastructure  
701 Development Project, Geological Mapping Lot 1. Sheet Explanation: 32 Sheets;  
702 Scale: 1/250000, Report No. B6.f. National Directorate of Geology, Republic of  
703 Mozambique.
- 704
- 705 Oliveira, C.H.E.O., Chemale Jr, F., Jelinek, A.R., Bicca, M.M., Philipp, R.P., U–Pb and  
706 Lu–Hf isotopes applied to the evolution of the late to post-orogenic transtensional basins of  
707 the dom feliciano belt, Brazil. *Precambrian Research* 246, 240–255.
- 708
- 709 Pereira, Z., Lopes, G., Fernandes, P., Marques, J., 2014. Palinoestratigrafia da Sondagem  
710 ETA 72 da Bacia Carbonífera de Moatize-Minjova, Província de Tete, Moçambique. In:  
711 Vasconcelos, L. (Ed.), Livro de Resumos, 2 Congresso Nacional de Geologia e 12  
712 Congresso de Geoquímica dos Países de Língua Portuguesa, Maputo, Moçambique, pp. 67–  
713 71.
- 714
- 715 Pereira, Z., Fernandes, P., Lopes, G., Marques, J., Vasconcelos, L., 2016. The Permian–  
716 Triassic transition in the Moatize–Minjova Basin, Karoo Supergroup, Mozambique: A  
717 palynological perspective. *Review of Palaeobotany and Palynology* 226, 1–19.
- 718

- 719 Pinna, P., Jourde, G., Calvez, J.Y., Mroz, J.P., Marques, J.M., 1993. The Mozambique  
720 Belt in northern Mozambique; Neoproterozoic (1100–850 Ma) crustal growth  
721 and tectogenesis, and superimposed Pan-African (800–550 Ma) tectonism. *Precambrian*  
722 *Research* 62, 1–59.
- 723
- 724 Sacchi, R., Cadoppi, P., Costa, M., 2000. Pan-African reactivation of the Lurio segment  
725 of the Kibaran Belt system: a reappraisal from recent age determinations in  
726 northern Mozambique. *Journal of African Earth Sciences* 30, 629–639.
- 727
- 728 Smith, R.M.H., Eriksson, P.G., Botha, W.J., 1993. A review of the stratigraphy and  
729 sedimentary environments of the Karoo-aged basins of Southern Africa. *Journal of African*  
730 *Earth Sciences* 16, 143–169.
- 731
- 732 Stern, R.J., 1994. Arc assembly and continental collision in the Neoproterozoic East  
733 African orogen: implications for the consolidation of Gondwanaland. *Annual Reviews of*  
734 *Earth and Planetary Sciences* 22, 319–351.
- 735
- 736 Thomas, R.J., Jacobs, J., Horstwood, M.S.A., Ueda, K., Bingen, B., Matola, R., 2010. The  
737 Mecubúri and Alto Benfica Groups, NE Mozambique: Aids to unravelling ca. 1 and 0.5 Ga  
738 events in the East African Orogen. *Precambrian Research* 178, 72–90.
- 739

740 Ueda, K., Jacobs, J., Thomas, R.J., Kosler, J., Jourdan F., Matola, R., 2012. Delamination-  
741 induced late-tectonic deformation and high-grade metamorphism of the Proterozoic  
742 Nampula Complex, northern Mozambique. *Precambrian Research* 196– 197, 275– 294.

743

744 Viola, G., Henderson, I.H.C., Bingen, B., Thomas, R.J., Smethurst, M.A., de Azavedo, S.,  
745 2008. Growth and collapse of a deeply eroded orogen: insights from structural and  
746 geochronological constraints on the Pan-African evolution of NE Mozambique. *Tectonics*  
747 27, TC5009, doi:10.1029/2008TC002284.

748

#### 4. ARTIGO SUBMETIDO À REVISTA TECTONOPHYSICS

TECTO: Your new submission received  Entrada 

 **Tectonophysics** <eesserver@eesmail.elsevier.com>  
para mim, marcosmb23, andrea.jelinek, ruy.philipp 

23:51 (Há 12 horas)   

 inglês  português  Traduzir mensagem Desativar para: inglês 

Dear Dr. Bicca,

Your submission entitled "Mesozoic-Cenozoic Denudation History of NW Mozambique Orogenic Belts by Apatite Fission Track Thermochronology: Implications on Rift Evolution Across Southeast African Margin" has been received by Tectonophysics for the article type Research Paper.

Please note that submission of an article is understood to imply that the article is original and is not being considered for publication elsewhere. Submission also implies that all authors have approved the paper for release and are in agreement with its content.

You will be able to check on the progress of your paper by logging on to <https://ees.elsevier.com/tecto/> as Author.

Your manuscript will be given a reference number in due course.

Thank you for submitting your work to this journal.

Kind regards,

Journal Management

TECTO11837: Notice of manuscript number  Entrada 

 **Tectonophysics** <eesserver@eesmail.elsevier.com>  
para mim, marcosmb23, andrea.jelinek, ruy.philipp 

05:48 (Há 9 horas)   

 inglês  português  Traduzir mensagem Desativar para: inglês 

Dear Dr. Bicca,

Your submission entitled "Mesozoic-Cenozoic Denudation History of NW Mozambique Orogenic Belts by Apatite Fission Track Thermochronology: Implications on Rift Evolution Across Southeast African Margin" has been assigned the following manuscript number: TECTO11837.

You will be able to check on the progress of your paper by logging on <https://ees.elsevier.com/tecto/> as Author.

Thank you for submitting your work to this journal.

Kind regards,

Tectonophysics

1   **Mesozoic-Cenozoic Denudation History of NW Mozambique Orogenic Belts by**  
2   **Apatite Fission Track Thermochronology: Implications on Rift Evolution Across**  
3   **Southeast African Margin**

4

5   Marcos Müller Bicca<sup>a\*</sup>

6   Andrea Ritter Jelinek<sup>a</sup>

7   Ruy Paulo Philipp<sup>a</sup>

8

9   \* Corresponding author

10   E-mail addresses: [marcos.mb83@gmail.com](mailto:marcos.mb83@gmail.com) (M.M. Bicca); [andrea.jelinek@ufrgs.br](mailto:andrea.jelinek@ufrgs.br)  
11   (A.R. Jelinek); [ruy.philipp@ufrgs.br](mailto:ruy.philipp@ufrgs.br) (R.P. Philipp)

12

13   <sup>a</sup>Instituto de Geociências – Universidade Federal do Rio Grande do Sul, Campus do  
14   Vale. Av. Bento Gonçalves, 9500, Porto Alegre, Rio Grande do Sul, CEP 91509-900,  
15   Brazil.

16

17   **Highligths**

18   1 - Fanerozoic compressive/extensional tectonics affect the NW Mozambique Orogenic  
19   Belts;

20   2 – Differential denudation controlled landscape evolution in NW Mozambique  
21   basement;

22   3 – Jurassic-Cenozoic denudation patterns induced by the Africa-Antarctica rifting;

23   4 - Dynamic topography influenced Cenozoic denudation rates in NW Mozambique;

24

25

26     **Abstract**

27                 The southern African plate has underwent several processes of horizontal and  
28                 vertical stress since Permian times attributed to Gondwanides orogenesis and to mantle  
29                 plumes upwelling from the Gondwana separation stages, respectively. Since about 30  
30                 Ma the plume related to the East Africa Rift system affects the NE Africa leading to the  
31                 development of topographically high lands affecting denudation history in all region.

32                 The NW Mozambique central apatite fission track ages range from Mesozoic to  
33                 Cenozoic times and an accumulated denudation thickness of about 2 - 3.5 km since  
34                 Upper Triassic times. The very early denudation stages of NW Mozambique were  
35                 marked by very low and local denudation rates (1-10 m/Ma) reaching about to 500 m  
36                 thick of eroded material until Lower Cretaceous. The larges amonts have being eroded  
37                 from since Lower Cretaceous with rates of 3-17 m/Ma until Middle Paleocene when  
38                 high denudation rates of 31-47 m/Ma bring the samples to the present conditions.

39                 The early cooling events are associated with erosion produced by extensional /  
40                 transtractive processes associated with the early break-up stages of Gondwana recorded  
41                 in several rift basins with thick volcano-sedimentary sequences from Karoo Supergroup.  
42                 This period also marks the drift of Madagascar through the Davie Fracture Zone from  
43                 the coast of Tanzania to the coast of Mozambique and the opening of the Mozambique  
44                 and Somalia basins. The Upper Jurassic and Upper Cretaceous were a period of great  
45                 development of the Indian ocean and the start of the N-S drift of Antarctica in relation  
46                 to the African plate marked in most of the maximum paleotemperatures observed in the  
47                 region.

48                 From Lower Cretaceous to Paleocene high amounts of denudation was attributed  
49                 to the development of the African margin and the reconfiguration of inland drainage  
50                 patterns. A significant increase of the cooling rates (1.17 to 0.88 °C/Ma) implying in the

51 denudation of about 1.5 to 2 km thick from the beginning of the Neogene to the Recent  
52 times. These cooling event was related to dynamic topography induced by the East  
53 African Rift mantle plume upwelling, which has been active since the Paleogene period.

54

55 **Keywords:** Apatite Fission Track, NW Mozambique, Denudation rates, East Africa Rift  
56 System, Gondwana break-up

57

## 58 1. Introduction

59 The architecture of the continental margin of northern Mozambique shows a  
60 close relationship to pre-existing Pan-African structures of the East African–Antarctic  
61 Orogen (Jacobs and Thomas, 2004; Fig. 1A) which plays an important role in margin  
62 configuration and landscape evolution (Emmel et al., 2011). Several crustal  
63 readjustments were observed during Phanerozoic period registered as brittle/ductile  
64 structures and sedimentation patterns all over south-central Africa (Catuneanu et al.,  
65 2005). Gondwana break-up was preceded by intracontinental Permian-Triassic rifting,  
66 marked by the deposition of thick sequences of Karoo Supergroup along south-central  
67 Africa (Catuneanu et al., 2005; Bicca et al., 2017), ending with a magmatic event (basalt  
68 flows) that took place during the final phase of Gondwana stability between 205 and  
69 175 Ma (Salman and Abdula, 1995). After that, the opening of the Indian Ocean sea  
70 floor was marked by the southward drifting of the East Antarctica/Madagascar/India  
71 Seychelles block guided by the Davie transform fault (Fig. 1B) away from East Africa  
72 between *ca.* 158 and 119 Ma (Salman and Abdula, 1995; Emmel et al., 2014).

73 The ongoing of Gondwana break-up led to the high denudation rates on the East  
74 Africa - Antarctica Orogen (Daszinnies et al., 2009; Emmel et al., 2011; Emmel et al.,  
75 2014; Bauer et al., 2016) and provide the development of distinct onshore and offshore

76 basins along east Africa passive margin. These basins are mostly filled with sediments  
77 discharged since Jurassic times (post-Gondwana disruption) over Karoo igneous rocks  
78 (Salman and Abdula, 1995; Reeves, 2000; Mahanjane, 2012; Castelino et al., 2015).

79 The study of exhumation and landscape evolution of Precambrian belts using  
80 low temperature thermochronological methods has become a robust tool for the  
81 improvement of regional tectonic models. With this in mind we used the apatite fission-  
82 track dating method to reconstruct the low-temperature cooling history (120–60 °C) of  
83 the Precambrian basement rocks of northwestern and central Mozambique (Fig. 1C).  
84 The aim of this study was to identify distinct denudation patterns on the hinterland  
85 determining the thermal ages and denudation rates of the Precambrian basement  
86 associations which contributed to sedimentation of intracratonic rift basins and with the  
87 depositional history in the north of Mozambique Basin. Therefore, we collected 27 rock  
88 samples from Mozambican shield, distributed comprehensively in the whole area in  
89 order to understand all regional structures and geotectonic domains identifying all  
90 differential denudation patterns.

91

## 92 **2. Geological Settings**

93 The northern and central region of Mozambique comprises a wide range of  
94 Precambrian and Cambrian igneous and metamorphic rocks formed in two distinct  
95 orogenic periods concerning the formation of the Rodinia and Gondwana  
96 Supercontinents (Norconsult Consortium, 2007). These associations can be subdivided  
97 into a northern, central and a southern provinces, by a series of E-W, N-S and NW-SE  
98 ductile crustal scale structures reactivated in a brittle regime during the Phanerozoic,  
99 caused by far compressive stress fields in the south-southwestern margin of Gondwana

100 (Fig. 1C; Castaing, 1991; Salman and Abdula, 1995; Norconsult Consortium, 2007;  
101 Bicca et al., 2017).

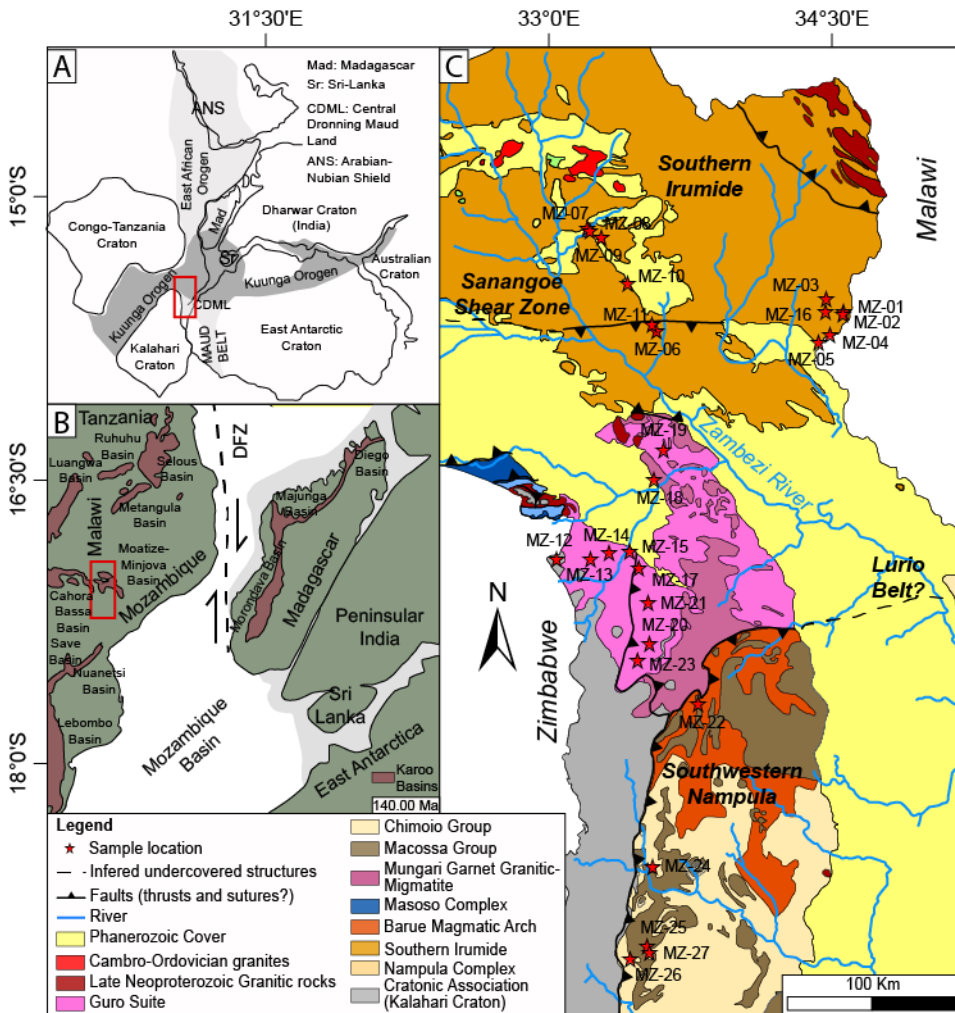
102 The south and central provinces are delimited by an ENE-trending structure  
103 attributed as a probable southern continuation of the Lurio Belt and the Sanangoe Shear  
104 Zone (Fig. 1C) (Norconsult Consortium, 2007; Jacobs et al., 2008; Viola et al., 2008;  
105 Bingen et al., 2009; Ueda et al., 2012). The ENE-trending structure converge  
106 southwards and mark the tectonic contact between the Southern Nampula Complex and  
107 the Kalahari Craton associations (Chaúque et al., 2017).

108 In the central area there are mostly Neoproterozoic ortho- and paragneisses  
109 which protoliths are related to juvenile magmatism of Rodinia break-up and marginal  
110 sedimentary basins deformed and thrust during Pan-African Orogeny (Chaúque, 2012;  
111 Manjate, 2015). These associations are surrounded by the sequences of the Karoo  
112 Supergroup (Late Carboniferous - Middle Jurassic) that comprises continental  
113 sediments and a bimodal magmatism erupted between 195-180 Ma attributed to an early  
114 aborted stage of Gondwana breakup (Salman and Abdula, 1995; Reeves, 2000) and  
115 younger igneous and sedimentary sequences related to the post-break-up period (Late  
116 Jurassic - Recent). They are hosted into E-W and NW-SE rift basins that compound the  
117 Zambezi Valley basins drained by the Zambezi River and its tributaries comprise one of  
118 the greater actual fluvial systems of Africa (Castaing, 1991; Norconsult Consortium,  
119 2007; Fernandes et al., 2015; Bicca et al., 2017). The Zambezi delta is responsible for  
120 carry sediments into the offshore Mozambique Basin (Fig. 1B).

121 The Sanangoe Shear Zone (SSZ) cut off the study area over a distance of about  
122 350 km (Fig. 1C) and represents a probable Pan-African connection between West and  
123 South Gondwana (Fig. 1A; Macey et al., 2013). In the north of this structure occur the  
124 Southern Irumide Belt (Fritz et al., 2013) comprising a large land mass of

125 Mesoproterozoic association intruded by Late Neoproterozoic granitoids and  
126 structurally overprinted by Pan-African Orogeny. Just south of the Sanangoe Shear  
127 Zone there is a large and merely NW-SE elongated segment of the Southern Irumide  
128 Belt that corresponds to a stratiform gabbro-anorthositic association tectonically  
129 transported with a SE-vergent during Pan-African Orogeny.

130 The great structures were affected by brittle reactivations under a sinistral  
131 transtensional regime induced by compressive stress fields in south-southwest  
132 Gondwana margin propagating throw NW-SE Zambezi pre-transform fault system from  
133 Late-Carboniferous to Middle Triassic. These reactivations are registered by periods of  
134 intense subsidence in the related rift basins generating great accommodation space for  
135 sedimentation and controlling depositional patterns and Mesozoic magmatic events  
136 (Castaing, 1991; Bicca et al., 2017). After that, the Gondwana break up led to large  
137 sedimentation patterns and tectonics within the extensional sedimentary basins along  
138 the east African margin basins which mostly show a continuous post-Jurassic record of  
139 sediment deposition (Salman and Abdula, 1995), reflecting high denudation histories in  
140 the onshore Mozambique basement (Salman and Abdula, 1995; Reeves, 2000;  
141 Mahanjane, 2012; Castelino et al., 2015).



142      Figure 1: A) Reconstruction of Gondwana during the Cambrian after Meert (2003), with  
 143      the locations of the East African Orogen and Kuunga Orogen shown. B) Gondwana at  
 144      *ca.* 140 Ma after the initial break-up between Madagascar and East Africa with Karoo  
 145      basins of East Africa and Madagascar (after Emmel et al., 2014). C) Simplified  
 146      geotectonic map of northwestern and central Mozambique with sample location (After  
 147      Norconsult Consortium, 2007 and Macey et al., 2013).

149

150      The Mozambique Basin (MB) covers the onshore and offshore parts of central  
 151      and southern areas of the Mozambique margin (Fig. 1B). The MB comprises one of the  
 152      oldest extensional sedimentary basins developed along the eastern African margin and  
 153      the stratigraphic record of the basin is dominated by marine deposits changing gradually  
 154      from deepest to shallower through time (Castelino et al., 2015). This basin registers a  
 155      Mesozoic sedimentation of 5-10 cm/kyr and 1-3 cm/kyr rates during Paleogene being

156 the former associated with high subsidence rates in the basin until Early Cretaceous  
157 times. The decrease in sedimentation rates from *ca.* 140 Ma until *ca.* 90 Ma is attributed  
158 to tectonic uplift in the onshore African basement which in consequence led to its rapid  
159 denudation increasing in the sediment influx into the basin until *ca.* 60 Ma. This uplift  
160 would be related to an epeirogenic event with Kimberlite emplacement in the African  
161 continent (Partridge and Maud, 1987). Another period of low sedimentation rates occur  
162 in the Low Paleogene attributed to a sediment-starved basin during a relative quiet  
163 tectonic phase onshore, but a tectonic uplift in the onshore basement around 30 Ma  
164 leading to another fast exhumation period onshore high sedimentation rates until  
165 Quaternary (Castelino et al., 2015).

166

## 167 **2.1 Thermochronological Constraints**

168 In the NW region of Mozambique apatite fission track (AFT) data are restricted  
169 to the Moatize-Minjova Basin which hosts the volcano-sedimentary sequences of Karoo  
170 Supergroup and also younger volcano-sedimentary sequences (Fig. 2). Four samples  
171 from two wells (*ca.* 500 m each) of the sedimentary rocks of Karoo Supergroup were  
172 analyzed providing a geothermal paleogradiente of 40 ° C/ km and apatite fission track  
173 ages between 146 to 84 Ma (Fernandes et al., 2015). According to the models, peak  
174 burial temperatures were attained shortly after deposition (3-10 Ma) and indicates two  
175 episodes of cooling and exhumation. The first between 240 and 230 Ma implying 2500  
176 and 3000 m of denudation, while the second from 6 Ma onwards implying 1000 and  
177 1500 m of denudation. The first denudation period was attributed to tectonic  
178 reactivation related to the Cape Fold Belt in South Africa and the latter to the southward  
179 propagation of the East African Rift System into Mozambique (Fernandes et al., 2015).

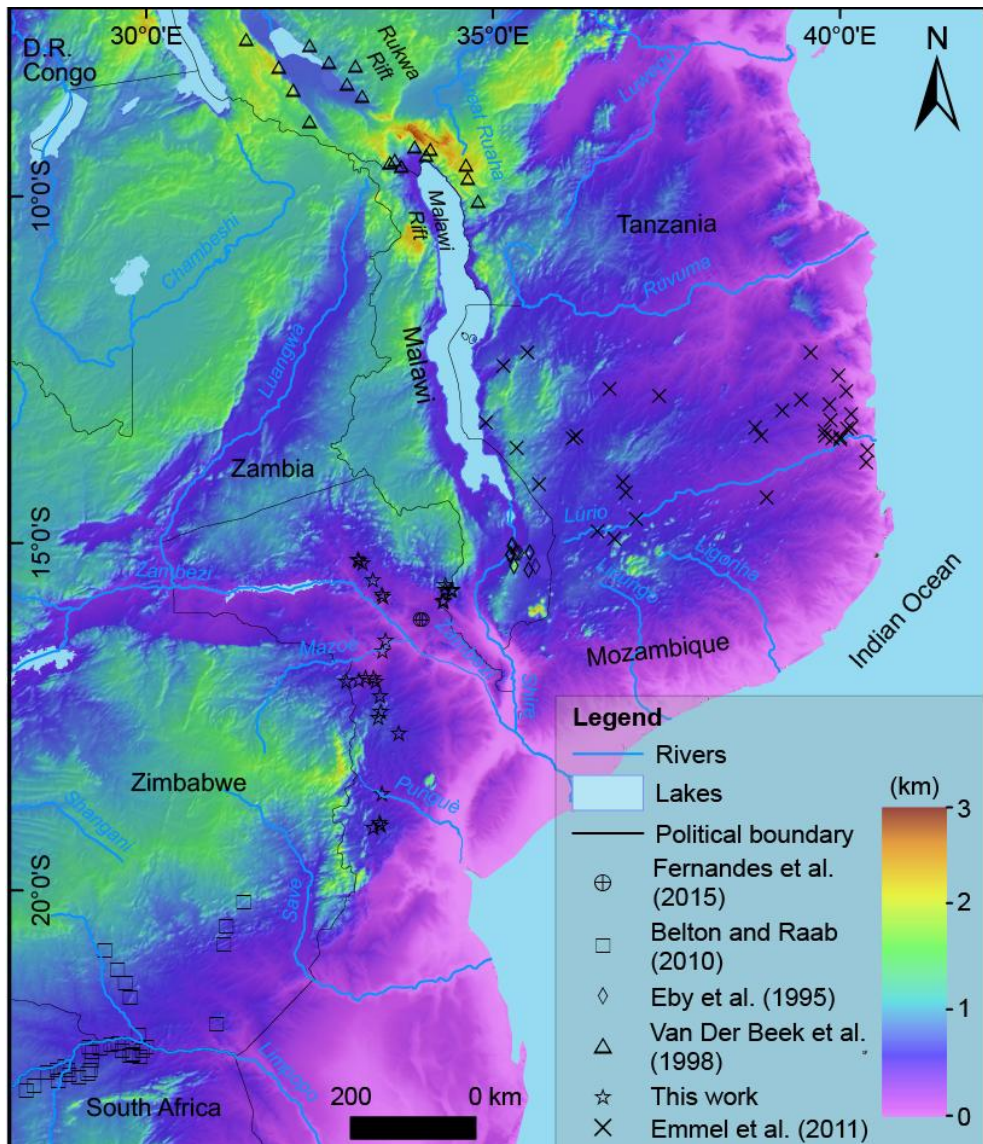
180 On the other hand, in the NE Mozambique there are a large spectrum of  
181 thermochronometric data for the basement provinces north and south of the Lurio Belt  
182 (Fig. 2; Daszinnies, 2006; Daszinnies et al., 2009; Emmel et al., 2011; Bauer et al.,  
183 2016). According to these data the region underwent differential post-orogenic thermal  
184 history (Emmel et al., 2011) as defined from titanite, zircon and apatite fission track  
185 data. The first two fission track methods provided ages north of the Lurio Belt ranging  
186 between *ca.* 578 Ma and 310 Ma, while in the south they are constrained between *ca.*  
187 460 Ma and 219 Ma. Apatite fission track analysis from samples in the north provide  
188 ages between *ca.* 326 Ma and 91 Ma contrasting with younger ages to south (147 to 59  
189 Ma; Fig. 2), suggesting that the southern province experience highest exhumation rates  
190 during Gondwana break-up. Thermal ages determine that the northern basement  
191 characterize rapid post orogenic cooling and exhumed to present levels during the  
192 Paleozoic, although the southern basement only underwent slow post-orogenic cooling.  
193 (Emmel et al., 2011).

194 Additionally, thermal activity during Cretaceous times was also described by Eby  
195 et al. (1995) studying the Cretaceous Chilwa Alkaline Province of southern Malawi (Fig.  
196 2). These authors presented K-Ar in amphibole and titanite fission-track ages indicating  
197 that igneous activity occurred in distinct periods starting at *ca.* 133 Ma with thermal  
198 igneous activity ending at *ca.* 113 Ma with the emplacement of large syenite-peralkaline  
199 granite plutons. The apatite fission-track ages and track-length measurements indicated  
200 that the emplacement of the large syenite-granite pluton caused local doming, leading to  
201 a rapid exhumation rate. However, more distal plutons show a slower cooling rate,  
202 suggesting that they were on the flanks of the local uplift and more deeply buried. These  
203 authors interpreted the Chilwa magmatism produced by crustal extension which  
204 reactivate pre-existing orogenic anisotropies leading to decompressional melting.

205 Similar K-Ar ages are described by alcaline rocks in NW Mozambique lying between  
206 *ca.* 106-166 Ma (GTK Consortium, 2006).

207 Further north of the study area, Van der Beek et al. (1998) identified from AFT  
208 data, fast cooling and denudation processes on the flanks of Malawi and Rukwa rifts  
209 (Fig. 2) during the periods of 250-200 Ma, *ca.* 150 Ma and  $\leq$  40-50 Ma. These present  
210 correlation with different sedimentation and rifting processes in the basin associated to  
211 the rift, where erosion, tectonic and isostatic rebound would be responsible for the  
212 reconfiguration of the surface during these events. The first interval corresponds to the  
213 final processes of erosion and deposition of the Karoo Supergroup, while in ca. 150 Ma  
214 occurs a reactivation of the rift separating Gondwana. Finally, the event between  $\leq$  40-  
215 50 Ma was interpreted as the result of the flexural isostatic response of the lithosphere  
216 to extensional unloading during rifting.

217 Through the Limpopo Belt (at the south of the study area, Fig. 2; Belton and  
218 Haab, 2010) extensive regions experienced kilometer-scale exhumation at around 130  
219 Ma and 90 Ma (Fig. 2). These period maks the strike-slip motion of the local fault  
220 patterns in this region due to the breakup of Gondwana as also igneous intrusions at *ca.*  
221 120 Ma and *ca.* 90 Ma and demonstrated that the sedimentation and subsidence rates on  
222 the Mozambique margin are in agreement with this data.



223

224 Figure 2: Geomorphological map (Jarvis et al., 2008) of central-eastern Africa with the  
 225 sample locations for this study and previous works.

226

### 227 3. Methods

228 We have applied apatite fission track thermochronology technique on 27  
 229 samples from Precambrian basement rocks of NW Mozambique assemblages as  
 230 indicated in Figure 1, and their lithological characteristics are listed in Table 1. The  
 231 samples were collected in an area that comprehensively covers the main tectonic  
 232 domains of the northwestern and central regions of Mozambique at distinct altitudes  
 233 ranging from 217 to 843 m (Tab. 1 and Fig. 3A).

234       The analytical procedures were performed at Rio Grande do Sul Federal  
235      University. The apatite grains were concentrated by conventional magnetic, heavy  
236      liquid and hand-picking techniques and mounted in epoxy resin. Afterwards, the mounts  
237      were polished and etched, using 5.5 M HNO<sub>3</sub> at 21 °C for 20s to reveal the spontaneous  
238      fission tracks (Ketcham et al., 2007). The apatite mounts were covered with mica sheets  
239      to obtain the fission track ages using the external detector method (Gleadow, 1981).  
240      Neutron irradiation was performed at the FRM-II reactor in Garching (TU München,  
241      Germany). After irradiation, the mica detectors were etched with 48% HF for 18 min to  
242      reveal the induced fission tracks.

243       Fission-track counting was performed with a Leica DM6000 Microscope at  
244      1000x magnification. The fission track ages were calculated using the zeta calibration  
245      approach (Hurford, 1990) with CN5 dosimeter glass and the Durango apatite age  
246      standard. At least 20 grains were counted per sample; while 100 horizontal confined  
247      tracks were measured for the track length distribution (Gleadow et al., 1986; Gallagher  
248      et al., 1998), as its orientation relative to the c-axis. Commonly a hundred or more  
249      confined tracks were observed and measured in the samples, but some did not have the  
250      same abundance. Yet we decided to retain them nonetheless due to their agreement with  
251      the nearby samples that do have good-quality measurements. The ages are expressed as  
252      central ages with percent variation (Galbraith and Lasllet, 1993). Throughout this study,  
253      fission track age errors are quoted at the 1 $\sigma$  confidence level and were derived by the  
254      conventional method (Green, 1981). For each apatite grain analyzed, a mean value for  
255      the kinetic parameter Dpar (Donelick et al., 2005) was determined from five  
256      measurements. The  $\chi^2$  -squared test was used to quantify age homogeneity (Galbraith  
257      and Laslett, 1993) using the software “RadialPlotter” (Vermeesch, 2009).

258 Thermal history modeling was carried out using the QTQt software (Gallagher,  
259 2012) with the multi-kinetic annealing model of Ketcham et al. (2007). The priors on  
260 the general time-temperature were set by the software based on the ages observed in  
261 each sample. Each inversion model was run at 100,000 Burnin and 100,000 Post-burn-  
262 in iterations to provide more stable solutions (see discussion in Gallagher, 2012).  
263 Denudation histories were based on geothermal gradients estimated for the African  
264 plate. We assume a constant and linear geothermal gradient over geological times and  
265 suppose that the geothermal gradient is linear (25 °C/km; Martinelli et al., 1995).

266

#### 267 **4. Results**

268 AFT ages and confined mean track length (MTL) measurements from the  
269 basement samples are presented in Table 1. The central AFT ages do not present a clear  
270 correlation with the altitude sampled and no vertical profile match was obtained,  
271 suggesting that these samples have experienced a complicated thermal history (Fig. 3A).  
272 The mean confined fission track lengths against the AFT ages houfly present a  
273 boomerang shape (Fig. 3B) indicating differential denudation patterns (Gallagher and  
274 Brown, 1997) as also medium to high standard deviation distributions (Fig. 3C)  
275 suggesting that all samples register a long residence time within the partial annealing  
276 zone.

277 Broadly speaking, AFT central ages (Table 1; Fig. 4A) measured from the  
278 basement rocks ranges from Middle Triassic ( $225 \pm 15$  Ma) to Upper Cretaceous ( $83 \pm$   
279 9 Ma) and the mean confined track lengths obtained from 27 samples range from  $9.67 \pm$   
280  $0.52$   $\mu\text{m}$  to  $13.13 \pm 0.16$   $\mu\text{m}$ , with track length distributions predominantly unimodal.  
281 All central AFT ages passed in the  $\chi^2$  indicating one age population. The Dpar values  
282 (Table 1 and Fig. 3D) indicate a reasonably similar chemical compositions ( $> 1.75$   $\mu\text{m}$ )

283 and relatively chlorine-rich apatite grains with a higher resistance to annealing  
284 (Donelick et al., 2005).

285 The oldest ages are dominantly located at the extreme northwest of the area (Fig.  
286 4A) referring to the South Irumide Belt region (mostly NW), also presenting the smaller  
287 lengths measured (*ca.* 10  $\mu\text{m}$ ; Fig. 3C and 4A). Nevertheless, the largest lengths (> 10  
288  $\mu\text{m}$ ) occur around the regional structures, predominantly in the southern region  
289 (Southwest Nampula Complex). This brief variation in the confined track lengths  
290 indicates that samples near the structural trends are fastly denuded.

291 Thermal history models for samples of the northernmost area were modeled in  
292 three major groups being one to the northeast and the other two to the northwest. The  
293 choice of the samples to be grouped was based mainly on the obtained results in their  
294 individual thermal histories and their geographical position (Fig. 4). The other samples  
295 were also pooled based on the same principles as described below.

296 Samples from Southern Irumide NE-SW transect (Fig. 1C; Fig. 4 and 4A) near  
297 the East African Rift System, indicate a maximum paleotemperature of 99 °C at 136  
298 Ma and show a slow cooling pattern until 10 Ma at a temperature of 64 °C (Fig. 4 and  
299 4A). Thereafter, the samples soffers a rapidly cooled to present surface conditions. On  
300 the other hand, the samples of the Southern Irumide north and NW-SE transect (Fig.  
301 1C) record two distinct cooling behavior. Samples MZ-7 and MZ-8 (Fig. 4, 4B and 4C)  
302 show the oldest AFT ages of the whole area ( $225 \pm 15$  Ma and  $216 \pm 15$  Ma,  
303 respectively) and indicate a very long time of residence into the partial annealing zone  
304 with moderate reduced mean fission trak length of  $9.96 \pm 0.24$   $\mu\text{m}$  and  $10.86 \pm 0.16$   
305  $\mu\text{m}$ , respectively. Accelerated cooling until present day surface conditions was only  
306 acheaved in the latter *ca.* 50 Ma.

307

308

Table 1: Apatite fission track data from the northwestern Mozambique.

| Sample | Elevation<br>(m) | Rock type                      | N  | $\rho_s$ (Ns)<br>(x10 <sup>5</sup> ) | $\rho_i$ (Ni)<br>(x10 <sup>5</sup> ) | $\rho_d$ (Nd)<br>(x10 <sup>5</sup> ) | P ( $\chi^2$ ) | U Content<br>(%) | $\frac{\text{Age}^* \pm}{1\sigma}$<br>(Ma) | Dpar<br>( $\mu\text{m}$ ) | n   | Mean track length<br>( $\mu\text{m}$ ) $\pm 1\sigma$ | Std. Dev.<br>( $\mu\text{m}$ ) |
|--------|------------------|--------------------------------|----|--------------------------------------|--------------------------------------|--------------------------------------|----------------|------------------|--------------------------------------------|---------------------------|-----|------------------------------------------------------|--------------------------------|
| MZ-01  | 843              | Tonalitic Gneiss               | 20 | 27.2 (471)                           | 39.0 (674)                           | 9.30 (9302)                          | 98.0           | 53.2             | 106 $\pm$ 10                               | 2.50                      | 113 | 10.75 $\pm$ 0.18                                     | 1.89                           |
| MZ-02  | 801              | Tonalitic Gneiss               | 20 | 6.36 (238)                           | 10.4 (390)                           | 9.30 (9302)                          | 100.0          | 14.2             | 94 $\pm$ 10                                | 2.46                      | 92  | 11.79 $\pm$ 0.20                                     | 1.92                           |
| MZ-03  | 822              | Tonalitic Gneiss               | 20 | 7.25 (356)                           | 11.6 (572)                           | 9.30 (9302)                          | 81.0           | 15.9             | 97 $\pm$ 10                                | 2.76                      | 100 | 11.69 $\pm$ 0.24                                     | 2.37                           |
| MZ-04  | 637              | Tonalitic Gneiss               | 20 | 13.2 (583)                           | 21.7 (955)                           | 9.30 (9302)                          | 72.0           | 29.6             | 97 $\pm$ 10                                | 2.23                      | 127 | 10.59 $\pm$ 0.18                                     | 2.08                           |
| MZ-05  | 451              | Metagabbro                     | 17 | 11.2 (126)                           | 9.38 (106)                           | 9.30 (9302)                          | 100.0          | 12.8             | 188 $\pm$ 14                               | 2.57                      | 31  | 9.67 $\pm$ 0.52                                      | 2.89                           |
| MZ-06  | 427              | Mylonite                       | 20 | 8.61 (124)                           | 13.5 (195)                           | 9.30 (9302)                          | 87.0           | 18.5             | 109 $\pm$ 10                               | 2.48                      | 100 | 10.70 $\pm$ 0.22                                     | 2.20                           |
| MZ-07  | 451              | Gabbro                         | 20 | 21.3 (494)                           | 13.1 (305)                           | 8.14 (16276)                         | 48.0           | 20.5             | 225 $\pm$ 15                               | 2.16                      | 102 | 9.96 $\pm$ 0.24                                      | 2.40                           |
| MZ-08  | 456              | Monzogranite                   | 20 | 26.6 (705)                           | 15.9 (421)                           | 8.14 (16276)                         | 88.0           | 24.8             | 216 $\pm$ 15                               | 1.79                      | 108 | 10.86 $\pm$ 0.16                                     | 1.66                           |
| MZ-09  | 487              | Monzogranite                   | 20 | 21.0 (1791)                          | 26.1 (2223)                          | 8.14 (16276)                         | 0.0            | 40.7             | 111 $\pm$ 11                               | 2.36                      | 30  | 11.64 $\pm$ 0.46                                     | 2.53                           |
| MZ-10  | 492              | Garnet mafic granilite         | 20 | 10.2 (423)                           | 8.07 (335)                           | 8.14 (16276)                         | 40.0           | 12.6             | 183 $\pm$ 14                               | 2.15                      | 13  | 9.86 $\pm$ 0.67                                      | 2.42                           |
| MZ-11  | 419              | Monzogranite                   | 20 | 31.3 (1100)                          | 30.9 (1089)                          | 8.14 (16276)                         | 0.0            | 48.3             | 147 $\pm$ 12                               | 2.36                      | 39  | 10.43 $\pm$ 0.34                                     | 2.10                           |
| MZ-12  | 611              | Tonalitic-throndjemitic gneiss | 20 | 19.9 (299)                           | 24.0 (360)                           | 9.30 (9302)                          | 96.0           | 32.8             | 124 $\pm$ 11                               | 2.58                      | 100 | 12.55 $\pm$ 0.16                                     | 1.56                           |
| MZ-13  | 482              | Tonalitic-throndjemitic gneiss | 20 | 15.5 (163)                           | 17.0 (179)                           | 9.30 (9302)                          | 97.0           | 23.3             | 136 $\pm$ 12                               | 2.30                      | 46  | 11.63 $\pm$ 0.30                                     | 2.03                           |
| MZ-14  | 452              | Tonalitic-throndjemitic gneiss | 20 | 14.8 (124)                           | 18.5 (155)                           | 9.30 (9302)                          | 100.0          | 25.2             | 119 $\pm$ 11                               | 2.36                      | 56  | 12.20 $\pm$ 0.16                                     | 1.20                           |
| MZ-15  | 284              | Sienogranitic-Gneiss           | 20 | 7.60 (136)                           | 9.72 (174)                           | 9.30 (9302)                          | 99.0           | 13.3             | 129 $\pm$ 11                               | 2.70                      | 57  | 11.33 $\pm$ 0.23                                     | 1.74                           |
| MZ-16  | 718              | Quartz Diorite                 | 20 | 11.9 (179)                           | 14.0 (212)                           | 9.30 (9302)                          | 100.0          | 19.2             | 127 $\pm$ 11                               | 2.27                      | 103 | 11.95 $\pm$ 0.17                                     | 1.72                           |
| MZ-17  | 462              | Granite-Gneiss with garnet     | 20 | 26.5 (459)                           | 32.2 (557)                           | 9.30 (9302)                          | 99.0           | 44.0             | 125 $\pm$ 11                               | 2.14                      | 100 | 12.49 $\pm$ 0.18                                     | 1.79                           |
| MZ-18  | 217              | Tonalitic Gneiss               | 20 | 10.1 (325)                           | 10.3 (331)                           | 9.30 (9302)                          | 80.0           | 14.0             | 153 $\pm$ 12                               | 2.87                      | 109 | 11.50 $\pm$ 0.18                                     | 1.91                           |
| MZ-19  | 314              | Tonalitic Gneiss               | 20 | 11.3 (263)                           | 14.8 (346)                           | 9.30 (9302)                          | 69.0           | 20.3             | 123 $\pm$ 11                               | 2.97                      | 102 | 12.52 $\pm$ 0.18                                     | 1.85                           |
| MZ-20  | 627              | Gn. Sienogr.                   | 20 | 37.9 (629)                           | 52.3 (868)                           | 9.30 (9302)                          | 100.0          | 71.4             | 108 $\pm$ 10                               | 2.56                      | 100 | 11.94 $\pm$ 0.15                                     | 1.48                           |
| MZ-21  | 591              | Leucogranite                   | 20 | 28.2 (463)                           | 37.4 (613)                           | 9.30 (9302)                          | 90.0           | 50.4             | 120 $\pm$ 11                               | 1.94                      | 101 | 9.77 $\pm$ 0.16                                      | 1.58                           |
| MZ-22  | 640              | Granite                        | 20 | 18.2 (329)                           | 24.5 (444)                           | 9.30 (9302)                          | 100.0          | 33.5             | 113 $\pm$ 11                               | 2.64                      | 100 | 13.13 $\pm$ 0.16                                     | 1.56                           |
| MZ-23  | 784              | Granite-gnaisse                | 20 | 16.3 (294)                           | 19.2 (346)                           | 9.30 (9302)                          | 79.0           | 26.2             | 130 $\pm$ 11                               | 2.24                      | 27  | 11.99 $\pm$ 0.40                                     | 2.09                           |
| MZ-24  | 484              | Granite                        | 20 | 5.36 (105)                           | 5.61 (110)                           | 9.30 (9302)                          | 98.0           | 7.7              | 150 $\pm$ 12                               | 2.15                      | 21  | 12.38 $\pm$ 0.39                                     | 1.78                           |

|       |     |            |    |            |            |             |       |      |              |      |     |                  |      |
|-------|-----|------------|----|------------|------------|-------------|-------|------|--------------|------|-----|------------------|------|
| MZ-25 | 607 | Ortogneiss | 20 | 17.5 (307) | 25.5 (447) | 9.30 (9302) | 100.0 | 34.9 | $104 \pm 10$ | 2.80 | 100 | $12.79 \pm 0.17$ | 1.71 |
| MZ-26 | 644 | Ortogneiss | 20 | 8.09 (161) | 12.1 (240) | 9.30 (9302) | 94.0  | 16.5 | $108 \pm 10$ | 2.24 | 62  | $11.67 \pm 0.18$ | 1.44 |
| MZ-27 | 654 | Ortogneiss | 20 | 18.9 (347) | 35.0 (644) | 9.30 (9302) | 96.0  | 47.8 | $83 \pm 9$   | 2.33 | 102 | $11.91 \pm 0.17$ | 1.76 |

N: number of grains analysed to determine track densities; ps: measured spontaneous track density; NS: number of spontaneous tracks counted ; pi: measured induced track density; Ni: number of induced tracks counted; pd: track density measured in external detector adjacent to glass dosimeter during irradiation; Nd: number of tracks counted in determining pd ; P ( $\chi^2$ ): probability of obtaining observed  $\chi^2$  value for n degrees of freedom (n = number of crystals -1); n: number of confined tracks lengths measured. \* Apatite ages calculated using a zeta of 320.2 for CNS glass on German reactor. Analyst: M.M.Bicca.

309

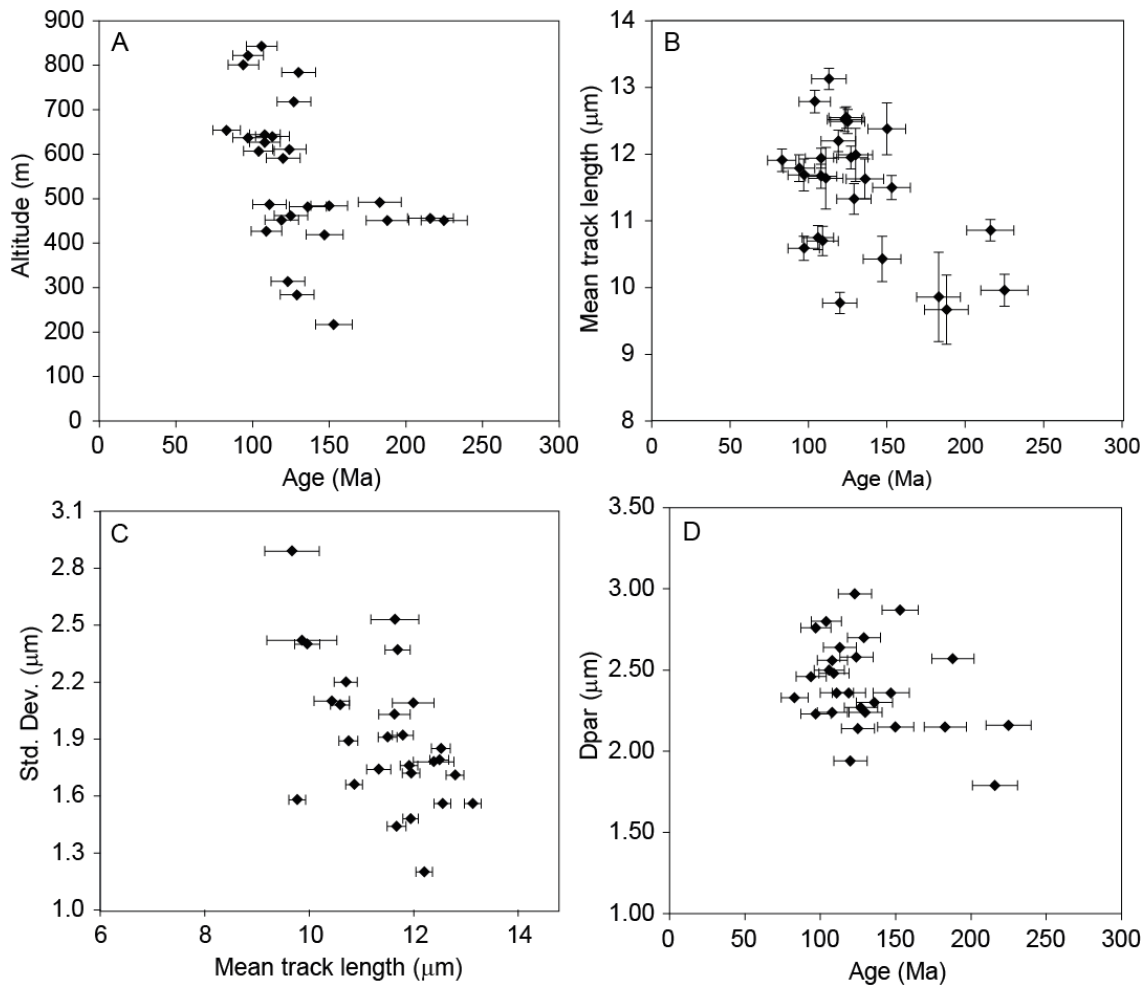
310

311

312

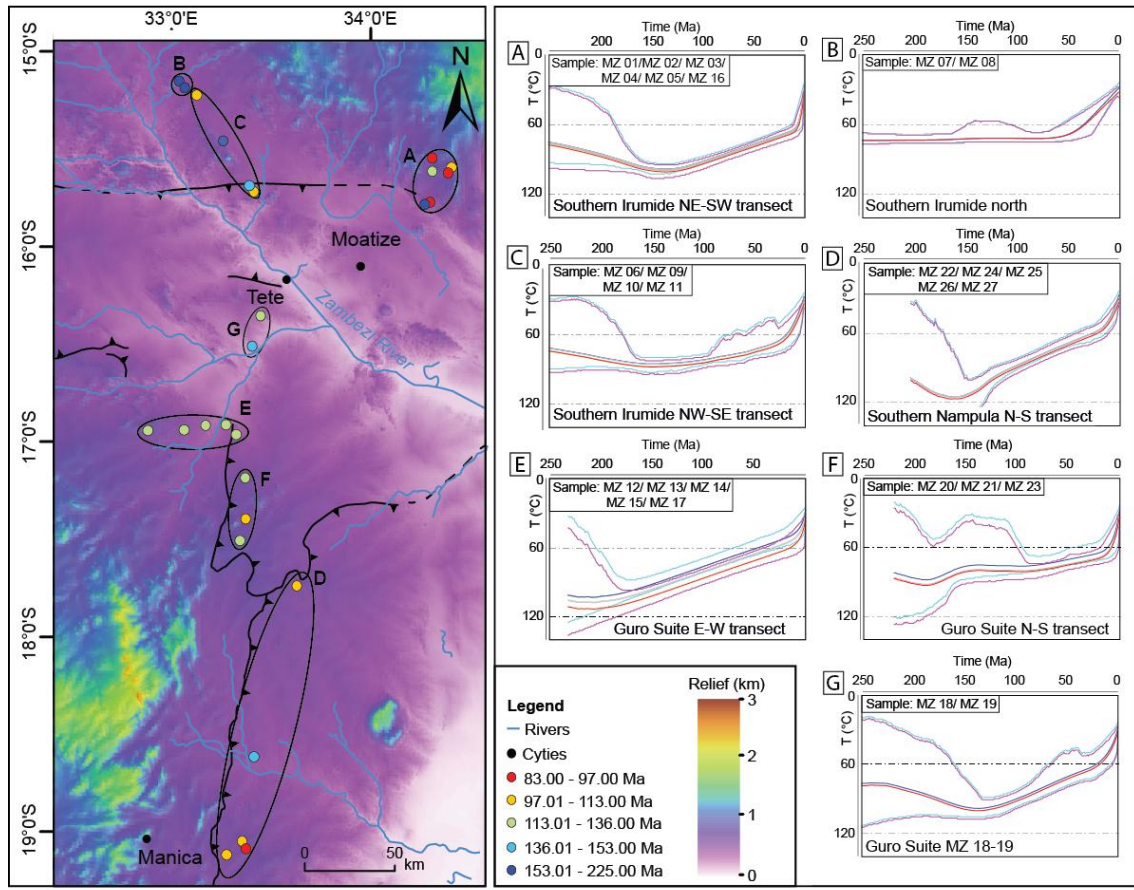
313

314



315

316 Figure 3: Relationship between AFT ages, samples elevation, MTL and Dpar values. A)  
 317 AFT ages plotted against sample elevation showing no clear relationship. B) AFT ages  
 318 against MTL showing a roughly boomerang shape. C) MTL plotted against Std. Dev.  
 319 showing a broad standard deviation pattern of the MTL, compatible with a very slow  
 320 cooling history. D) Dpar plotted against AFT ages show that the samples are of chlorine-  
 321 rich apatite grains.



322

323 Figure 4: Geomorphologic map (Jarvis et al., 2008) of the study area with the sample  
 324 locations and the thermal history models of all samples. They were grouped based on their  
 325 thermal history behavior and their geographic location.

326

327 The Nampula Complex N-S transect (Fig. 1C) registers a similar cooling pattern,  
 328 with a relatively slow cooling from maximum paleotemperature of 116 °C at 165 Ma to 56  
 329 °C at 17 Ma continuing with a faster cooling pattern until present-day surface conditions  
 330 (Fig. 4 and 4D).

331 Samples from the central region were separated into three groups (Fig. 1 and Fig. 4).  
 332 The first comprises the Guro Suite E-W transect (Fig. 4 and 4E) with five samples. Thermal  
 333 history of this group is represented by a steady-state cooling history from 208 Ma to 15 Ma

334 with a maximum paleotemperature of 103 ° C decreasing until 50 ° C in a time span of *ca.*  
335 190 Ma, followed by a fast cooling period to the present-day thermal conditions (Fig. 4E).  
336 The thermal behavior observed by the second group (formed by three samples and grouped  
337 as the Guro Suite N-S transect, Fig. 4 and 4F) differs from the former, presenting a rapid  
338 cooling between 190 Ma and 150 Ma, from temperetures of 88 ° C to 76 ° C, followed by a  
339 period of a stationary cooling history until 94 Ma. From this moment samples started to  
340 cooling in the same stady-state pattern until 18 Ma when achieved present-day conditings  
341 after a fast cooling event from paleotemperature of 64 ° C. The third one comprises the  
342 samples MZ-18 and MZ-19 located in the Guro Suite of the central portion of the graben of  
343 the structural controlled Zambezi Valley (Fig. 1C) at altitudes of 217 and 314 m,  
344 respectively (Table 1), being lower than the others of this region. As the other samples, the  
345 thermal model indicates a slow cooling of paleotemperatures of the order of 99 ° C to 136  
346 Ma to 60° C at 21 Ma. From 21 Ma these samples soffers a fast cooling until present-day  
347 conditions (Fig. 4G).

348

## 349 **5. Discussions**

350 The data demonstrate that the thermal histories of the analyzed samples correspond  
351 to prossess much younger than the stratigraphic age of the rocks sampled indicating that  
352 intense exhumation processes affected the region during the Mesozoic Era. The AFT  
353 central ages and the maximum modeled paleotemperatures can be attributed to important  
354 regional and local tectonic activity and mantle dynamics controlled by the tectonic  
355 evolution related to the opening of the Indian Ocean.

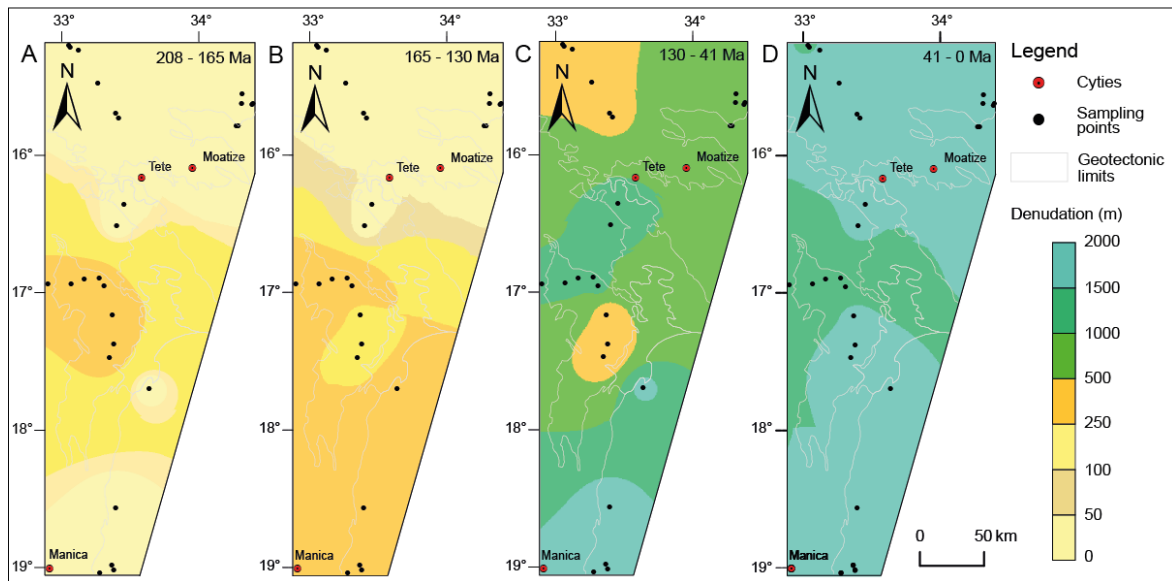
356 The time interval choosed to construct the denudation maps were based on the  
357 maximun paleotemperatures obseved in the thermal modeling (Fig. 4B to 4G). From this,

358 four main intervals were analysed separately as presented in Figure 5. The older ages are  
359 situated close to the latter stages of the Cape Fold Belt tectonic activity attributed to the  
360 subduction of the Panthalassa seafloor and may represent cooling episodes caused by  
361 erosion and denudation associated with tectonic reactivations induced by a far stress field  
362 propagating along the African crust. The process is well documented by Karoo  
363 sedimentation in the Zambezi Valley basins. Permian-Triassic times was a period of high  
364 subsidence rates in these basins filled by *ca.* 10 km of volcano-sedimentary pile (Catuneanu  
365 et al., 2005) implying high denudation rates in the source areas southwards (Key et al.,  
366 2015; Bicca et al., 2017).

367 Cooling episodes around 200-250 Ma was also described by Van Der Beek et al.  
368 (1998) in the north of the Malawi rift, which they attributed to late Karoo erosion have  
369 affected the entire area. High denudation rates from *ca.* 190-180 Ma (Norconsul  
370 Consortium, 2007) would be expected due to thermal uplift of the rift shoulders produced  
371 by the Karoo magmatism in the north of Mozambique (Fig. 6), which extends to *ca.* 170  
372 Ma in other parts of Africa and Antarctica (Catuneanu et al., 2005; Klausen, 2009;  
373 Mahanjane, 2012; Castelino et al., 2015). Middle Jurassic Drift onset (170-166 Ma) depict  
374 the initiation of movement on the Davie Ridge transform, which is marked by spreading in  
375 the Somali basin (Mahanjane, 2014). This period comprises the early stages of Gondwana  
376 break-up and were poorly preserved in the thermal history of our samples and the highest  
377 denudation thicknesses (about to 300 m) were observed in the central area (Fig. 5A; Guro  
378 Suite E-W and N-S transects) in a period from Upper Triassic to Middle Jurassic implying  
379 in <0.3 °C/Ma, while in the north and south these periods were not registered suggesting no  
380 thermal or tectonic influence.

381 From Middle Jurassic to Lower Cretaceous the central and southern regions presents  
382 the highest denuded amounts (around 300 m; Fig. 5B), demonstrating that this area  
383 underwent important erosive processes that may be associated with the NW-SE and N-S  
384 structural trends that comprise important inherited structural patterns the Precambrian  
385 basement of the region (Fig. 1). Fast cooling history around 150 Ma were also documented  
386 in the Malawi Rift (Van der Beek et al., 1998) which these authors associated with a  
387 renewed rifting phase. This moment is documented in the southern region of Malawi with  
388 the development of alkaline magmatism (abouto to 130-100Ma) associated with extensional  
389 tectonics (Eby et al., 1995), near to the NE region of the study area (see Fig. 2 for location).  
390 This period (around 150 Ma) comprises the early stages of the Antarctica southwards  
391 drifting with respect to Africa (Mahanjane, 2012; Castelino et al., 2015) and the  
392 Madagascar southwards drift from Tanzania margin by the Davie shear zone with seafloor  
393 spreading in the Somali Basin during the Lower and Upper Cretaceous times (140 Ma to 90  
394 Ma; Emmel et al., 2011; Mahanjane, 2014). After that, Madagascar occupied its present  
395 position as part of the African plate (Salman and Abdula, 1995; Castelino et al., 2015).

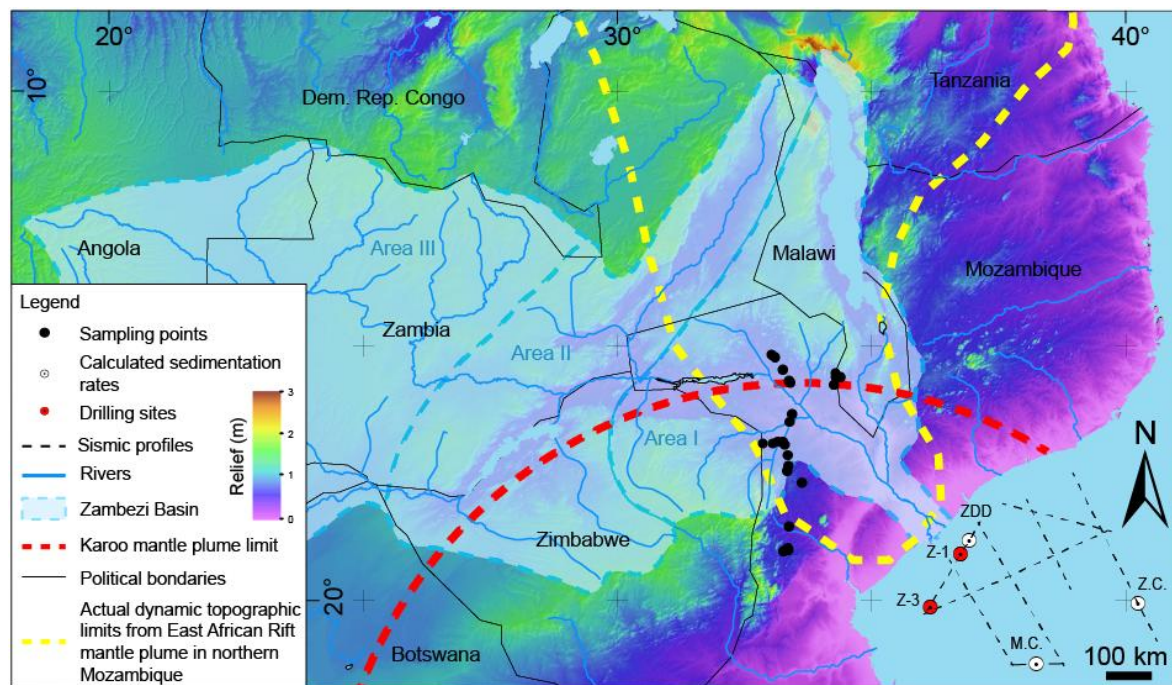
396



397

398 Figure 5: Reconstructed denudation history of the NW Mozambique basement. The maps  
 399 show the inferred amount and the spatial variation of denudation at: A) 208 – 165 Ma, B)  
 400 165–130 Ma, C) 130 – 41 Ma, and D) 41 – 0 Ma.

401



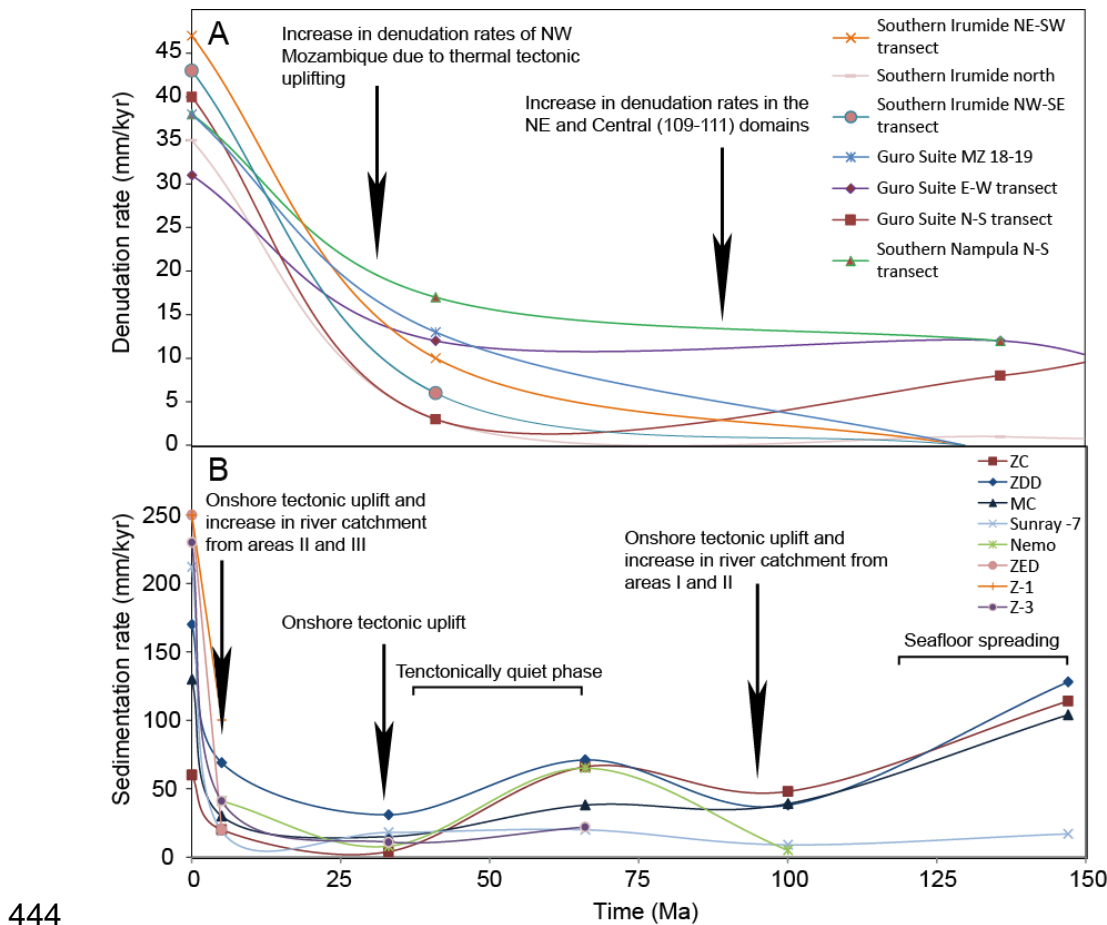
402

403 Figure 6: Geomorphological map (Jarvis et al., 2008) of central-eastern Africa highlighting  
 404 important thermal limits and the extension of the Zambezi Basin. Seismic and drilling data  
 405 are after Castelino et al. (2015); Karoo mantle plume limits are after Cox (1989a and  
 406 1989b); and dynamic topography limits is after Moucha and Forte (2011).

407 These arguments are also in agreement with the intensification of denudation  
408 observed in all the study area (Fig. 5C) from Upper Cretaceous to Middle Paleocene  
409 eroding thicknesses from 254 m to 1659 m due to the development of the Mozambique  
410 margin, being the largest thicknesses were removed from the northeast, central and south  
411 regions. Accelerated denudation processes during Lower and Upper cretaceous are also  
412 described by Belton and Raab (2010) for the Kalahari cratonic area and by Emmel et al.  
413 (2011) for NE Mozambique corroborating the regional uplift model of the hinterland in the  
414 east margin of the African plate and accelerated denudation patterns.

415 A well-defined pattern of rapid cooling around 40 Ma taking the samples out of the  
416 partial cooling zone with denudation rates of 31-47 m/Ma and amounts of 1.5-2 km thick of  
417 surface denuded section until the current thermal conditions. The south and north of the  
418 area have suffered the greatest influnce during this period. Until this moment the total  
419 amount of denuded sheet of NW Mozambique have reached 2.5-3.5 km. Similar conditions  
420 were detected in the Karoo sequences in the area implying 1000 and 1500 m of denudation  
421 onwards from 6 Ma (Fernandes et al., 2015). This moment is approaching crustal uplifting  
422 in the northeastern region of Africa attributed to a superswell related to the African mantle  
423 plume movements responsible for the evolution of the East African Rift System. According  
424 to the models developed by simulations of the mantle convection for the last 30 Ma  
425 (Moucha and Forte, 2011) it was possible to observe a drastic increase of topography in the  
426 NE region of Africa (since *ca.* 15 Ma) propagating south towards the north of Mozambique  
427 (Fig. 6). This southwards uplift is due to the northwards movement of the African plate due  
428 to the movement of the mantle, leading to distensive processes reactivating ancient crustal  
429 structures raising the rates of cooling and denudation throughout the northwest region of  
430 Africa (Moucha and Forte, 2011).

431 This dynamic topography came to contribute to the sedimentation rates in the  
432 onshore and offshore Mozambique basin sites, since the erosion amount determined from  
433 NW Mozambique does not match the higher sedimentation rates described in the basin  
434 despite of provide a good fit with the timing of major crustal uplift (Fig. 7). These  
435 additional amounts of sediment were added to the river systems from other interior regions  
436 covered by the Zambezi river basin. The African plate due to thermal uplifting firstly  
437 related to the Karoo Igneous Province and more recently by the mantle dynamics of the  
438 East African Rift System induced the capture of the Zambezi tributaries due to the  
439 structural reactivation. The Zambezi river basin possess three main regions known as basins  
440 I, II and III (Fig. 6, Castelino et al., 2015). The most distal ones have only became part of  
441 the basin from the Miocene-Paleocene times as determined by Castelino et al. (2015) from  
442 sedimentation rates in the north of the Mozambique Basin, which is in agreement with the  
443 uplift periods of the northeast region of the African plate (Moucha and Forte, 2011).



444      Figure 7: Plots of denudation rates from NW Mozambique (A) and thermal burial histories  
445      of the north of the Mozambique Basin nearer the Zambezi Delta determined from well and  
446      seismic data (see figure 6 for location; after Castelino et al., 2015).

448

449      With these in mind, it is possible to determine our high Pleistocene denudation rates  
450      which fit with the predicted uplift periods and river catchment as determined by Castelino  
451      et al. (2015). Although, most of the samples indicate a protracted cooling history since  
452      Late-Jurassic- Early Cretaceous with an acceleration of the cooling history only in the last  
453      *ca.* 41 Ma, probably associated with mantle upwelling of the East African Rift System and  
454      extensional tectonics related to it. The main period of uplift around 90 Ma were not clearly  
455      distinguished in our data.

456 **6. Conclusions**

457 The northern region of Mozambique comprises important pieces to assemble the  
458 puzzle related to the plates dynamics during the formation and separation of the Gondwana.  
459 The southern African plate has underwent several processes of horizontal and vertical stress  
460 since Permian times attributed to Gondwanides orogenesis and to mantle plumes upwelling  
461 from the Gondwana separation stages, respectively. The AFT age data provided range from  
462 Upper Triassic to Upper Cretaceous indicating that the region underwent intense  
463 denudation during earlier times, erasing these stages from thermal history. This  
464 interpretation is corroborated by intense tectonic reactivation in the Zambezi Valley region,  
465 leading to the formation of great accommodation spaces in the rift basins, filled by thick  
466 sedimentary sequences of the Karoo Supergroup. Maximum paleotemperatures in the  
467 basement samples were reached at around 200-150 Ma which led to denudation amounts of  
468 0.3-2 km at rates varying from 3-17 m/Ma until Middle Pleistocene. The early stages of  
469 cooling is compatible with the increasing opening stage of the Indian Ocean seafloor. Since  
470 Middle Pleistocene a fast-cooling event affected the entire region taking samples to the  
471 current thermal conditions at denudation rates between 31-47 m/Ma and a final denuded  
472 section since Late Triassic of 2-3.5 km. This change were caused by important shift in the  
473 northeast portions of the African plate, mainly in terms of topography and drainage patterns  
474 induced by mantle plume activity that have uplifted the whole NE region of Africa  
475 extending to the north of Mozambique, due to a thermal induced drift of Africa northwards.

476

477 **7. Acknowledgements**

478 This study incorporate part of the doctoral thesis of the first author at Programa de  
479 Pós-Graduação em Geociências of Universidade Federal do Rio Grande do Sul. We thanks

480 to Conselho Nacional do Desenvolvimento Científico e Tecnológico (CNPq) of Brazil, for  
481 scholarship financially supported of the first author. We also would like to thank to Mr.  
482 António Rizzo Alface for the geology field assistance.

483

484 **8. References**

485 Bauer, F.U., Jacobs, J., Emmel, B.U., van Soest, M.C., 2016. New (U-Th)/He titanite data  
486 from a complex orogenepassive margin system: A case study from northern Mozambique.  
487 Journal of African Earth Sciences 120, 56-69.

488

489 Bingen, B., Jacobs, J., Viola, G., Henderson, I.H.C., Skar, O., Boyd, R., Thomas, R.J.,  
490 Solli, A., Key, R.M., Daudi, E.X.F., 2009. Geochronology of the Precambrian crust  
491 in the Mozambique belt in NE Mozambique, and implications for Gondwana assembly.  
492 Precambrian Research. 170, 231-255. <http://dx.doi.org/10.1016/j.precamres.2009.01.005>.

493 005.

494

495 Castaing, C., 1991. Post Pan-African tectonic evolution of South Malawi in relation to  
496 the Karoo and recent East African Rift System. Tectonophysics 191, 55-73.

497

498 Castelino, J.A., Reichert, C., Klingelhoefer, F., Aslanian, D., Jokat, W., 2015. Mesozoic  
499 and Early Cenozoic sediment influx and morphology of the Mozambique Basin. Marine  
500 and Petroleum Geology 66, 890-905. <http://dx.doi.org/10.1016/j.marpetgeo.2015.07.028>.

501

- 502 Catuneanu, O., Wopfner, H., Eriksson, P.G., Cairncross, B., Rubidge, B.S., Smith, R.M.H.,  
503 Hancox, P.J., 2005. The Karoo basins of south-central Africa. *Journal of African Earth  
504 Sciences* 43, 211–253.
- 505
- 506 Chaúque, F. R., 2012. Contribution to the knowledge of the tectonic evolution of the  
507 Mozambique Belt, Mozambique. Thesis (Ph.D) - Institute of Geosciences, University of  
508 São Paulo, São Paulo, 187pp.
- 509
- 510 Chaúque, F. R., Cordani, U.G., Jamal, D.L., Onoe, A.T., 2017. The Zimbabwe Craton in  
511 Mozambique: A brief review of its geochronological pattern and its relation to the  
512 Mozambique Belt. *Journal of African Earth Sciences*. doi: 10.1016/j.jafrearsci.  
513 2017.01.021.
- 514
- 515 Cox, K.G., 1989a. Hot plumes from the mantle. *Nature* 340, 341-341.
- 516
- 517 Cox, K.G., 1989b. The role of mantle plumes in the development of continental drainage  
518 patterns. *Nature* 342, 873-877.
- 519
- 520 Daszinnies, M.C., 2006. The Phanerozoic Thermo-tectonic Evolution of Northern  
521 Mozambique Constrained by  $^{40}\text{Ar}/^{39}\text{Ar}$ , Fission Track and (U-Th)/He Analyses. PhD  
522 Thesis University of Bremen 227.
- 523
- 524 Daszinnies, M.C., Jacobs, J., Wartho, J.-A., Grantham, G.H., 2009. Post Pan-African  
525 thermo-tectonic evolution of the north Mozambican basement and its implication

- 526 for Gondwana rifting. Inferences from  $40\text{Ar}/39\text{Ar}$  hornblende, biotite and  
527 titanite fission-track dating. In: Lisker, F., Ventura, B., Glasmacher, U. (Eds.),  
528 Thermochronological Methods: From Palaeotemperature Constraints to Landscape  
529 Evolution Models: Geological Society of London, Special Publications, 324,  
530 pp. 25–50.
- 531
- 532 Donelick, R.A., O'Sullivan, P.B., Ketcham, R.A., 2005. Apatite Fission-Track Analysis. In:  
533 Reiners, P.W., Ehlers, T.A. (Eds.), Low-Temperature Thermochronology: Techniques,  
534 Interpretations, and Applications. Reviews in Mineralogy and Geochemistry 58.  
535 Mineralogical Society of America, Washington, pp. 49–94.
- 536
- 537 Emmel, B., Kumar, R., Jacobs, J., Ueda, K., Van Zijl, M., R.J., Matola, R., 2014.  
538 The low-temperature thermochronological record of sedimentary rocks from the central  
539 Rovuma Basin (N Mozambique) — Constraints on provenance and thermal history.  
540 Gondwana Research 25, 1216–1229.
- 541
- 542 Emmel, B., Kumar, R., Ueda, K., Jacobs, J., Daszinnies, M.C., Thomas, R.J., Matola, R.,  
543 2011. Thermochronological history of an orogen-passive margin system — an example  
544 from N Mozambique. Tectonics 30. <http://dx.doi.org/10.1029/2010TC002714>.
- 545
- 546 Fernandes, P., Cogné, N., Chew, D.M., Bruno Rodrigues, B., Jorge, R.C.G.S., Marques, J.,  
547 Jamal, D., Vasconcelos, L., 2015. The thermal history of the Karoo Moatize-Minjova  
548 Basin, Tete Province, Mozambique: An integrated vitrinite reflectance and apatite fission  
549 track thermochronology study. Journal of African Earth Sciences 112, 55–72.

- 550
- 551 Fritz, H., Abdelsalam, M., Ali, K.A., Bingen, B., Collins, A.S., Fowler, A.R., Ghebreab,W.,
- 552 Hauzenberger, C.A., Johnson, P.R., Kusky, T.M., Macey, P., Muhongo, S., Stern, R.J.,
- 553 Viola, G., 2013. Orogen styles in the east African orogen: a review of the Neoproterozoic
- 554 to Cambrian tectonic evolution. *J. Afr. Earth Sci.* 86, 65e106. <http://dx.doi.org/10.1016/j.jafrearsci.2013.06.004>.
- 555
- 556
- 557 Galbraith, R.F., Laslett, G.M., 1993. Statistical models for mixed fission track ages. *Nucl.*
- 558 *Tracks Radiat. Meas.* 21, 459–470.
- 559
- 560 Gallagher, K., 2012. Transdimensional inverse thermal history modeling for quantitative
- 561 thermochronology. *Journal of Geophysical Reserch* 117.<http://dx.doi.org/10.1029/2011JB008825>.
- 563
- 564 Gallagher, K., Brown, R., 1997. The onshore record of passive margin evolution.
- 565 *Geological Society of London* 154, 451-457.
- 566
- 567 Gallagher, K., Brown, R., Johnson, C., 1998. Fission track analysis and its applications
- 568 to geological problems. *Annual Review of Earth and Planetary Sciences* 26, 519–572.
- 569
- 570 Green, P.F., 1981. A new look at statistics in fission-track dating. *Nucl. Tracks* 5 (1), 77–
- 571 86.
- 572

- 573 Hurford, A.J., 1990. International union of geological sciences subcommission on  
574 geochronology recommendation for the standardization of fission track dating calibration  
575 and data reporting. *Nucl. Tracks Radiat. Meas.* 17 (3), 233–236.
- 576
- 577 Gleadow, A.J.W., Duddy, I.R., Green, P.F., Lovering, J.F., 1986. Confined fission track  
578 lengths in apatite: a diagnostic tool for thermal history analysis. *Contributions Mineralogy*  
579 and Petrology 94, 405-415.
- 580
- 581 Jacobs, J., Thomas, R.J., 2004. A Himalayan-type indenter-escape tectonic model for the  
582 southern part of the Late Neoproterozoic/Early Paleozoic East African–Antarctic  
583 Orogen. *Geology* 32, 721–724.
- 584
- 585 Jacobs, J., Bingen, B., Thomas, R.J., Bauer, W., Wingate, M., Feitio, P., 2008. Early  
586 Palaeozoic orogenic collapse and voluminous late-tectonic magmatism in Dronning  
587 Maud Land and Mozambique: insights into the partially delaminated orogenic root of the  
588 East African-Antarctic Orogen? In: Satish-Kumar, M., Motoyoshi, Y., Osanai, Y., Hiroi,  
589 Y., Shiraishi, K. (Eds.), *Geodynamic Evolution of East Antarctica: A Key to the East–West*  
590 *Gondwana Connection*. Geological Society of London, Special Publications 308, 69–90.
- 591
- 592 Jarvis, A., Reuter, H.I., Nelson, A., Guevara, E., 2008, Hole-filled SRTM for the globe  
593 Version 4, available from the CGIAR-CSI SRTM 90m Database. <http://srtm.cgiar.org>.
- 594
- 595 Ketcham, R.A., Carter, A.C., Donelick, R.A., Barbarand, J., Hurford, A.J., 2007. Improved  
596 modeling of fission-track annealing in apatite. *Am. Mineral.* 92, 799–810.

- 597
- 598 Key, R.M., Cotterill, F.P.D., Moore, A.E., 2015. The Zambezi River: An Archive of  
599 Tectonic Events Linked to the Amalgamation and Disruption of Gondwana and Subsequent  
600 Evolution of the African Plate. *South African Journal of Geology* 118(4), 425-438.
- 601
- 602 Klausen, M.B., 2009. The Lebombo monocline and associated feeder dyke swarm:  
603 diagnostic of a successful and highly volcanic rifted margin? *Tectonophysics* 468, 42-62.
- 604
- 605 Lavè, J., 2015. Landscape inversion by stream piracy. *Nature* 520, 442-444.
- 606
- 607 Macey, P.H., Miller, J.A., Rowe, C.D., Grantham, G.H., Siegfried, P., Armstrong, R.A.,  
608 Kemp, J., Bacalau, J., 2013. Geology of the Monapo Klippe, NE Mozambique and  
609 its significance for assembly of central Gondwana. *Precambrian Research* 233, 259-281.  
610 <http://dx.doi.org/10.1016/j.precamres.2013.03.012>.
- 611
- 612 Mahanjane, E.S., 2012. A geotectonic history of the northern Mozambique Basin including  
613 the Beira High – a contribution for the understanding of its development. *Marine and  
614 Petroleum Geology* 36, 1–12. <http://dx.doi.org/10.1016/j.marpetgeo.2012.05.007>.
- 616
- 617 Mahanjane, E.S., 2014. The Davie Fracture Zone and adjacent basins in the offshore  
618 Mozambique Margin - A new insights for the hydrocarbon potential. *Marine and Petroleum  
619 Geology* 57, 561-571. <http://dx.doi.org/10.1016/j.marpetgeo.2014.06.015>  
620 2012.05.007.

- 621
- 622 Manjate, V. A., 2015. Caracterização Geocronológica dos granitoides do Complexo de  
623 Bárue e da Suíte de Guro, Centro-Oeste de Moçambique, e suas relações com a  
624 metalogênese. Thesis (Ph.D) - Institute of Geosciences, University of São Paulo, São Paulo,  
625 149pp. (unpubl.)
- 626
- 627 Martinelli, G., Dongarra, G., Jones, M.Q.W., Rodriguez, A., 1995. Geothermal features of  
628 Mozambique: country update. Proceedings of the World Geothermal Congress,  
629 Florence, Italy, 251–273.
- 630
- 631 Meert, J.G., 2003. A synopsis of events related to the assembly of eastern Gondwana.  
632 Tectonophysics 362, 1e40.
- 633
- 634 Moucha, R., Forte, A.M., 2010. Changes in African topography driven by mantle  
635 convection. Nature Geoscience 4, 707-712.
- 636
- 637 Norconsult Consortium, 2007. Mineral resources management capacity building  
638 project. Republic of Mozambique, Component 2: Geological Infrastructure Development  
639 Project, Geological Mapping Lot 1, Report.
- 640
- 641 Patridge, T.C., Maud, R.R., 1987. Geomorphic evolution of souther Africa since the  
642 Mesozoic. South African Journal of Geology 90, 179-208.
- 643
- 644 Reeves, C., 2000. The Geophysical mapping of Mesozoic dyke swarms in southern

- 645 Africa and their origin in the disruption of Gondwana. *Journal of African Earth*  
646 *Sciences* 30, 449-513.
- 647
- 648 Salman, G., Abdula, I., 1995. Development of the Mozambique and Ruvuma sedimentary  
649 basins, offshore Mozambique. *Sedimentary Geology* 0738, 7-41.
- 650
- 651 Eby, R M., Roden-Tice, G.N., Krueger, H.L., Ewing, W., Faxon, E.H., Woolley, A.R.,  
652 1995. Geochronology and cooling history of the northern part of the Chilwa Alkaline  
653 Province, Malawi. *Journal of African Earth Sciences* 20(3-4), 215-288.
- 654
- 655 Ueda, K., Jacobs, J., Thomas, R.J., Kosler, J., Jourdan, F., Matola, R., 2012. Delamination-  
656 induced late-tectonic deformation and high-grade metamorphism of the Proterozoic  
657 Nampula Complex, northernMozambique. *Precambrian Research* 196–197, 275–294.
- 658
- 659 Van der Beek, P., Mbede, E., Andriessen, P., Delvaux, D., 1998. Denudation history of the  
660 Malawi and Rukwa Rift flanks (East African Rift System) from apatite fission track  
661 thermochronology. *Journal of African Earth Sciences* 26(3), 363.365.
- 662